Department of Geosciences
University of Fribourg (Switzerland)

Air Convection in Coarse Blocky Permafrost: A Numerical Modelling Approach to Improve the Understanding of the Ground Thermal Regime

THESIS

presented to the Faculty of Science and Medicine of the University of Fribourg (Switzerland)
in consideration for the award of the academic grade of
Doctor of Philosophy in Geosciences

by

Jonas Wicky

from

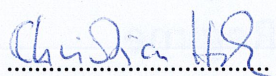Freiburg i. Üe. and Escholzmatt

2022

Accepted by the Faculty of Science and Medicine of the University of Fribourg (Switzerland) upon the recommendation of Dr. Lukas Arenson, Prof. Christian Hauck, Prof. Martin Hoelzle, Dr. Sébastien Morard and Prof. Andreas Vieli
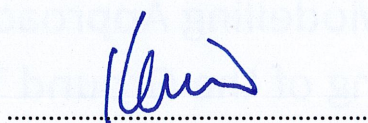
Freiburg, 16.03.2022

Thesis supervisor   Dean

Prof. Christian Hauck   Prof. Gregor Rainer

....

Summary

Permafrost is a thermal phenomenon, defined as subsurface material with a temperature remaining below 0°C for at least two consecutive years. Permafrost occurs at high latitudes and high altitudes in mountain ranges. In the Swiss Alps, permafrost can be expected to occur above roughly 2400 m a.s.l., depending on the energy input at the surface, mostly depending on altitude and aspect, as well as on the sub-surface processes governing the ground temperatures.

The focus of this thesis are these subsurface thermal processes. In mountain ranges, the surface is often covered with coarse blocks hosting a lot of air. As long as air is not moving, it is thermally insulating due to its low thermal conductivity. Once moving, air has the potential to convectively transfer heat, meaning that through the movement of warm (cold) air, the medium is getting warmer (colder). Transferred to a mountainous environment, the following annual cycle of convective air flow can be observed: During the summer, the exterior air temperature is higher compared to the temperature of the air in between the blocks. The thermal stratification is thus stable, as the warmer, lighter air is on top of the colder, denser air. Heat is transferred through conduction and air plays its insulating role. During winter, the situation changes. The exterior air temperature drops leading to cold, heavy air on top of the relatively warm air in between the blocks. This stratification is unstable and the cold, heavy, exterior air starts flooding the blocks. This leads to an enhanced heat transfer due to convection during the winter months, leading to a net-cooling effect over the year. In the literature, this effect has been called "thermal-semiconductor-effect", describing this seasonal asymmetry.

This effect is well known and has been observed in various contexts. The contribution of this thesis towards a better understanding of the influence of air convection in the ground is achieved by means of numerical modelling. Although numerical modelling is widely applied in permafrost research, the explicit modelling of air convection has so far only been done in permafrost engineering. There, crushed rocks, which allow for air convection, are used to maintain low ground temperatures beneath infrastructure constructions. In numerical modelling temperatures in permafrost, convective heat transfer by air flow was normally either neglected or strongly parametrised. In this thesis, a physics-based approach is presented using the porous media assumption for the coarse blocky layer, solving for heat transfer through conduction and convection with air flow described by Darcy's law and adopting a Boussinesq-approximation to account for the buoyancy induced free convection effects. The model approach is specifically refined and adapted to different landforms to assess the influence of air convection in the ground on the thermal regime of the permafrost.

The model was applied on two typical landforms hosting permafrost in the alpine environment: (i) talus slopes and (ii) rock glaciers. Two different types of talus slopes (i) were modelled. First, a talus slope within the belt of alpine permafrost was used to constrain the model. It could be modelled that convection has the potential to lead to a significant temperature difference between the upper and the lower part of a slope, which can explain the typical distribution of permafrost along a talus slope. The cold, ice-rich part is found at its base, whereby the upper part is often permafrost free – contradicting the intuitive expectation of an altitudinal dependence of permafrost occurrence. Further modelling was performed on a low altitude talus slope, where the mean annual air temperature is positive and thus permafrost is not expected, but has been sporadically observed. The reproduction of the observed permafrost occurrences was possible when accounting for ground air convection, confirming that this is the process governing these unusually cold ground temperatures at lower altitudes. In addition, the aggregation and melting of ground ice was also successfully reproduced.

Rock glaciers (ii), the arguably most famous permafrost landform, were a further subject of numerical modelling. While in their core the voids are normally (super-) saturated with ice, the thaw layer on top is often composed of large blocks with interstices filled with air. There again the convective air flow shows comparable cooling effects to a talus slope albeit not on the same spatial scale and extent. The effect of air convection in the active layer of a rock glacier on permafrost temperatures has been modelled and demonstrated to be very significant. The convective behaviour could be described by the concept of the Rayleigh number, a dimensionless number known from fluid mechanics. The temperature gradient within the active layer and the permeability of the active layer have been identified as the most important parameters controlling the ground air convection and its influence on the thermal regime. The permeability is the parameters describing how well the pores are linked and thus how fast a fluid passes through a porous medium. Reliable permeability measurements are not available, this parameter shows thus the highest sensitivity.

Overall, this thesis describes a consistent approach to modelling air convection in porous ground and its influence on permafrost temperatures. Although air convection in the ground has been observed and described for quite a long time, its representation in a numerical model on a real two-dimensional field-scale, applying measured data as boundary and afterwards as validation, is novel. The approach confirms most of the field observations that were made, but it allows for an extended qualitative description of the air convection in the ground as well as for attempts of absolute quantification of the influence of air convection on permafrost temperatures. In addition, the use of an equation-based numerical model allows various links to other branches of science, such as engineering or fluid mechanics, which allows new and interesting interpretations of heat transfer processes in mountain permafrost.

Zusammenfassung

Permafrost ist ein thermisches Phänomen, das sich durch litosphärisches Material, dessen Temperatur für mindestens zwei aufeinanderfolgende Jahre unter 0°C ist, definiert. Permafrost tritt in hohen Breitengraden und in großen Höhen in Gebirgszügen auf. In den Schweizer Alpen kann Permafrost oberhalb von etwa 2400 m ü. M. erwartet werden, abhängig von den Energiebilanz an der Oberfläche, die vor allem von der Höhenlage und der Ausrichtung abhängt, sowie von den Wärmeübertragungsprozessen im Boden selbst.

Der Schwerpunkt dieser Arbeit liegt auf den Wärmeübertragungsprozessen im Boden. In Gebirgen befinden sich an der Oberfläche oft grosse Blöcke, in deren Zwischenräumen sich Luft befindet. Solange sich die Luft nicht bewegt, ist sie aufgrund der geringen Wärmeleitfähigkeit isolierend. Sobald sich die Luft bewegt, hat sie das Potenzial, Wärme konvektiv zu übertragen, d. h. durch die Bewegung der warmen (kalten) Luft wird das Medium wärmer (kälter). Überträgt man dies nun auf die Blockschicht im Gebirge, so lässt sich der folgende Jahreszyklus beobachten: Im Sommer ist die Außenlufttemperatur höher als die Temperatur der Luft zwischen den Blöcken. Die thermische Schichtung ist somit stabil, da sich die wärmere, leichtere Luft oben befindet. Die Wärmeübertragung erfolgt durch Wärmeleitung, und die Luft hat ihre isolierende Funktion inne. Im Winter ändert sich die Situation. Die Temperatur der Außenluft sinkt, so dass sich kalte, schwere Luft über der relativ warmen Luft zwischen den Blöcken befindet. Diese Schichtung ist instabil und die kalte, schwere Außenluft beginnt, die Blöcke zu fluten. Dies führt zu einer verstärkten Wärmeübertragung durch Konvektion während der Wintermonate, was im Jahresverlauf zu einer Nettokühlung führt. In der Literatur wird diese jahreszeitliche Asymmetrie als "thermischer Halbleitereffekt" bezeichnet.

Dieser Effekt ist gut bekannt und wurde in verschiedenen Zusammenhängen beobachtet. Der Beitrag dieser Arbeit zu einem besseren Verständnis des Einflusses der Luftkonvektion im Boden wird durch numerische Modellierung erzielt. Obwohl die numerische Modellierung im Bereich der Permafrostforschung weit verbreitet ist, wurde die explizite Modellierung der Luftkonvektion bisher nur im Permafrostingenieurwesen durchgeführt. Dort wird zerkleinertes Gestein, das Luftkonvektion zulässt, verwendet, um die Bodentemperaturen unter Infrastrukturbauten niedrig zu halten. Bei der Modellierung von Permafrostlandformen wurde die konvektive Wärmeübertragung normalerweise entweder vernachlässigt oder stark parametrisiert. Hier wird ein physikalisch basierter Modellansatz vorgestellt, der die grobblockige Schicht als ein poröses Medium beschreibt und für Wärmeübertragung durch Wärmeleitung und Konvektion löst, wobei die Luftströmung durch das Darcy-Gesetz beschrieben wird und eine Boussinesq-Approximation verwendet wird, um die auftriebsbedingten freien Konvektionseffekte zu berücksichtigen. Der Modellansatz wurde spezifisch verfeinert und an verschiedene Landformen angepasst, um den Einfluss der Luftkonvektion im Boden auf das thermische Regime des Permafrosts zu bewerten.

Das Modell wurde an zwei typische Landformen des Gebirgspermafrostes angewandt: Blockhalden und Blockgletscher. Zwei verschiedene Typen von Blockhalden wurden modelliert. Zum einen wurde eine Blockhalde innerhalb des Gürtels des alpinen Permafrosts modelliert. Es konnte nachgebildet werden, dass Konvektion zu einem erheblichen Temperaturunterschied zwischen dem oberen und dem unteren Teil einer Blockhalde führen kann, was die typische Permafrostverteilung in einer Blockhalde erklären kann. Der kalte, eisreiche Teil befindet sich an der Basis, während der obere Teil oft frei von Permafrost ist - was der intuitiven Erwartung einer Höhenabhängigkeit der Permafrostverbreitung widerspricht. Eine weitere Modellierung wurde an einer niedrig gelegenen Blockhalde durchgeführt, wo die Jahresluftmitteltemperatur positiv ist und daher Permafrost nicht erwartet wird, aber sporadisch beobachtet wurde. Die Reproduktion des in der Vergangenheit aufgetretenen Permafrostvorkommens war möglich, wenn die Luftkonvektion im Boden

berücksichtigt wurde, was bestätigt, dass dies der Prozess ist, der für die ungewöhnlich kalten Bodentemperaturen in niedrigeren Höhenlagen ausschlaggebend ist. Darüber hinaus konnten auch die Aggregation und das Schmelzen von Bodeneis erfolgreich reproduziert werden.

Blockgletscher, die wohl bekannteste Permafrostlandform, waren die Grundlage einer weiteren numerischen Modellierung. Während in ihrem Kern die Hohlräume normalerweise mit Eis gesättigt oder gar übersättigt sind, besteht die darüber liegende Auftauschicht oft aus großen Blöcken, deren Zwischenräume mit Luft gefüllt sind. Auch hier zeigt die konvektive Luftströmung vergleichbare Effekte, wenn auch nicht in demselben räumlich Ausmass. Die Auswirkung der Luftkonvektion in der aktiven Schicht eines Blockgletschers auf die Permafrosttemperaturen wurde modelliert und deren Einfluss hat sich als signifikant erwiesen. Die Konvektion konnte mit dem Konzept der Ralyeigh-Zahl beschrieben werden, einer dimensionslosen Zahl, die aus der Strömungsmechanik bekannt ist. Der Temperaturgradient innerhalb der aktiven Schicht und die Permeabilität der Auftauschicht wurden als die wichtigsten Parameter identifiziert, die die Luftkonvektion im Boden und ihren Einfluss auf das thermische Regime des Permafrostes steuern. Die Permeabilität ist der Parameter, der beschreibt, wie gut die Poren miteinander verbunden sind und wie schnell ein Fluid durch ein poröses Medium fliessen kann. Verlässliche Permeabilitätsmessungen sind nicht verfügbar, dieser Parameter weist daher die höchste Sensitivität auf.

Über das Ganze gesehen, beschreibt diese Arbeit einen konsistenten Ansatz zur Modellierung der Luftkonvektion im porösen Boden und deren Einfluss auf die Permafrosttemperaturen. Obwohl die Luftkonvektion im Boden seit langem beobachtet und beschrieben wird, ist die Darstellung in einem zweidimensionalen numerischen Modell auf der Skala einer ganzen Landform, unter Verwendung von Messdaten als Randbedingung und als Validierung, neu. Der Ansatz bestätigt die meisten der zuvor gemachten Beobachtungen, erlaubt aber eine erweiterte qualitative Beschreibung der Luftkonvektion im Boden sowie den Versuch einer absoluten Quantifizierung des Einflusses der Luftkonvektion auf die Permafrosttemperaturen. Darüber hinaus ermöglicht die Verwendung eines gleichungsbasierten, numerischen Modells verschiedene Verbindungen zu anderen Wissenschaftszweigen, wie dem Ingenieurwesen oder der Strömungsmechanik, was neue und interessante Interpretationen der Wärmeübertragungsprozesse im Gebirgspermafrost ermöglicht.

Contents

1 Introduction

1.1 Context

This thesis presents a numerical modelling approach developed to better understand the importance, influence and implications of convective heat transfer through air flow in porous mountain permafrost. One may ask, why this specific process is of interest – the following section frames the motivations and the resulting research questions.

People living in or close to the mountains have to deal with mountain permafrost. The main issues linked to mountain permafrost are the terrain stability, whether it be to construct infrastructure or as a natural hazard threatening people and their infrastructure. Furthermore, the hydrological cycle is also affected by permafrost, whereby in some regions the contribution of mountain permafrost to the hydrological cycle is estimated to be significant (Jones et al., 2018). Within the background of a changing climate, the ground thermal regime of mountain permafrost is warming and undergoing substantial changes (Biskaborn et al., 2019; Etzelmüller et al., 2020; Harris et al., 2003). Understanding the processes governing the thermal regime of mountain permafrost is thus a precondition to understand and interpret its past development as well as to make statements and projections about the future development. It is generally agreed that heat conduction is the most important heat transfer mode governing the ground thermal regime in permafrost, but other modes of heat transfer are also of importance (Kane et al., 2001). In mountainous landscapes, the ground is often covered with coarse blocks, where convective heat transfer has a significant influence on the ground temperatures. Etzelmüller (2013) concludes in a publication on advances in permafrost research that one of the main research topics to be addressed in future is the quantification and understanding of spatial heterogeneities of thermal processes in coarse surface material - Haeberli et al. (2011) and Harris et al. (2009) come to the same conclusion.

Coarse surface material hosts a lot of air, which is free to move. Heat is transferred through the circulation of air – convection takes place. Convective heat transfer through air is known to have a cooling effect on ground temperatures (Harris and Pedersen, 1998). A brief and simple explanation is that convection due to density differences takes only place when the heavier (colder) air is on top of lighter (warmer) air and therefore convection is most active when the outdoor air is colder than the air within the coarse surface sediment. The enhanced heat transfer through convection takes only place during the cooling phase (Balch, 1900; Guodong et al., 2007). This is most prominent in isolated patches of low altitude permafrost (e.g. Delaloye et al., 2003).

The convective cooling has been recognised early on by Balch (1900) and its effect on the ground thermal regime of alpine permafrost has so far mainly been studied with field-based empirical approaches. Indirect measurements of the convection process, often relying on interpretations of temperature differences and gradients as well as visual observations of cold or warm air outflows, allow for a good conceptual model of the convection process (amongst others: Delaloye et al., 2003; Hanson and Hoelzle, 2004; Morard et al., 2010). Direct measurements, either through anemometers (Morard and Delaloye, 2008) or through effective thermal conductivity sensors (Panz, 2008), give further valuable insights but proved to be rather unreliable in the harsh alpine environment for a more long-term process monitoring. In this regard, an ongoing attempt of the innosuisse project PERMA-XT (Amschwand et al., 2021) may achieve more robust measurements in future.

To overcome the uncertainty of these measurements and to refine the conceptual model of ground convection in the coarse blocky permafrost as well as to be able to isolate the convection process to quantify its influence on the ground thermal regime be it qualitatively or quantitatively, the development of a physics-based model is an obvious choice. Physics-based models are developed

based on physical equations describing the observed processes. As these equations often cannot be solved analytically, a numerical solution is required and therefore the well-known term numerical modelling is often used. Numerical modelling of ground temperature in permafrost is already performed on different spatial, temporal and complexity scales but convection as a relevant process is normally either neglected or parametrised. On rock glaciers, heat-source or sink terms (Scherler et al., 2014) or a parametrization through a ventilation parameter (Pruessner et al., 2018) have been applied, just to mention a few. In talus slopes, even less has been done – Tanaka et al. (2000) presents an interesting approach with a prescribed stream function. On a more general term, either from a process-oriented modelling approach (Gruber and Hoelzle, 2008; Marmy et al., 2016; Pruessner et al., 2018; Scherler et al., 2013) or from a permafrost mapping perspective (Boeckli et al., 2012), the need of a better understanding of the processes governing the ground thermal regime beneath a coarse blocky surface has been formulated. An explicit approach in modelling the convective air flow within periglacial landforms on a real field scale was so far missing.

To fill this gap, a look at the methods and developments of cold regions engineering helps. Constructions in the Arctic are exposed to the risk of thawing permafrost. Measures have to be taken to avoid heat transfer from the construction to the ground which could lead to degradation of the permafrost below and therefore a terrain instability damaging the construction. Engineering solutions of many kinds have been developed to avoid this. Especially for transport infrastructure, like roads and railways through permafrost regions, embankments made out of coarse-grained blocks have been developed to artificially create ground convection. This leads to passive cooling of the underlying permafrost and protects the infrastructure from damage. Methods to model such structures and their passive cooling effect have been developed and successfully applied (e.g. Arenson and Sego, 2006; Goering and Kumar, 1996; Guodong et al., 2007, see section 3.3).

1.2 Objectives

This thesis now presents an explicit physics-based numerical modelling approach to account for convective heat transfer in the coarse blocky permafrost found in an alpine setting. This is achieved by adapting and refining modelling concepts that were developed and approved in cold regions engineering to real-scale field sites for transient long-term modelling. Measured data is used for the model forcing and validation. The model approach is adjusted to different field sites with different land forms – an alpine talus slope (paper I), rock glaciers (paper II) and a low-altitude talus slope (paper III).

The central thread through all the publications and therefore the main question of this thesis is, if and to what extent air convection in the ground influences the ground thermal regime of the aforementioned landforms?

This leads to the additional questions of how ground convection manifests itself in terms of intensity, seasonality and characteristics and whether a numerical model approach can confirm the conceptual models developed from empirical observations.

1.3 Structure of the thesis

This thesis is cumulative and paper-based. The three publications are embedded in an outline text which consists of the following parts:

- An introduction, explaining the context, the aim and the structure of this thesis.
- A section on permafrost, where important concepts and notions are introduced and explained with a focus on the topics relevant to this thesis

- A model background, to understand where the modelling approach comes from, and how it has been used and evolved throughout this thesis
- An overview of the field sites, to geographically classify the thesis
- The main research work, divided into three paper publications:

  - Paper I (published in The Cryosphere) dealing with an alpine talus slope and the title: "Numerical modelling of convective heat transport by air flow in permafrost talus slopes"
  - Paper II (published in Frontiers in Earth Science) modelling the convective heat transfer in the active layer of rock glaciers with the title: "Air Convection in the Active Layer of Rock Glaciers"
  - Paper III (in prep., submission to Permafrost and Periglacial Processes foreseen) applies and refines the model on a low altitude cold talus slope with the title: "Modelling the link between air convection and the formation of short-term permafrost in low altitude cold talus slopes"

- An unpublished work section, presenting briefly three pre-/pilot studies which were not part of the three papers but which may still be of interest, and address some open questions of paper I-III
- A discussion section, where the main concepts present in all papers are summarised and where their relevance is discussed in a broader context followed by a conclusion
- At the end, the data availability statement, references, conference contributions related to this thesis, acknowledgements and a CV are included

1.4 Project MODAIRCAP

This thesis was realised with the support of the Swiss National Science Foundation SNSF through a 4-year project funding. The project was called *Modelling of air circulation and energy fluxes in the coarse debris layer of high Alpine permafrost sites* (short: MODAIRCAP, project number no. 169499) and was completed in May 2021. The proposal for this project was partly based on my master thesis, which explored the possibilities of convection modelling in permafrost and its influence. The financing then allowed a further development and application of the model approach and led to advances in the understanding of the convective heat flux caused by air flow in porous permafrost – the topic of this doctoral thesis.

The objectives of the research proposal were formulated as follows:

i. Adapt an existing engineering software that has already been tested for application in mountain permafrost for real field cases in the Swiss Alps
ii. Quantify the amount of cooling due to convective air circulation within the coarse blocky surface layer (in addition to enhanced thermal insulation and in comparison to all other parts of the energy balance)
iii. Validate the simulation results by ground surface temperature and borehole temperature data at two well-studied and well-equipped field sites, talus slope Lapires and rock glacier Murtèl.

2 Permafrost

2.1 What and where

Permafrost is defined as ground (soil or rock and included ice and organic material) that remains at or below 0°C for at least two consecutive years (van Everdingen, 1998). The definition comprises exclusively temperature as a parameter, the presence of water, frozen or unfrozen, is not a precondition. Permafrost is found in high latitudes (Arctic and Sub-Arctic) and mountain ranges at higher altitudes. The latter is called alpine or mountain permafrost (Pewe, 1983). This thesis deals with thermal processes that are of high significance for mountain permafrost although under certain conditions this can also be significant for arctic permafrost, or porous soils in general.

Mountain permafrost can be found in mountain ranges where the mean annual air temperature (MAAT) is below 0°C (Pewe, 1983). During the summer, the uppermost meters of the soil thaw. The thawed layer is called the active layer and the thaw depth corresponding to the vertical extent of this layer is called active layer thickness (van Everdingen, 1998). During winter, the whole active layer is again in the sub-zero temperature range. Even below the active layer, the permafrost body is subjected to temperature variations, whereby the annual temperature signal is almost fully damped at the "depth of zero annual amplitude" (van Everdingen, 1998). Typical active layer thicknesses in the Swiss Alps range from 2 to 5 m and the depth of zero annual amplitude is reached at around 20 m (PERMOS, 2019).

Permafrost conditions in the Swiss Alps can be found roughly above 2400 m a.s.l. on north-facing slopes (FOEN, 2005). Permafrost occupies barren terrain, (bed-)rock walls and debris-covered slopes. Characteristic landforms bearing ground ice are rock glaciers and talus slopes, often showing a coarse blocky substratum at the surface. Rock glaciers are used as an indicator of permafrost (Barsch, 1996) and are composed of blocks up to ten meters diameter, the block size may vary depending on the site and lithology, and the voids filled or supersaturated with ice (Arenson et al., 2002). The term talus slope, as used in this thesis, describes the accumulation of coarse loose debris at the foot of a rock wall, resulting in a slope covered with scree. Hence, in some publications, the term scree slope is used. Talus slopes in permafrost areas might show a considerable amount of ground ice in their lower part, whereby the upper part is generally ice (and often permafrost) free (Lambiel and Pieracci, 2008). Alpine talus slopes and rock glaciers are the subjects of paper I and II respectively.

Moreover, in some places, isolated patches of permafrost are observed. They are located at a lower elevation, sometimes far below the tree line. The mean annual air temperature exceeds 0°C and can reach up to 5 °C (Morard et al., 2010). The landforms associated with these isolated patches of permafrost show highly permeable substratum, mostly in the form of talus slopes (Delaloye et al., 2003; Gude et al., 2003; Kneisel et al., 2000; Morard et al., 2010; Sawada et al., 2003; Zacharda et al., 2007). The processes governing the ground thermal regime at low elevation cold talus slopes are the topic of paper III.

2.2 Heat transfer

2.2.1 Processes

The main heat transfer mechanism in permafrost soils is heat conduction (Kane et al., 2001), as described by (Fourier, 1822). Depending on soil and environmental properties, non-conductive heat transfer mechanisms gain in importance (Kane et al., 2001). Heat can be transferred through radiation, meaning the radiative heat transfer, and through convection, meaning that the heat transfer takes place through a moving liquid within the ground.

Radiation is not mentioned by Kane et al. (2001) as a possible non-conductive heat transfer mechanism in permafrost. Later, Scherler et al. (2014) identify the radiative heat flux as a part of the energy balance in the active layer of the Murtèl glacier and Lebeau and Konrad (2016) showed through numerical modelling in the specific context of coarse-grained substrate, that radiation is, compared to convection, of minor importance. Still, radiation within the porous medium has the potential to influence the effective thermal conductivity.

2.2.2   Forced and free convection

Two types of convection can be distinguished, forced and free convection. Forced convection takes place when the liquid is moved with an external force. Free convection, also called natural convection, takes place within the fluid without any external force and is the result of density differences within the fluid, which might be induced by temperature differences. The onset and thus the existence of free convection is linked to the Rayleigh number (referring to the Rayleigh number for convective flow in porous media, or the Rayleigh-Darcy number), which is a dimensionless number from fluid dynamics (Nield and Bejan, 2017). When the Rayleigh number reaches a critical threshold, the critical Rayleigh number, the onset of convection can be observed. The Rayleigh number is described in section 2.2.3 and discussed in paper II and section 7.2.

2.2.3   Rayleigh number

The Rayleigh number Ra describes the potential and the strength of free convection in a porous media, using the ratio of buoyancy to viscous forces (Kane et al., 2001) and is defined as follows (Nield and Bejan, 2017):

$$Ra = \frac{\rho^2 C_a \, g \, \beta \, \kappa \, H \, \Delta T}{\mu \, k} \qquad (1)$$

with ρ the density, C_a the specific heat capacity of air, g the gravitational acceleration, β the coefficient of thermal expansion, κ the permeability, H the vertical dimension of the active layer, ΔT the temperature difference within the active layer, μ the dynamic viscosity of the fluid and k the thermal conductivity.

Ra describes the strength and the onset of free convection at a critical threshold, called the critical Rayleigh number Ra_{crit}. Theoretically, depending on the boundary conditions, different values from 3 to $4\pi^2$ can be derived for Ra_{crit}. In practice, the value of $4\pi^2$ (~40) has prevailed (Goering and Kumar, 1996; Guodong et al., 2007; Juliussen and Humlum, 2008; Lebeau and Konrad, 2009; Pham et al., 2008; Wagner et al., 2019). Apart from the threshold value of Ra_{crit}, Ra is very useful parameter to understand the efficiency of convection and the influence of various parameters.

2.3 Convection in permafrost

2.3.1   Free convection of air

Free convection of air is the focus of this thesis. In a flat porous ground, free convection can be observed in form of vertical convection cells, also referred to as Rayleigh-Bénard circulation. In porous media modelling, the occurrence and especially the onset of vertical convection cells is treated as the Horton–Rogers–Lapwood problem (Horton and Rogers, 1945; Lapwood, 1948; Nield and Bejan, 2017). In permafrost science, convection is known since long time to influence the ground thermal regime. The vertical exchange of air is often referred to as the Balch effect (Balch, 1900). Convection takes also place on inclined terrain, where depending on boundary conditions and slope angle, the characteristics of the convection cells change (Bories and Combarnous, 1973; Guodong et al., 2007). Lateral convection along a slope, often also referred to as the chimney effect (Wakonigg, 1996) or as advection, leads to a heat transfer along the slope resulting in a temperature difference

between the upper and lower part of the slope. When only a single cell dominates the convective heat transfer, advection is sometimes also categorised as a form of forced convection driven by the slope, with the onset of free convection characterised by multiple convection cells at a critical threshold (Nield and Bejan, 2017). The occurrence of convection in the ground is not restricted to permafrost (Levintal et al., 2017; Weisbrod et al., 2009), but is well studied in this context (overview in section 2.3.3)

2.3.2 Other forms of convection

Other possible forms of convection are not explicitly treated in this thesis but discussed in the different papers. Empirical data indicate that forced air convection is less effective than vertical convection in the active layer of a rock glacier (Hanson and Hoelzle, 2004). It is important to note, that free convection and the related cooling effect is most pronounced during the winter when the soil is (mostly) decoupled from the atmospheric wind forcing due to the presence of a snow cover. Furthermore, a numerical modelling experiment conducted within this thesis showed that the free convective flow prevails over the influence of wind forcing (section 6.3). Still, there are also modelling and empirical studies that reveal the influence of atmospheric wind during the snow-free period (Pham et al., 2008, 2015; Wagner et al., 2019), respectively that are describing forced convection through atmospheric wind as the driving factor of near-surface ventilation (Pruessner et al., 2018). With more reliable validation data, future studies may treat this aspect more rigorously.

Free convection of water is possible in porous soils but of minor importance in alpine permafrost. The ground is normally unsaturated and during winter, when free convection is likely to take place, temperatures are far below the freezing point. Furthermore, and this applies also to the forced convection of water, coarse blocky and thus highly permeable grounds have a very low retention capacity and the water runoff is often immediate. Forced convection of water occurs through snow melt water, precipitation and groundwater flow. Kane et al. (2001) estimate that the influence of these sporadic events is of minor importance. Moore et al. (2011) showed that in rock clefts in an alpine setting that the free convective flux of air prevails over the convective flux of melt water. Forced convective heat transfer due to ground water fluxes (Sawada et al., 2003) and intra rock glacier taliks (Luethi et al., 2017) influence the ground temperatures on specific sites.

Typical situations of convective heat transfer in permafrost can thus be summarised as follows:

i. Free convection of air takes place in the ground when permeability is high enough and the critical Rayleigh number is reached – and this throughout the year, as air is always present
ii. Forced convection of air is possible through an atmospheric wind forcing at the surface, also called wind pumping
iii. Free convection of water is theoretically possible within a highly saturated permeable ground when the critical Rayleigh number is reached
iv. Forced convection of water, with the possible processes of infiltrating meltwater, infiltration of precipitation or through groundwater flux

2.3.3 Relevance of air convection for permafrost

Air convection in coarse-grained sediments arguably plays the most important role in isolated permafrost occurrences, where it is often the main process explaining the exceptionally cold temperatures. Described in the Swiss Alps (Kneisel et al., 2000; Morard et al., 2010; Schwindt, 2013), the Swiss Jura (Delaloye et al., 2003), lower mountain ranges of Central Europe (Gude et al., 2003; Zacharda et al., 2005, 2007), the Carpathians (Popescu et al., 2017), Japan (Sawada et al., 2003; Tanaka et al., 2000), the US (Millar et al., 2016; Schorghofer et al., 2017) and many more places, often also in non-scientific literature, this isolated patches of permafrost are often of particular

interest because they are usually characterised by a peculiar flora and fauna and their microclimates arouse curiosity. The cold microclimates typically lead to the occurrence of dwarf trees, relict insect species and lichens (Lendemer et al., 2009; Zacharda et al., 2005).

Furthermore, in mountain permafrost convective air circulation is known to have a significant influence on the ground thermal regime of talus slopes (Delaloye and Lambiel, 2005; Lambiel and Pieracci, 2008; Phillips et al., 2009; Scapozza et al., 2015). The thermal regime of rock glaciers is as well sensitive to convective heat transfer (Hanson and Hoelzle, 2004; Herz, 2006; Hoelzle et al., 1999; Panz, 2008; Pruessner et al., 2018; Scherler et al., 2014). In addition to landform-specific investigations, it was also shown that ground surface and subsurface temperatures are lower if the substrate is composed of coarse blocks (Gubler et al., 2011; Harris and Pedersen, 1998; Hoelzle et al., 1999; Schneider et al., 2012). Finally, in studies on permafrost mapping the importance of the spatial distribution of the ground cover is mentioned. Especially coarse-grained surfaces lead to a thermal offset and thus to uncertainties in permafrost mapping (Boeckli et al., 2012; Kenner et al., 2019a; Westermann et al., 2013).

Beyond permafrost, air convection is also known to affect the ground thermal regime. Ice caves are known to have a thermal regime which at times is highly influenced by convection (Edenborn et al., 2012; Faimon and Lang, 2013; Luetscher and Jeannin, 2004; Meyer et al., 2016; Morard, 2011), and where a chimney effect, analogous to the talus slopes, can develop. Studies from agricultural science (Levintal et al., 2017; Weisbrod et al., 2009) examined the gas exchange in the soil, driven by free convection and identified a significant potential.

2.3.4 Measuring convection

Explicit measurements of the convection in coarse-grained permafrost substratum with a quantitative character, going beyond the interpretation of temperature measurements, are still rare and difficult to obtain. Qualitative observations of melt holes or cold air outflows are manifold and are an illustrative description of the convection process (e.g. Morard, 2011). Popescu et al. (2017) conducted smoke experiments to qualitatively track the flow paths. Quantitatively, measurements were performed with anemometers (Morard, 2011; Morard and Delaloye, 2008) or with wind sensors that detect changes in effective thermal conductivity linked to convective air flow (Panz, 2008). No long-term monitoring of airflow or convective heat flux in the ground was yet documented in harsh alpine environment, especially because snow prevented a reliable functioning of the measurement devices for several annual cycles. Still, these measurements are of benefit. First, they describe convective cycles on shorter (compared to the temporal scale in this thesis) periods, and they give an order of magnitude of the observed air flow velocity within the substratum – they will be further discussed in section 7.3.2.

An ongoing attempt of direct measurements of convection-driven air flow in a cavity in the active layer of the rock glacier Murtèl (PERMA-XT project; Amschwand et al., 2021; Scherler et al., 2018) delivers promising results. Thermal anemometers for low wind speed and ultrasonic wind field measurements have the potential to provide a novel dataset for a more profound understanding of the convective heat flux in the ground (Amschwand et al., 2021). Unfortunately, calibration issues currently still restrict the usability of the data. They may be resolved in near-future.

3 Model

3.1 Temperature modelling in permafrost

In permafrost science the ground temperature is the most important parameter – it solely decides if permafrost exists or not. Therefore, the modelling of ground temperatures in permafrost regions is of interest. Two main motivations can be determined regarding the modelling of permafrost temperatures. The first is to represent the spatial distribution of permafrost. Amongst others, for the Swiss Alps, this has been done based on empirical-statistical models (Boeckli et al., 2012; Deluigi et al., 2017; Hoelzle, 1996; Keller, 1992; Kenner et al., 2019a) or physically-based approaches (Haberkorn et al., 2017; Hoelzle et al., 2001; Noetzli and Gruber, 2009; Stocker-Mittaz et al., 2002).

The second group of thermal permafrost modelling studies, and that is also where this work is to be situated, applies modelling as a tool to better understand a specific process, or a specific site (Cicoira et al., 2019; Gruber and Hoelzle, 2008; Luethi et al., 2017; Pruessner et al., 2018, 2021; Scherler et al., 2014; Tanaka et al., 2000), sometimes with projections for the future evolution (Marmy et al., 2016; Scherler et al., 2013). These usually physically-based models are applied by expressing the processes governing the ground thermal regime as (differential) equations which are subsequently solved. Different tools and methods on different spatial scales and with different complexity are applied. Common to all these models are in general the heat conduction equation, which solves for heat conduction as described by Fourier (1822).

3.2 Convection modelling in permafrost

In the arctic, the ground is often not permeable enough to allow for air convection, which can be neglected accordingly (Kane et al., 2001), whereas in an alpine setting the ground is often highly permeable and convective processes are an important part of the energy balance (Scherler et al., 2014). Approaches to integrate convection into a thermal numerical model are sparse and not of explicit nature. Tanaka et al. (2000) present an approach with a defined stream function in a talus slope in Korea and are able to represent the seasonally reversing circulation (called "convective overturning") in their model approach. In an alpine context, Gruber and Hoelzle (2008) propose an approach, where the cooling effect is represented as an effective thermal conductivity. Scherler et al. (2014) then developed a heat sink/source term to account for the winter cooling effect at the Murtèl rock glacier. During winter, a heat sink is active whereas during summer a heat source compensates for the air convection. Other studies explore the effect of advected water in the permafrost, either in rock clefts (Hasler et al., 2011) or as a talik formation in a rock glacier (Luethi et al., 2017). Later, Pruessner et al. (2018) proposes an alternative approach to a heat sink/source term (Scherler et al., 2014) to account for the winter cooling: A ventilation factor is introduced and tuned to the wind speed at the Corvatsch/Murtèl site, even though free and not forced convection is the prevailing thermal process in the active layer (Hanson and Hoelzle, 2004).

3.3 Modelling in cold regions engineering

In contrast to permafrost research in geosciences, the modelling of convection has extensively been performed in the domain of cold regions engineering. It has been found that crushed rocks do have an efficient passive cooling capacity, which helps to prevent the melting of the underlying permafrost and by this favour a sustainable construction of infrastructure in arctic regions. The first modelling approaches of this effect were performed by Goering and Kumar (1996), which can be seen as the foundation stone of modelling of passive cooling capacities in road embankments. This has then been developed further in the US and Canada (amongst others: Arenson and Sego, 2006; Lebeau and Konrad, 2009, 2016; Darrow and Jensen, 2016) and also in Tibet, where the Chinese authorities constructed the Tibetan Highway and the Tibetan Railway. A plethora of modelling studies was

published on the passive cooling of railway and road stretches in the Tibetan plateau (e.g. Guodong et al., 2007; Sun et al., 2010; Zhang et al., 2009). Further, the passive cooling capacities of crushed rocks are also used to keep mine waste piles frozen and to avoid leaking (Arenson et al., 2007; Pham et al., 2008, 2015). In addition to this extensive modelling work, laboratory studies to determine the properties of crushed rocks were conducted (Côté et al., 2011; Rieksts et al., 2020; Zhang et al., 2013).

The research from engineering sciences proved that an approach with a heat conduction equation combined with a Darcy approach adopting the Boussinesq approximation for the air flow leads to stable and satisfying results. Shortcomings can be found in the assumption of incompressible gases (Boussinesq approximation) (Lebeau and Konrad, 2009), neglecting drag terms (such as the Forchheimer term to account for Non-Darcy effects, Lebeau and Konrad, 2016) and radiation within the porous media (Lebeau and Konrad, 2016) as well as the assumption of a local thermal equilibrium (LTE) (Heinze, 2020). These shortcomings are discussed in paper II.

The transition to a real-scale field site nevertheless entails some challenges. Engineering studies often either use a steady-state modelling approach (Lebeau and Konrad, 2016), neglecting transient effects, or use harmonic functions to prescribe the atmospheric forcing at the upper boundary (Goering and Kumar, 1996; Guodong et al., 2007; Lebeau and Konrad, 2016). Appling real, measured data as atmospheric boundary (in the case of the presented papers either ground surface or borehole temperatures) instead of a harmonic function revealed to be challenging. The degree of non-linearity in the model increases considerably and it is thus harder to get a stable, converging model setup.

3.4 Model description

3.4.1 Equations

The general model approach is the same for papers I, II, and III. The governing equations are described in Nield and Bejan (2017), COMSOL (2018b, 2018c) and GeoStudio (2013c, 2013b, 2013a) as well as in each of the papers. The coupled set of differential equations that describe the conductive and convective heat flow in the porous medium are listed below. Eqs. 2 and 3 govern hereby the heat transfer by conduction and convection, where q is the heat flux, Q is the storage term, q_0 the boundary flux, k the (effective) thermal conductivity, C_p the (effective) volumetric heat capacity, ρ the density, V the velocity, T the temperature and t the time.

$$\rho C_p \frac{\partial T}{\partial t} + \rho C_p V \nabla T + \nabla q = Q + q_0 \qquad (2)$$

$$q = -k \nabla T \qquad (3)$$

Airflow in the porous medium is described in eqs. 4 and 5, where Φ is the porosity, Q_m the boundary flux, κ the permeability, μ the dynamic viscosity, g the gravitational acceleration and p the pressure.

$$\frac{\partial}{\partial t}(\phi \rho) + \nabla(\rho V) = Q_m \qquad (4)$$

$$V = -\frac{\kappa}{\mu}(\nabla p - \rho g) \qquad (5)$$

3.4.2 Model environment

The modelling environment changes from paper I to paper II and III. In paper I the modelling environment was GeoStudio2012 from GEO-SLOPE International Ltd. (now part of Seequent) with the relative packages TEMP/W for temperature modelling (GeoStudio, 2013c), SEEP/W for seepage

modelling (GeoStudio, 2013b) and AIR/W (GeoStudio, 2013a) to integrate the airflow into the seepage modelling. GeoStudio2012 allows for a direct coupling while solving all three packages. GeoStudio is a geotechnical engineering software that has been used in the context of cold regions engineering modelling (Arenson and Sego, 2006; Darrow and Jensen, 2016) and also in permafrost research (Koenig et al., 2021; Mottaghy and Rath, 2006). GeoStudio2012 TEMP/W, SEEP/W and AIR/W are relatively slim and easy to use but are somewhat limited in their computational performance when using them on real scale field sites and applications, where a dense mesh (element size in the order of centimetres) is of importance to represent the prevailing processes. Furthermore, the equations cannot be accessed directly and custom modifications and work-around for specific problematics are not easily achieved, as the implementation of an add-in C+ is quite laborious. Another weak point is the formulation of the AIR/W package. Even though it relies on a Darcy approach (see paper I), the equation is formulated with an air conductivity [m s^{-1}] (analogous to a hydraulic conductivity) and not with an air permeability [m^2], which is the standard approach and parameter in the literature to describe flow in porous media.

For papers II and III, the COMSOL Multiphysics (COMSOL, 2018a) environment with the additional modules of heat transfer and subsurface flow was used in version 5.3 for paper II and 5.6 for paper III. COMSOL Multiphysics is a general FEM modelling software environment to integrate any kind of modelling tasks involving partial differential equations with a very broad application spectrum and a big user group. COMSOL proved to be more stable and much faster than GeoStudio2012, allowing for more complex model setups. Furthermore, COMSOL is directly equation-based, meaning that the equations are accessible and can easily be customised and reformulated to apply them for a specific task. COMSOL has also been used in cold regions engineering (Pham et al., 2008; Wang et al., 2021) and permafrost science (Hasler et al., 2011; Noetzli and Gruber, 2009).

3.4.3   Model evolution
The model evolved with the site-specific characteristics and questions, even though the model approach is comparable for all three papers. In this section, the main advances, respectively developments in-between the different research papers are highlighted (cf Table 1). The respective model approach is always thoroughly described in the corresponding section of each paper.

From paper I to paper II the changes in the model approach are considerable. The shift from GeoStudio to COMSOL as a modelling environment can be seen as a major advance. This allows for a more complex model set-up, longer simulating periods and customised solutions. The changes lie in the boundary conditions, where the thermal boundary is now a first-order Dirichlet condition prescribing the upper temperature boundary as a borehole temperature value and not a measured GST value as in paper I. The lower thermal boundary is of Neumann type, prescribing the geothermal heat flux and not a constant temperature measured in a borehole. Furthermore, the atmospheric boundary condition at the surface is prescribed as an altitude dependent zero-pressure boundary, whereas in paper I an air domain had to be integrated, adding a lot of uncertainty and computational effort. COMSOL allowed also for the material properties to vary with temperature (air, water). Latent heat was additionally integrated, even though damping of the latent heat was needed to obtain numerically stable results (details see paper II). The new formulation allowed also for the integration of permeability instead of air conductivity as material property, allowing for comparison with published literature. Easily applicable parameter switches allowed in COMSOL to model for a range of parameters and geometries to better understand the model sensitivities.

From paper II to paper III, the model was developed further to respond to the special characteristics of a low elevation cold talus slope. The main advances are the integration of geophysical data to represent the spatial heterogeneity of the subsurface in the talus slope. The permeability was linked

to the electrical resistivity of the ground, allowing for a heterogeneous talus. At the upper thermal boundary, the condition was also refined. Whereas in paper II both of the two rock glaciers studied were modelled with a homogeneous surface temperature from the uppermost thermistor of the on-site boreholes, a new approach was chosen for paper III. All available GST measurements at the surface were integrated. For each time step, a linear gradient between the measured temperatures was calculated. The forcing temperature at the surface is consequently different at each node. Furthermore, a water-bearing layer was added below the talus, where the seasonal and at times perennial aggregation of an ice layer is modelled, fully integrating latent heat effects with an increased heat capacity of water around the freezing point. To be able to accurately simulate the measured temperature data a so-called "permeability switch" was implemented, damping the permeability within the talus when the outside temperature is higher than the mean interior talus temperature to consider possible seasonal preferential flow paths.

Table 1 Overview of the evolution of the model properties

	Paper I	**Paper II**	**Paper III**
Environment	GeoStudio2012	COMSOL 5.3	COMSOL 5.6
Dimensions	2D	2D	2D
Model domain extent (x,y)	170 m, 110 m	150 m, 180 m	150 m, 130 m
Initial conditions	Constant initial and 7 yr mean forcing temperature spin up	Two-step: Steady-state and 30 yr median forcing temperature spin up	Two-step: Steady-state and 10 yr first-year forcing temperature spin up
Thermal upper boundary condition	Temperature from one GST logger	Temperature from the uppermost thermistor of one borehole	Temperature gradients in between different GST loggers along the slope profile
Thermal lower boundary condition	Constant borehole temperature (Dirichlet)	Geothermal heat flux (Neumann)	Geothermal heat flux (Neumann)
Upper pressure boundary condition	Additional domain of viscous air to mimic atmospheric exchange	Altitude dependent zero pressure head	Altitude dependent zero pressure head
Material properties porous media	Homogeneous porosity and air conductivity	Homogenous porosity and permeability	Heterogeneous porosity and permeability, linked to geophysical properties
Simulation time	2000 - 2012	2000–2018	2006-2018
Water/Ice	Dry.	Ice. Melting possible, damped latent heat. No water flow.	Domain with saturated porous morainic material. Melting and aggradation of ice, full latent heat. No water flow.

4 Site overview

This section gives a brief overview of the field sites, from which the forcing data for the model simulations presented throughout this thesis originate. The choice of these sites was mainly driven by (i) the availability of high-quality data, (ii) the prior research history allowing for more precise model constraints as well as (iii) the difference in landforms (alpine talus slope, low altitude talus slope and rock glaciers). The use of measured boundary and validation data allows for a valuable reference to reality even though the model is primarily developed to represent a process and its implications rather than to precisely represent a field site with all detailed, specific characteristics. Data from the different field sites were made available by the PERMOS network (PERMOS, 2016, 2019). Model approaches as presented in this thesis are not possible without a solid data basis and data of the PERMOS network is thus of inestimable value.
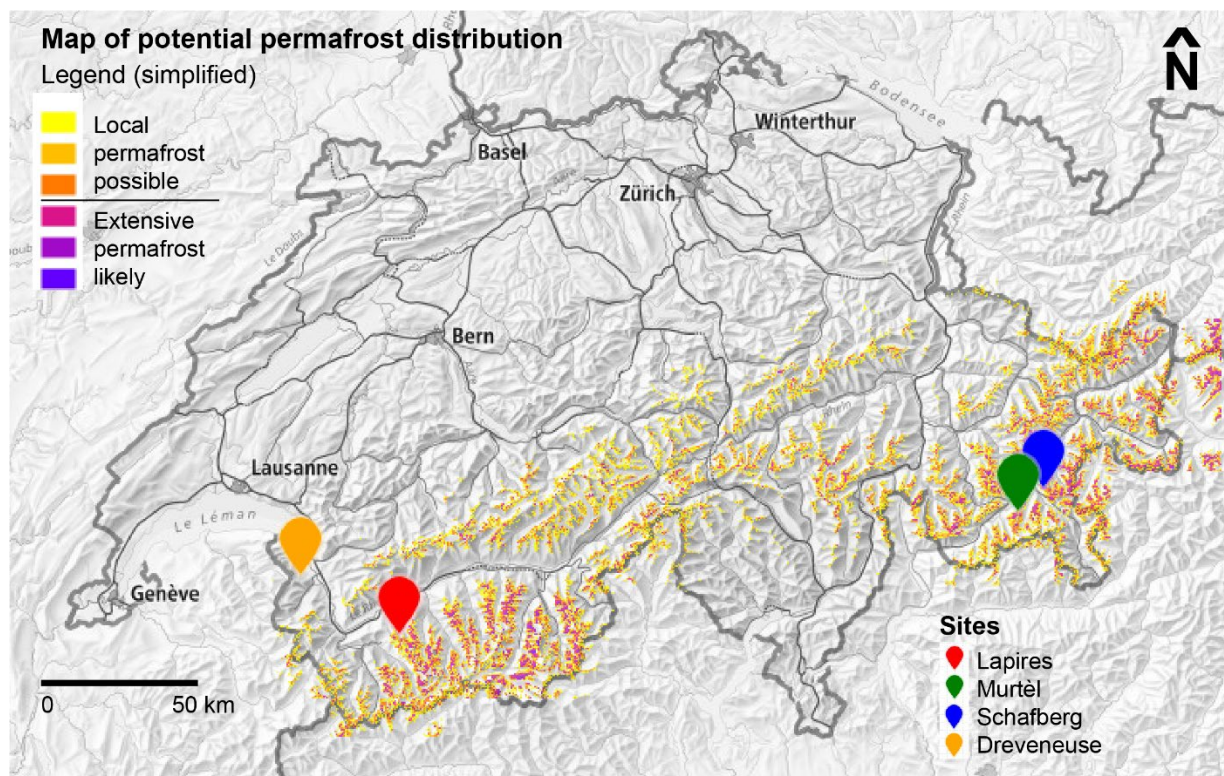

Figure 1 Location of the field sites, from which data was used in this thesis. The red marker represents the Lapires site (paper I), blue and green markers represent the Schafberg and Murtèl/Corvatsch sites (paper II) and the Dreveneuse site is marked in orange (paper III). The background shows the potential permafrost distribution in Switzerland (FOEN, 2005).

4.1 Lapires

Forcing data in paper I stem from the Lapires talus slope located in the Valais Alps (WGS 84 lat/lon 46.10752, 7.28766, Figure 1, red). This talus slope lies within the skiing domain of Verbier, ranges from 2400 and 2700 m a.s.l. with an NE aspect. Long-term data is available for ground temperature (borehole), ground surface temperature measurements and geophysical monitoring (PERMOS, 2019). Validation and ground truth data are available from four boreholes, regarding temperature, material composition and stratigraphy of the sediments (Scapozza et al., 2015) as well as from geophysical measurements for the analysis of spatial heterogeneity (Delaloye, 2004; Delaloye and Lambiel, 2005; Hilbich, 2010; Mollaret et al., 2020; Scapozza, 2013; Scapozza et al., 2015) and temporal evolution (Maierhofer et al., 2021; Mollaret et al., 2019). The bedrock consists of gneiss and is located deeper than 40m, as it has never been reached by the drillings (Scapozza, 2013; Scapozza et al., 2015).

4.2 Murtèl

A part of paper II uses forcing data from the Murtèl-Corvatsch rock glacier, located above Surlej in the Engadine Valley, Eastern Switzerland (WGS 84 lat/lon 46.42880, 9.82182; Figure 1 green). The Murtèl rock glacier is arguably one of the best-studied rock glaciers in the world. It lies within the skiing domain of St. Moritz at an altitude of 2650 m a.s.l. on a north-western slope at the foot of Piz Corvatsch. The rock mainly consists of granodiorite. At the surface, ogive-like structures originating from downward motion are very pronounced. The first borehole, which is still operational, was drilled in 1987 (Haeberli et al., 1988). Two other boreholes were drilled in 2000 (Arenson et al., 2010; Vonder Mühll et al., 2003), and in 2015 a new borehole was drilled close to the 1987 borehole to ensure the continuity of the data series in case of failure of the old borehole (PERMOS, 2019). The first drilling reached the bedrock at 49m, whereas the drillings form the year 2000 did not reach the bedrock at the same depth (Arenson et al., 2002). Geophysical investigations at the surface and in the boreholes, also through drill cores, provide a detailed description of the internal structure (Arenson et al., 2002; Hilbich et al., 2009; Maurer and Hauck, 2007; Mollaret et al., 2020; Vonder Mühll et al., 2000; Vonder Mühll and Haeberli, 1990) and temporal evolution (Mollaret et al., 2019).

4.3 Schafberg

In addition to Murtèl rock glacier, data from Schafberg rock glacier is used as forcing data in paper II. The Schafberg rock glacier (WGS 84 lat/lon 46.49881, 9.92521; Figure 1 blue) is located above Pontresina in the Engadin valley (Eastern Switzerland) at an altitude of 2750 m a.s.l. and facing north, turning to west in the lower part. The rock is biotite gneiss. Two boreholes with ground temperature monitoring are operational within the PERMOS network (PERMOS, 2019). Research started early on with the drilling of the boreholes in 1990, where borehole logs are published (Vonder Mühll and Holub, 1992) but no cores were retrieved. Creep rates and ice content were derived from borehole deformation monitoring (Hoelzle et al., 1998). Surface geophysical surveys describing the subsurface heterogeneity were performed already at an early stage (Geotest, 1990; VAW, 1991, 1992). More recent subsurface geophysical measurements are available at the University of Fribourg. In addition, there are hydrological (Pruessner et al., 2021) and kinematic (Cicoira et al., 2019) model studies. Schafberg rock glacier is quite a complex landform with several lobes. The frontal lobe ends in a torrent that reaches the village of Pontresina and is thus a potential source of debris flows (Kenner et al., 2019b).

4.4 Dreveneuse

For paper III, forcing data from the Dreveneuse low altitude cold talus slope is applied. The site is located in the Valais Prealps (Switzerland) above the Rhone valley on its western flank (WGS 84 lat/lon 46.27344/6.88959, Figure 1 orange). The slope stretches from 1560 m a.s.l. to 1650 m a.s.l and is oriented to E/ENE. The rock mainly consists of malm limestone as part of the Préalpes médianes rigides. Permafrost was observed at twice (2005-07 and 2010-12) during the monitoring period even though the mean annual air temperature MAAT is around 5°C (Morard et al., 2010). The lowest part is covered by dwarf spruces, representative of the cold microclimate. Dreveneuse has been extensively studied with temperature monitoring (two boreholes, GST loggers and BTS campaigns) and geophysical measurements (Delaloye, 2004; Lambiel, 2006; Morard, 2011; Morard et al., 2010), geophysical ERT monitoring (Mollaret et al., 2019) and soil moisture characteristics (Pellet and Hauck, 2017). Further, Dreveneuse was part of the Swiss permafrost monitoring network (PERMOS) to represent low-elevation permafrost sites but was later withdrawn from the network because of the absence of permafrost conditions since 2012. A comprehensive overview of the research history of Dreveneuse is given in the PERMOS report for the years 2014-2018 (PERMOS, 2019).

5 Publications

Paper I is dealing with the thermal regime of an alpine talus slope. The model calculations are performed in GeoStudio. Boundary data is used for the well-studied site Lapires, located in the skiing domain of Verbier in the Valais Alps, Switzerland. The data is provided by PERMOS and GST as well as borehole temperature data are used.

Title: Numerical modelling of convective heat transport by air flow in permafrost talus slopes.

Author contributions: Jonas Wicky designed and performed the model calculations and analysed the data, produced all the figures, and wrote the manuscript with substantial inputs from Christian Hauck.

Reference: Wicky, J. and Hauck, C. (2017). Numerical modelling of convective heat transport by air flow in permafrost talus slopes. The Cryosphere 11(3): 1311-1325.

The Cryosphere

Numerical modelling of convective heat transport by air flow in permafrost talus slopes

Jonas Wicky and Christian Hauck

Department of Geosciences, University of Fribourg, Fribourg, 1700, Switzerland

Correspondence to: Jonas Wicky (jonas.wicky@unifr.ch)

Abstract. Talus slopes are a widespread geomorphic feature in the Alps. Due to their high porosity a gravity-driven internal air circulation can be established which is forced by the gradient between external (air) and internal (talus) temperature. The thermal regime is different from the surrounding environment, leading to the occurrence of permafrost below the typical permafrost zone. This phenomenon has mainly been analysed by field studies and only few explicit numerical modelling studies exist. Numerical simulations of permafrost sometimes use parameterisations for the effects of convection but mostly neglect the influence of convective heat transfer in air on the thermal regime. In contrast, in civil engineering many studies have been carried out to investigate the thermal behaviour of blocky layers and to improve their passive cooling effect. The present study further develops and applies these concepts to model heat transfer in air flows in a natural-scale talus slope. Modelling results show that convective heat transfer has the potential to develop a significant temperature difference between the lower and the upper parts of the talus slope. A seasonally alternating chimney-effect type of circulation develops. Modelling results also show that this convective heat transfer leads to the formation of a cold reservoir in the lower part of the talus slope, which can be crucial for maintaining the frozen ground conditions despite increasing air temperatures caused by climate change.

1 Introduction

Mountain permafrost is currently undergoing substantial changes due to climate change as a whole and especially due to the observed air temperature increase. Among the typical mountain permafrost substrates, i.e. rock, fine sediments and coarse blocky surfaces, the latter have an important role on the subsurface because of their high insulating characteristics due to the low thermal conductivity of the air voids between the blocks (Harris and Pedersen, 1998; Herz et al., 2003; Juliussen and Humlum, 2008). In addition, natural air convection with upward transport of warmer air from the permafrost body and downward transport of cold air from the surface can take place within the coarse blocky layer, both vertically (in flat terrain) as well as in form of a 2-D circulation within a slope. These two effects lead firstly to much lower surface and subsurface temperatures for terrain with coarse blocky surface layers compared to fine-grained or bedrock surfaces (e.g. Hanson and Hoelzle, 2004; Schneider et al., 2012; Gubler et al., 2011) and then to persisting permafrost occurrences at the lower limit of permafrost (including rock glaciers and ice-cored moraines) and even to azonal permafrost occurrences at low elevation (e.g. Kneisel et al., 2000, 2015; Gude et al., 2003; Delaloye et al., 2003). For the latter, mean annual air temperatures may be positive and permafrost would not exist without this effect. This permafrost mostly occurs in undercooled scree and talus slopes and has been well researched in a number of publications (Funk and Hoelzle, 1992; Wakonigg, 1996; Kneisel et al., 2000; Gude et al., 2003; Sawada et al., 2003; Delaloye et al., 2003; Gorbunov et al., 2004; Delaloye and Lambiel, 2005; Zacharda et al., 2007; Morard et al., 2008a, b; Phillips et al., 2009; Gądek and Leszkiewicz, 2012; Stiegler et al., 2014; Kneisel et al., 2015).

Previous review articles about mountain permafrost research have highlighted the need for improved process understanding and model studies for the complex subsurface material of Alpine terrain (Harris et al., 2009; Haeberli

et al., 2010; Etzelmüller, 2013). While the energy balance for the coarse blocky surface layer of rock (and debris-covered) glaciers and talus slopes has been addressed in several field and modelling studies (e.g. Hanson and Hoelzle, 2004; Scherler et al., 2014; Reid and Brock, 2010), the effect of the internal 2-D air circulation driven by the gradient between outside (air) and internal (talus) temperature has not been treated in detail or quantified with respect to the other terms in the energy balance. Transient numerical simulations of permafrost usually neglect the influence of convective heat transfer in air on the thermal regime or parameterise it with an apparent thermal conductivity (Gruber and Hoelzle, 2008) or with an artificial heat sink (Scherler et al., 2013, 2014). Only very few and idealised modelling studies of the air circulation in undercooled talus slopes exist to date (e.g. Tanaka et al., 2000, 2006).

In contrast, many studies have been carried out in civil engineering to investigate the thermal behaviour of artificial blocky layers (such as railroad embankments) and to improve their passive cooling capacity (e.g. Goering and Kumar, 1996; Cheng, 2005; Gudong et al., 2007; Pham et al., 2008; Zhang et al., 2005; Arenson et al., 2006, 2007). In this study we will adapt the modelling concepts from civil engineering to investigate the feasibility of using a commercially available finite-element modelling software (GeoStudio, 2013a, b, c) to explicitly model the 2-D heat transfer by air flow within an idealised talus slope and to quantify the cooling effect with respect to different sensitivity parameters. The simulations are driven by observational data from the Lapires talus slope in the western Swiss Alps (Delaloye and Lambiel, 2005; Scapozza et al., 2015; Staub et al., 2015).

2 Theory and data

2.1 Conceptual model

Convection is the transport of energy by a fluid, in the present case the transport of heat by air flow through the available pore space. This is in contrast to heat transport by conduction or radiation, which are other important processes for the energy balance within coarse blocky surface layers (Scherler et al., 2014). Convective processes are responsible for the specific (cold) temperature regime in undercooled talus and scree slopes. In 1900, Balch described the asymmetry of seasonal air circulation in ice caves with gravity-induced descending cold air in winter and an absence of circulating air in summer (Balch, 1900). Wakonigg (1996) described the so-called chimney effect in talus slopes, where a seasonally switching air circulation produces descending cold air in summer and ascending warm air in winter. The cold air exits at the foot of the slope in summer and warm air exits through melt holes in the snow cover at the top of the slope in winter, as has been observed in field studies on various talus and scree slopes (e.g. Gude et al., 2003; Sawada et al.,

2003; Delaloye, 2004; Delaloye et al., 2003; Zacharda et al., 2005, 2007; Morard et al., 2008a, b; Lambiel and Pieracci, 2008; Morard, 2011).

Figure 1 shows this process schematically in its most basic form (Morard et al., 2010). Here, the sediments in the talus slope are assumed to be homogeneous and the induced air circulation is most effective when the temperature gradient between the outside air (T_{ao}) and the voids in the porous substrate (T_{ai}) is high and if the voids between the blocks have a high connectivity. Material composition can be heterogeneous, which means that the cooling effect does not affect the whole talus slope in the same way (Delaloye and Lambiel, 2005). In any case, the internal air circulation can lead to rapid ground cooling, in particular at the bottom of the talus slope, where cold air is aspirated in winter.

Model studies trying to explicitly simulate this process are rare. In a 1-D study of the energy balance within the coarse blocky surface layer of a rock glacier, Scherler et al. (2014) estimated the impact of this seasonally varying convective heat transfer (heat source in winter, heat sink in summer) in comparison with other elements of the energy balance, and therefore also with observed data. However, this approach does not treat the underlying process and prohibits an explicit modelling of the 2-D air circulation. Tanaka et al. (2000) investigated the air circulation at two sites (Ice Valley, Korea, and Nakayama, Japan) using field data and analytical and numerical models. In their most complex 2-D model they could confirm that the cooling effect in summer stems from a gentle katabatic flow in stable stratified conditions, whereas the winter circulation is due to an unstable convective overturning in a 50 m long convection cell. In general, these convection cells form by natural convection, i.e. air movement occurs as a function of density (temperature) differences, as opposed to forced convection caused by the influence of surface (atmospheric) wind (e.g. Arenson and Sego, 2007). Hereby, the air movement due to natural convection has to be strong enough with respect to the bulk thermal conductivity of the material to yield a sustained convective cell. This relation is expressed by the Rayleigh number, which relates the air permeability, the thickness of the porous layer, the thermal conductivity of the material and the temperature gradient within the porous layer, i.e. the talus material. The higher the air permeability, the thickness of the talus and the temperature gradient with respect to the thermal conductivity, the higher the Rayleigh number and the stronger and longer the convective cell(s) (Arenson and Sego, 2007). However, as some of the important parameters of the Rayleigh number may be temporally and spatially variable, the air circulation will change in both space and time. Consequently, an explicit modelling of the air circulation in two dimensions is necessary to be able to simulate the development and seasonality of the occurrence of convection cells in talus slopes. Convective heat transfer in permafrost was explicitly modelled in several engineering studies. First numerical simulations were conducted by Goering and Kumar (1996) and showed
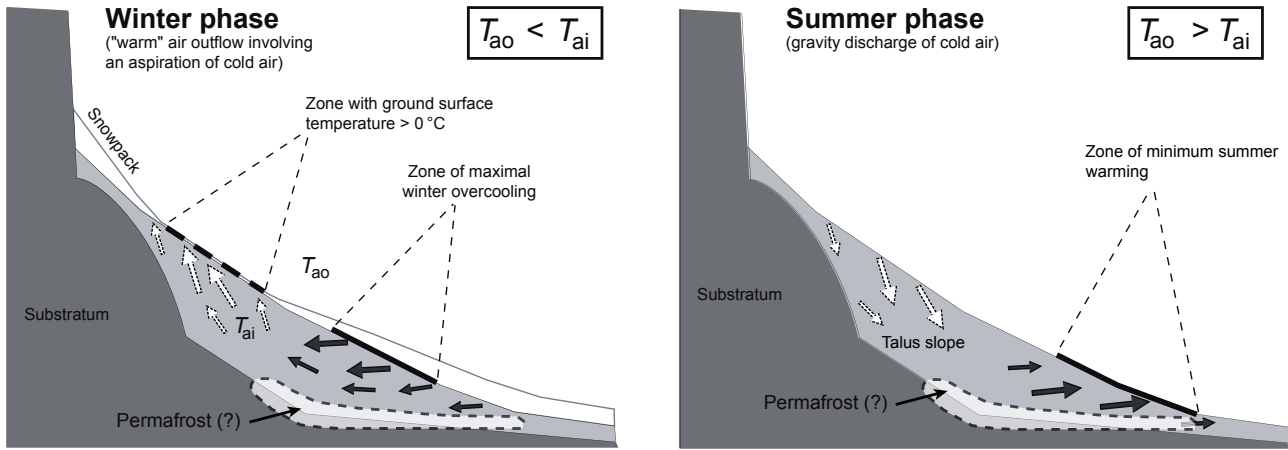
Figure 1. Schematic view of a seasonally alternating air circulation within a talus slope (modified from Morard et al., 2010). T_{ao} and T_{ai} denote air temperature outside and inside the blocky material, respectively.

a passive cooling effect of convective cells within coarse-grained road embankments. The same effect, corresponding to a Rayleigh–Bénard circulation was described by Guodong et al. (2007) as a thermal semi-conductor which cools road or train embankments in permafrost regions in winter, whereas no heat can penetrate in summer, due to the stable temperature stratification within the coarse material. Further engineering studies (e.g. Arenson and Sego, 2006; Arenson et al., 2007; Pham et al., 2008; Pei et al., 2014) investigated and simulated these small-scale cooling effects to optimise passive cooling systems on mine waste piles and road- and railway embankments in permafrost regions.

In the following we will describe the model set-up for an explicit simulation of the larger- and natural-scale lateral heat transfer by 2-D air circulation within an Alpine talus slope.

2.2 Governing equations

The general heat flow equation including convective transfer by water and air can be formulated as follows (GeoStudio, 2013a):

$$
\left(\rho_s c_{ps} + L w \frac{\partial W_u}{\partial T} \right) \frac{\partial T}{\partial t} = \frac{\partial}{\partial y} \left[K_t \frac{\partial T}{\partial y} \right] + c_{pa} \frac{\partial (\dot{m}_a T)}{\partial y}
$$
$$
+ \rho_w c_{pw} \frac{\partial (q_w T)}{\partial y} + Q, \qquad (1)
$$

where L is the latent heat of water (J m^{-3}), W_u is the unfrozen water content (m^3 m^{-3}), w is volumetric water content (m^3 m^{-3}), T is temperature (K), y is the coordinate(s) (m), K_t is thermal conductivity (W m^{-1} K^{-1}), Q is the boundary flux (W m^{-3}), t is time (s), $\rho_{s/w}$ is the density of soil/water (g m^{-3}), c_{ps} is the specific heat capacity of soil (J g^{-1} K^{-1}), $c_{pa/pw}$ is the specific heat capacity of air/water (J g^{-1} K^{-1}), $\dot{m}_a$ is the mass flow air (g s^{-1}) and q_w is the flow rate (Darcy) of water (m s^{-1}).

Water (Eq. 2) and air (Eq. 3) flow can be described as follows and have to be jointly solved, as air and water pressure are dependent variables (GeoStudio, 2013b, c):

$$
m_w \gamma_w \frac{\partial H_w}{\partial t} = \frac{\partial}{\partial y} \left[K_w \frac{\partial H_w}{\partial y} \right] + m_w \frac{\partial P_a}{\partial t} + Q_w, \qquad (2)
$$
$$
\left(\frac{\theta_a}{RT} + \rho_a m_w \right) \frac{\partial P_a}{\partial t} = \frac{\partial}{\partial y} \left[\frac{\rho_a K_a}{\gamma_{oa}} \frac{\partial P_a}{\partial y} + \frac{\rho_a^2 K_a}{\rho_{oa}} \right]
$$
$$
- \left[\frac{\theta_a P_a}{R} \frac{\partial (\frac{1}{T})}{\partial t} \right] + \left[\rho_a \gamma_w m_w \frac{\partial H_w}{\partial t} \right], \qquad (3)
$$

where m_w is the slope of the water storage curve (m s^2 g^{-1}), γ_w is the unit weight of water (g m^{-2} s^{-2}), γ_{oa} is the relative unit weight of water (g m^{-2} s^{-2}), H_w is the total head (m), K_w is the hydraulic conductivity (m s^{-1}), Q_w is the boundary flux (s^{-1}), K_a is the air conductivity (m s^{-1}), P_a is the air pressure (Pa), ρ_a is the density of air (g m^{-3}), ρ_{oa} is the relative density of air (g m^{-3}), θ_a is the volumetric air content (m^3 m^{-3}) and R is the specific heat capacity of dry air (J g^{-1} K^{-1}).

2.3 Forcing data sets

Forcing data are used from the Lapires talus slope, which is situated between 2400 and 2700 m a.s.l. in the Valais Alps, western Swiss Alps (e.g. Staub et al., 2015). Several long-term mean annual ground near-surface temperature data series and four deep boreholes with temperature measurements are available from this site (Delaloye and Lambiel, 2005; Scapozza, 2013; Scapozza et al., 2015; Staub et al., 2015), which is part of the PERMOS network (PERMOS, 2016b).

For this study we used ground surface temperature (GST) data as the surface atmosphere boundary condition. Moreover, snow height data from the nearby weather station Les Attelas (Swiss IMIS network) were used to model the seasonal decoupling of the ground from the atmosphere by the

snow cover. Borehole temperature data were used to compare the modelled temperature distribution to the measured temperature series in the borehole.

Validation and ground truth data are available from four boreholes, regarding temperature, material composition and stratigraphy of the sediments (Delaloye et al., 2001; Scapozza, 2013; Scapozza et al., 2015), and from geophysical measurements for the analysis of spatial heterogeneity (Delaloye, 2004; Lambiel, 2006; Hilbich et al., 2008; Hilbich, 2010). The porosity within the permafrost layer ranges from 30 to 60 % and some parts of the talus slope (including the base of the slope) are sealed by ice (see Scapozza, 2013; Hilbich, 2010). The bedrock consists of gneiss and is located at 40 m depth at least, as observed in borehole cores (Scapozza, 2013; Scapozza et al., 2015).

3   Model set-up

The commercially available software GeoStudio has already been applied to coarse blocky permafrost substrates for of different engineering purposes, such as the investigation of the passive cooling effect in road embankments (Arenson et al., 2006) or the heat convection in coarse mine waste rock piles (Arenson et al., 2007). Furthermore, Mottaghy and Rath (2006) used it to validate their own model approach in a study of paleoclimate permafrost in porous media. In the engineering sciences modelling approaches of convective heat transport by air and the resulting passive cooling effect are numerous (e.g. Goering and Kumar, 1996; Guodong et al., 2007; Lebeau and Konrad, 2009). Such studies showed the important influence of convective heat transport on the ground thermal regime at fine scales.

In this study we pick up these concepts and adapt them to a natural-scale talus slope. With GeoStudio we use a finite element modelling approach that solves the partial differential heat equations, including convective heat transfer over a 2-D domain. The numerical domain is divided into subdomains with different material properties (Fig. 2). Measured daily temperature values (see Sect. 2.3) were used as temperature forcing data at the surface–atmosphere boundary for the transient modelling. This 2-D approach allows an explicit modelling of the air flow and the resulting convective heat exchange over the spatial domain of a natural-scale talus slope, allowing us to analyse its influence on the ground thermal regime.

3.1   Mesh geometry

Figure 2 shows the numerical domain with its four subdomains. Each subdomain represents a different material and therefore has different physical material properties (Sect. 3.2). The entire domain represents an idealised talus slope with a talus thickness of 17 m and a constant slope angle of 33°. An unstructured mesh of quadrilateral and trian-

gular elements was used with a mesh size of 1.2 m in the talus, increasing to 3 m in bedrock and air domain. An adaptive time stepping scheme was used. The maximum time step is 0.5 days, decreasing to 0.1 days until the Courant criterion is met to minimise numerical dispersion and oscillation (GeoStudio, 2013a, c). Convergence is met when the results of two different iterations differ by less than 0.01 °C or do not differ by more than 0.1 % for temperature and 0.001 % for pressure. The maximum number of iterations was set to 30, and our experiments showed that the model is numerically stable and produced interpretable results under these numerical conditions. Numerical configuration proved, however, to be a crucial and delicate point in defining the model boundaries and running the model.

3.2   Material properties

Table 1 summarises the material properties of the subdomains shown in Fig. 2 which were used in our simulations. The conductivities and heat capacities are taken from Schneider (2014), who empirically established the different values for several blocky periglacial landforms in the Murtèl–Corvatsch region. It can be assumed that these values are more accurate for natural-scale talus slopes than published values from laboratory experiments. The volumetric heat capacity for bedrock exposed at the surface is given by Schneider (2014) as $275\,\mathrm{kJ\,m^{-3}\,K^{-1}}$, which is approximately 8 times lower than other published values for deep-seated bedrock in permafrost (e.g. $1600\,\mathrm{kJ\,m^{-3}\,K^{-1}}$ in Gruber and Hoelzle, 2008; $>2000\,\mathrm{kJ\,m^{-3}\,K^{-1}}$ in Arenson and Sego, 2006; $2000\,\mathrm{kJ\,m^{-3}\,K^{-1}}$ in Noetzli et al., 2008; $2063\,\mathrm{kJ\,m^{-3}\,K^{-1}}$ in Wegmann et al., 1998). Considering that the model is simulating bedrock at depth and not at the surface, the volumetric heat capacity is set to $2500\,\mathrm{kJ\,m^{-3}\,K^{-1}}$. Arenson et al. (2006) point out that the heat capacity has a less prominent influence on the temperature distribution than other parameters in Table 1, especially the air conductivity.

The porosity is set to 0.5 for the material within the talus slope. This value corresponds to measured porosity values in the drill cores (Scapozza et al., 2015) and model-fitted values for the Lapires site (Marmy et al., 2016) as well as previously published values for other coarse-grained permafrost material (Gruber and Hoelzle, 2008; Scherler et al., 2014). The porosity of bedrock is assumed to be very low compared to the talus slope and is therefore set to a near-zero value. The so-called air conductivity is an intrinsic permeability which can be understood as a theoretical value of the potential air flow within the material. As Arenson et al. (2006) pointed out, the chosen air conductivity has to be in accordance with the other numerical parameter settings (time step, mesh size) to guarantee numerical stability and convergence. In our study, the air conductivity in the bedrock was set to a near-zero value, assuming that no air circulates within the bedrock. The air conductivity within the talus and in the air was set to a value of $10^4\,\mathrm{m\,day^{-1}}$. This value was
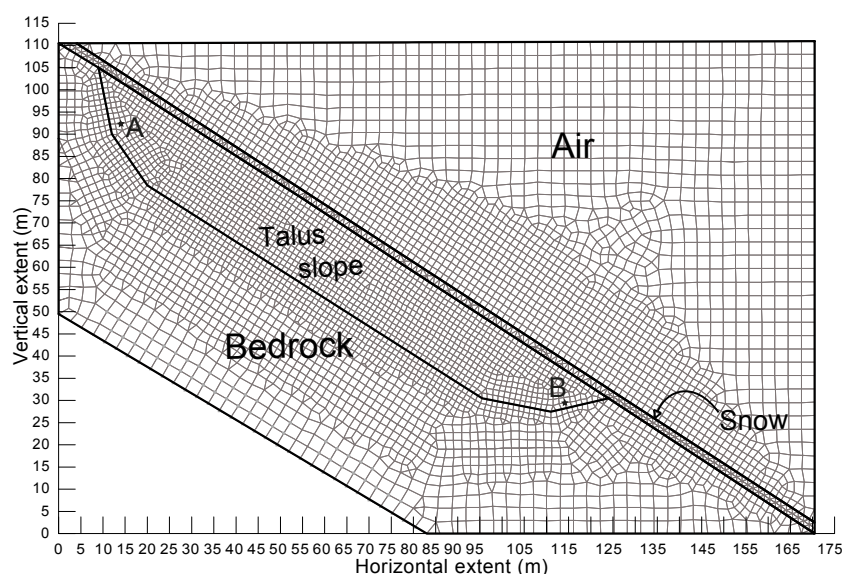
Figure 2. Model set-up and mesh showing the four subdomains used in the talus slope experiments. The points (nodes) marked by A and B are reference points which are further analysed below.

Table 1. Material properties used for the GeoStudio simulations in this study (based on Schneider, 2014; Arenson and Sego, 2006; Arenson et al., 2007; Scapozza et al., 2015; see text). The snow layer only acts as an idealised boundary that seasonally damps and prohibits air exchange between talus and atmosphere through coupling of the air conductivity value to the snow height. See text for further explanations.

Material	Thermal conductivity		Specific heat capacity	Vol. heat capacity	Porosity	Air conductivity
	$(W\,K^{-1}\,m^{-1})$	$(kJ\,day^{-1}\,m^{-1}\,K^{-1})$	$(J\,kg^{-1}\,K^{-1})$	$(kJ\,m^{-3}\,K^{-1})$		$(m\,day^{-1})$
Bedrock	2.4	207	99	2500	0.01	0.01
Talus	1.2	103	904	1256	0.5	10^4
Air	1.2	103	1	1.3	1	10^4
Snow	1.2	129	1	1.3	1	0–10^4

obtained through numerical test simulations, as in Arenson et al. (2007), who obtained the same value. Higher air conductivity values did not result in numerical convergence and lead to clearly unrealistic results. In comparison to that of the rock material, the heat capacity of the air above the surface is low. Air movement in the atmosphere and its influence on the talus are simplified. There are no turbulent atmospherical fluxes or external wind sources included in the model set-up. This is of course a simplification of real-world conditions, but it helps to isolate the process of the internal air circulation within the talus slope without the existence of external forcing by wind.

Finally, the effect of snow is simulated in an indirect way. The thermal effect of snow on the ground is represented through the explicit GST boundary condition at the atmosphere–surface boundary. However, the decoupling of the subsurface from atmospheric circulation regarding the air flow is not represented by this boundary condition. To ac-

count for this decoupling of air movement, the air conductivity above the surface is parameterised as a function of snow height. Snow height data from the IMIS station Les Attelas (close to the Lapires site, with representative snow data; see Staub et al., 2015) were used to parameterise air conductivity. For a snow height below 0.2 m the snow layer does not restrict the circulation. For snow heights between 0.2 and 0.8 m air conductivity linearly decreases from 10^4 to $0\,m\,day^{-1}$ and thus makes the exchange between the air and the talus impossible for snow heights above 0.8 m (see Scherler et al., 2013). Morard (2011) has shown that air aspiration is also possible through the snow, but little is known about the characteristics and importance of this effect.

3.3 Boundary and initial conditions

The lower boundary condition is set to a constant value of $+0.6\,°C$. Temperature data from the lowermost thermistor

Table 2. List and description of model experiments conducted.

Name	Processes included	Description
Conduction only (CON)	Conduction only	–
Closed (CLO)	Conduction and convection	No exchange with the air block
Open (OPE)	Conduction and convection	Unrestricted exchange with the air block
Seasonally closed (SEA)	Conduction and convection	Seasonally restricted exchange with the air block

in the Lapires borehole LAP_1108 at 39 m depth show values around $+0.6\,°C$ with no seasonal variability (PERMOS, 2016a). For the surface–atmosphere boundary condition a 13-year period (2000–2012) of the GST data series from the logger S15 at Lapires (see Sect. 2.3; Staub et al., 2015) is used. Initial conditions are set with a constant temperature of $-0.2\,°C$ in the talus and $0.2\,°C$ in the surrounding bedrock, followed by a 7-year spin-up using the daily mean values from the S15 GST data as forcing. After 7 years a quasi-equilibrium state from the constant initial conditions is reached. After the spin-up procedure the 13-year data series is used at the atmospheric boundary as forcing to show the effects of interannual variability of the driving meteorological variables.

3.4 Model experiments

Simulations with four different model set-ups have been conducted (Table 2). The first set-up (CON) allows no air circulation at all and hence only conductive heat transfer is represented, as in most permafrost models and land-surface schemes. This set-up serves as a reference simulation. The second set-up (CLO) consists of a permanently closed domain which allows air circulation within the talus, but no exchange with the air domain above the surface. In the third set-up (OPE) exchange with the modelled air domain above the surface is always possible, whereas the fourth set-up (SEA) allows only a seasonal circulation with the air block to represent the seasonal decoupling from talus and atmosphere by the snow cover.

4 Results

4.1 Air circulation

Figure 3 shows the simulated air circulation and temperature distribution in the full model domain for day 300 (27 October) for the experiment with open boundary conditions between the surface of the talus slope and the atmosphere (OPE). The ascending air flow within the talus slope can be clearly seen, with maximum flow velocities of around $100\,\mathrm{m\,day^{-1}}$, i.e. $\sim 0.001\,\mathrm{m\,s^{-1}}$, which is in the range of the values estimated in other model and observational studies (Tanaka et al., 2000). Meyer et al. (2016) estimated velocities of about $0.07\,\mathrm{m\,s^{-1}}$ for air flow within an ice cave, which

can be seen as the upper porosity limit for this kind of intra-talus air circulation. The thermal effect of this circulation is clearly seen with positive temperatures around $2\,°C$ in the upper part of the talus slope and negative ones around $-1\,°C$ in the lower part. Note that the near-surface layer shows homogeneously negative temperatures at this time of the year due to seasonal freezing from the surface, except for the 10 m around the exit region of the warm ascending air flow in the upper part of the slope, where ground temperatures remain positive.

The air circulation causes aspiration of cold atmospheric air into the lower part of the talus slope, where the lowest temperatures are found (horizontal distance 110 m). This temperature distribution is a clear effect of the induced convective air circulation. The pure conduction experiment (CON), which served as a reference experiment and only uses conduction for heat transfer, shows a spatially and temporally homogeneous temperature distribution. The small difference between nodes A and B in Fig. 6 is due to the slightly asymmetric model geometry. The spatial variability of the temperature difference to the OPE experiment is shown in Fig. S1 in the Supplement. Neither negative temperatures nor permafrost conditions are produced in this reference run.

Figure 4 shows the seasonal evolution of the intensity and direction of the air circulation shown in Fig. 3 for the different months. The seasonal reversal of the circulation, as postulated in Delaloye and Lambiel (2005) and Morard et al. (2010, see Fig. 1), amongst others, is clearly visible with downslope air flow within the talus slope between June and September and ascending air circulation from November to May. The strongest circulation (snow free and therefore high temperature gradient at the atmosphere – talus boundary) is simulated in July and August, whereas the winter circulation is less strong, but continues over a longer time period (7 months, in contrast to only 3–4 months in summer). Even low temperature gradients cause a circulation in the modelling results. However, a weak circulation has almost no thermal effect and thus conduction dominates.

Figure 5 shows the differences of the simulated seasonal circulation depicted in Fig. 4 between the three experiments CLO, OPE and SEA. The seasons are shown as 3-month averages regarding their typical conditions at high elevation, i.e. winter (JFM), spring (AMJ), summer (JAS) and autumn (OND). The transition period with reduced air circulation be-
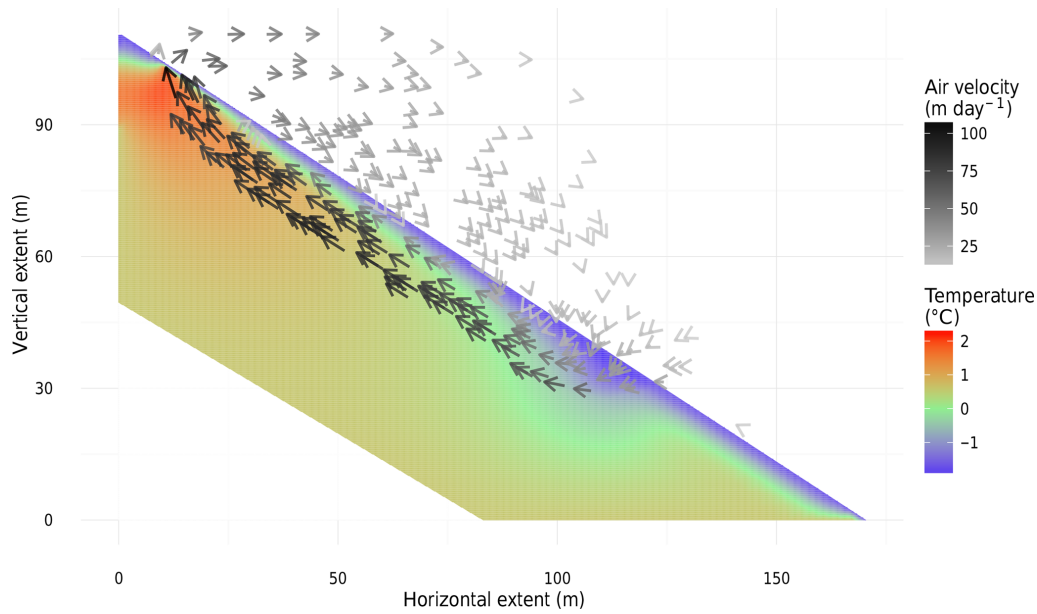
Figure 3. Simulated temperature distribution (colours) and air current vectors in the talus slope for the open experiment (OPE) for day 300 (winter circulation). The intensity of the circulation is marked by the grey/black vector arrows and is given in m day^{-1}.
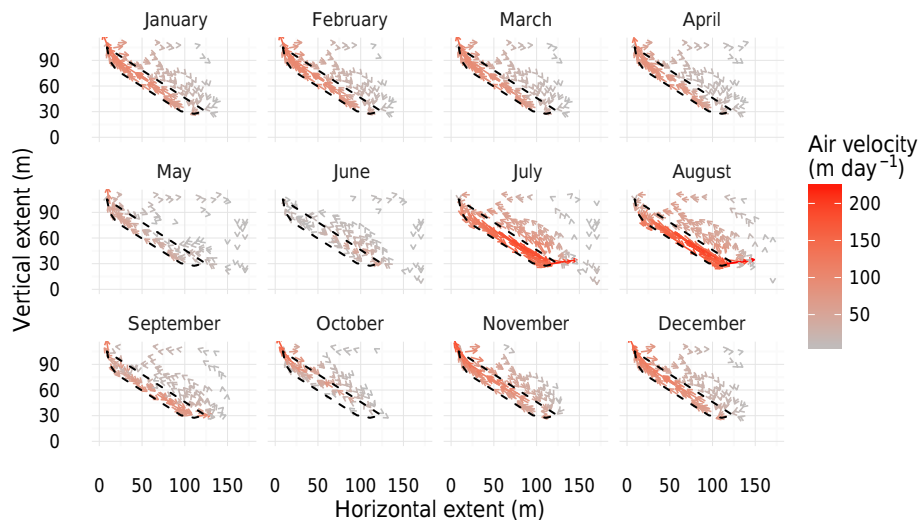

Figure 4. Mean monthly air flow of the open experiment (OPE) over the 13 modelled years. The dashed line marks the domain of the talus slope. The seasonal differences in intensity and direction of the air circulation are clearly shown by the direction and colour of the arrows.

tween April and June is seen in all experiments; however, it has to be noted that during these 3 months the circulation reverses (see Fig. 4) and downslope and upslope air flow will contribute to near-zero air flow in a 3-month average. The strong downslope air flow in summer is seen in OPE and SEA but much less so in CLO, as only little space in the near-surface part of the talus slope is available for the upward-directed backflow of air. In CLO the circulation is also weaker in winter, which clearly illustrates that an open boundary between atmosphere and talus slope is necessary to

produce stronger air circulation. However, it can be seen that in CLO a seasonally reversing air circulation also develops.

The OPE and SEA experiments differ regarding their open and seasonally closed boundary condition, the latter resembling the insulating effects of the seasonal snow cover. The comparison shows that between July and December almost no differences can be seen, as the snow cover is absent or not yet thick enough to dampen the air exchange between talus slope and atmosphere. In contrast, strong damping effects can be observed between January and June due to the presence of an up to 2 m thick snow cover (see Fig. 8).
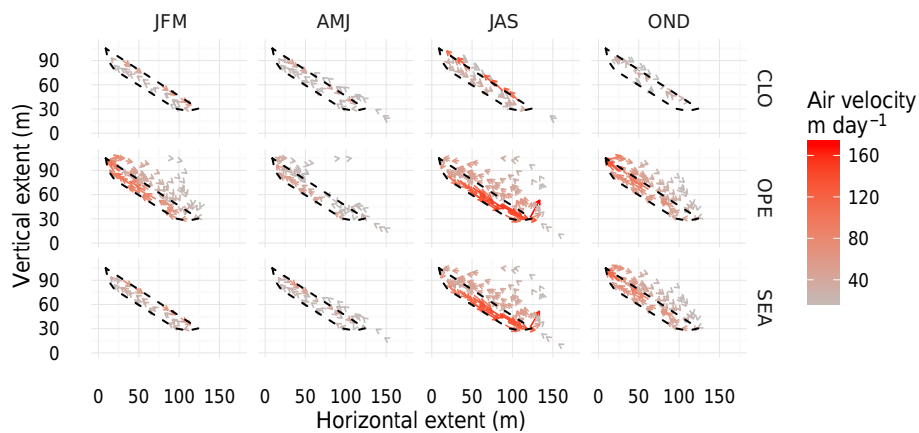
Figure 5. Modelled seasonal mean air flow for the modelled 13 years for the different atmospheric boundary conditions: (top) closed to atmosphere (CLO), (middle) open to atmosphere (OPE) and (bottom) seasonally closed to atmosphere (SEA). The dashed line is the talus slope.
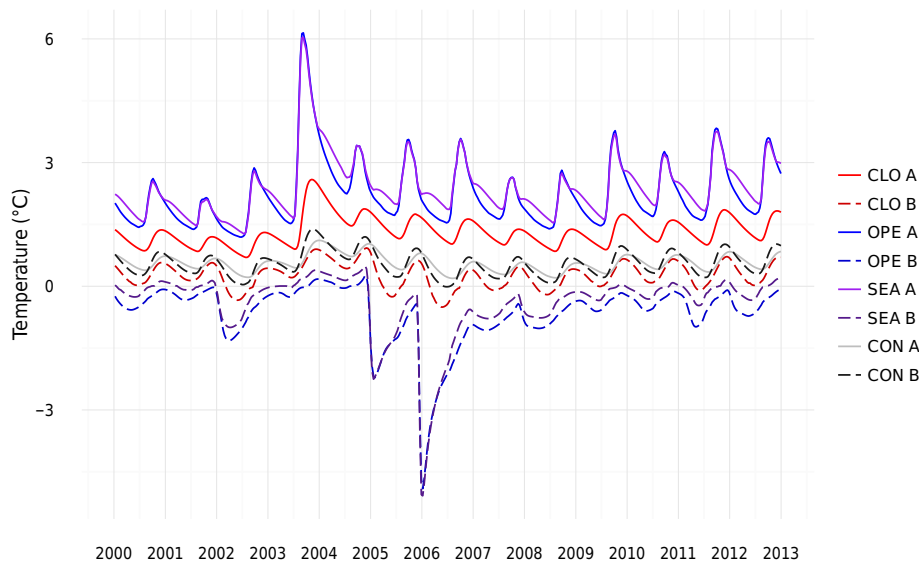

Figure 6. Temperature evolution at two different locations in the upper (node A, solid lines; see Fig. 2) and lower (node B, dashed lines; see Fig. 2) part of the talus slope for the CLO (red), the OPE (blue), the SEA (purple) and the CON (black) experiment.

4.2 Ground temperature

The effect of the seasonally reversible air circulation on the spatial ground temperature distribution was already shown in Fig. 3. Figure 6 shows the seasonal and interannual variations of this temperature effect for all four experiments. Temperature curves in the upper part of the talus slope (node A) indicate that temperatures are always positive with a seasonal variability of around $1\,°C$. An exception is summer 2003, where the effect of the exceptional heat wave (see Schär et al., 2004; Hilbich et al., 2008) is clearly shown by a temperature increase between $1\,°C$ (CON) and $3\,°C$ (OPE and SEA). Apart from this anomalous year, interannual variability is small in the upper part of the talus slope. In addition,

the effect of the snow cover (SEA A compared to OPE A) is small with no differences in summer and maximal temperature differences of around $0.2\,°C$ in winter.

In contrast, the interannual variability in the lower part of the talus slope is much more pronounced. Here, temperatures in the OPE and SEA experiments show permafrost conditions which are almost conserved during the summer 2003 heat wave. Temperature decreases exceeding $3\,°C$ can be observed during the cold winters 2004–2005 and 2005–2006. After that, temperatures increase again steadily but still show permafrost conditions at the end of the simulation period in 2012 for the OPE experiment.

The mean temperatures in the lower part of the talus at node B over the 13-year modelling period decrease by

0.28 °C (CLO), 0.94 °C (SEA) and 1.19 °C (OPE) compared to the CON experiment without convective cooling. Temperature differences between the upper and lower parts of the talus slope are up to 6 °C during the warm summer 2003 and the cold winters in 2004–2005 and 2005–2006, which is an effect of the air circulation alone, as no significant temperature differences were obtained in the conductive reference experiment (CON, grey and black lines on Fig. 6). Differences between the OPE and SEA experiments are around 0.2 °C for the lower part of the talus slope, demonstrating the critical role of the snow cover in damping the cooling effect of the talus slope circulation.

5   Discussion

The simulations qualitatively reproduce the internal air circulation observed in low- and high-elevation talus slopes and they are consistent with many different observations. For a critical analysis of the reliability of the model approach and its results, the degree of practicality of the processes in the model, its sensitivity to model parameters, a comparison with observed borehole temperatures in the Lapires talus slope as well as a discussion of the strengths and weaknesses of the model will be addressed below.

5.1   Process analysis

Figure 7 shows the velocity of the air flow within the talus slope as a function of driving GST data. It is clear that there is a strong correlation between highly positive GST data and strong downslope (positive) air flow and, correspondingly, negative GST data with upslope (negative) air flow. This is in good agreement with the underlying process, where a high temperature gradient between the inside and outside of the talus slope leads to ascending air if the interior is warmer and descending air if the interior is colder than the outside air (Fig. 1). As the temperature within the talus slope is close to 0 °C, a GST of 0 °C corresponds roughly to zero air displacement, as there is no temperature gradient. The high correlation coefficient (r^2) in the OPE and the SEA experiments shows that GST is a very important factor in explaining the air flow through the talus. The slightly lower r^2 in the CLO experiment is partly due to the weaker air circulation and thus greater influence of the values near the zero curtain, but it may also indicate that the closed model conditions are less representative.

Figure 8 shows an analysis of the simulated air flow in dependence of the presence or absence of a snow cover for the three different experiments. As shown in the previous figures, the velocities are lowest for the CLO experiment, and the air flows downslope in summer and upslope in winter in all experiments. In addition, velocities in summer for OPE and SEA show a similar behaviour, as no snow cover is present. Due to the more efficient ground cooling in winter, the OPE

experiment shows slightly higher air velocity values. However, large differences can be seen in late autumn and during winter. Clearly, winter velocities are highest for OPE, as there is no snow cover inhibiting the coupling between talus slope and atmosphere in this experiment. In contrast, maximal velocities for the ascending air flow are obtained in late autumn in the SEA experiment, which can be seen as the most realistic simulation, as it includes the non-linear damping effect of the snow cover. In late autumn, air (and also ground surface) temperatures can be negative due to strong radiative cooling at the surface at night. In the absence of a thick snow cover (e.g. in autumn–early winter 2005; Fig. 8) a strong air circulation can develop, as the temperature gradient between interior and outside is high. As soon as the snow cover completely insulates the ground, the air circulation is severely damped as can be seen by the increasing and then flattening velocity curve in the SEA experiment. A similar, but much weaker, effect can be seen in early summer when the snow cover thickness decreases again. However, as the temperature gradient is much weaker during the main snow melt period, its effect on the evolution of the air circulation is also much smaller.

5.2   Model sensitivity analysis

Sensitivity simulations with different slope angles showed a strong influence of the slope angle on the intensity of the air circulation and therefore on temperature evolution. Not surprisingly, higher slope angles lead to higher velocities and larger temperature contrasts due to the stronger gravitational forces, as was also noted in previous studies (e.g. Guodong et al., 2007). As the mesh geometry (see Fig. 2) changes with changing slope angles, the obtained temperature dependencies on slope angle cannot be compared quantitatively. In addition, the circulation pattern changes with increasing slope angle. For the simulations with high slope angles (such as the 33° depicted in Fig. 2, which was used in all simulations shown above) only one 2-D advection cell is present, with seasonal reversal of the flow direction (see Figs. 3–5). With decreasing slope angle this circulation cell decreases in strength and additionally 1-D vertical convection cells are formed, which do not extend over the full model domain (not shown). For slope angles lower than around 5° the air flow is dominated by several individual small vertical convection cells.

Guodong et al. (2007) describe a similar relation between slope angle and circulation patterns in laboratory experiments. They found a minimal slope angle of 15° for connected advection cells and a dependence on the Rayleigh number for higher slope angles (see also Sect. 2.1). In practice and in our model simulations it is difficult to distinguish clearly between horizontal advective and vertical convection cells as there is usually a gradual transition between the two phenomena. Using in situ measurements, Hanson and Hoelzle (2004) showed that for the case of rock glacier Murtèl, a
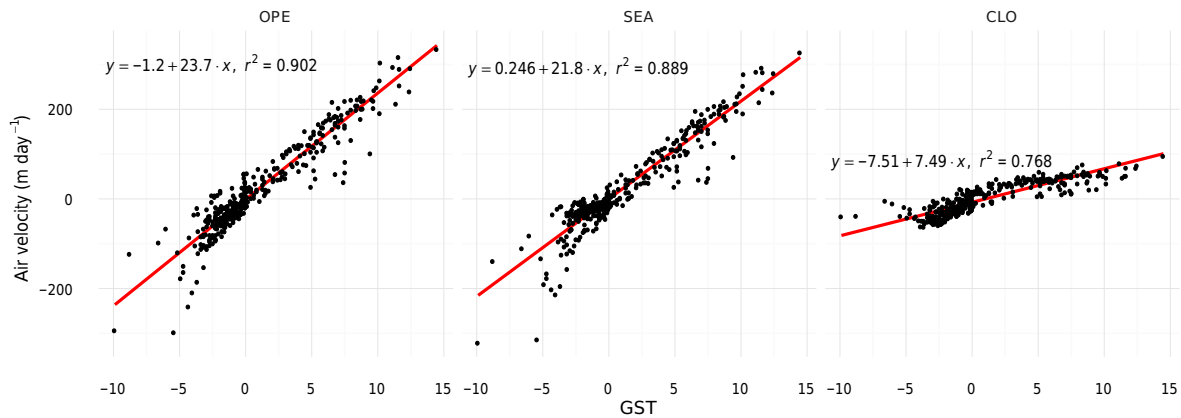
Figure 7. Relation between velocity of the air flow at node B (see Fig. 2) and the forcing ground surface temperature (GST) for the three different experiments OPE, SEA and CLO. Positive velocities indicate downslope movement and negative velocities indicate upslope movement of air.
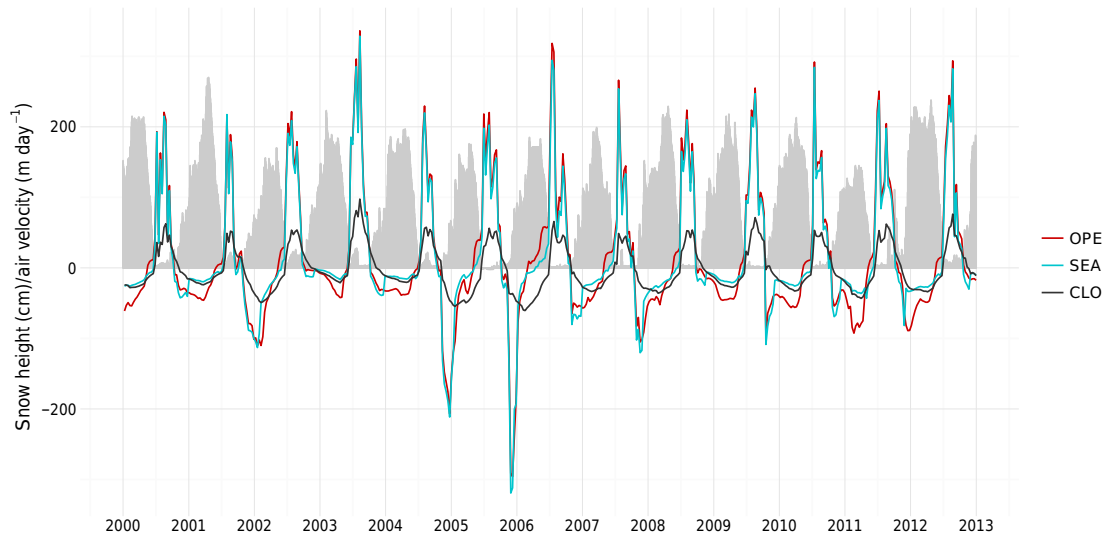

Figure 8. Velocity of the simulated air flow at node B (see Fig. 2) in the experiments OPE, SEA and CLO for the period 2010–2013 in relation to the presence of a snow cover (grey bars). Positive (negative) velocities correspond to downslope (upslope) air flow.

comparatively flat rock glacier with large furrows and ridges inhibiting the lateral air circulation, the vertical exchange of air is more important than advective processes. A thorough observation- and simulation-based analysis of these dependencies still needs to be carried out.

In addition, the model is very sensitive regarding the so-called air conductivity parameter introduced above. Arenson et al. (2006) concluded that finding a physically consistent combination of air conductivity and temporal and spatial discretization is the biggest practical problem affecting numerical stability in soil temperature simulations. In our simulations only a narrow range of air conductivities allow for convergent calculations that produce convective circulation patterns for a given mesh and time step. Similar results were obtained in GeoStudio (2013a) and Arenson et al. (2007), which suggests that the air circulation should be used as a

calibration parameter wherever subsurface temperature data are available, especially as there are generally no in situ air velocity measurements within the talus slopes.

5.3 Comparison of modelled and measured ground temperature data

Finally, the idealised experiments discussed above can be compared to the observed temperature evolution in a borehole situated in the central part of the Lapires talus slope. Even though the driving GST values were taken from this talus slope, this comparison can only be qualitative, as no temperature calibration has been attempted in our model and there are several differences between our model set-up and the real conditions. The most notable difference is the presence of a massive ice core at Lapires (Hilbich, 2010;
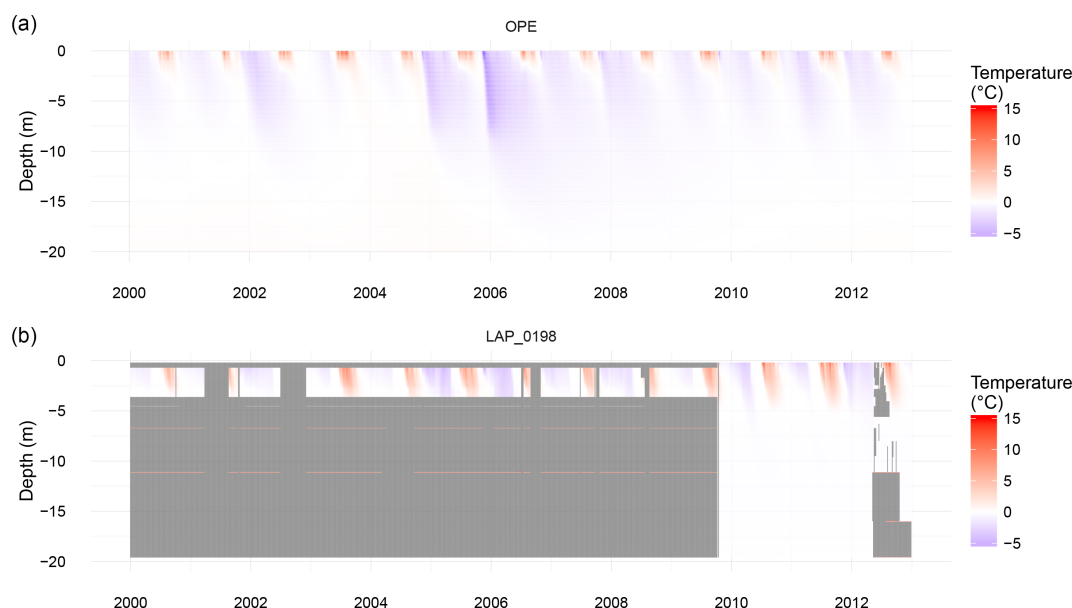
Figure 9. (a) Temperature plot along a perpendicular profile through node B for the OPE simulation for the 13-year period. **(b)** Borehole temperature from borehole LAP_0198 at the Lapires field site (PERMOS, 2016a). Missing values due to technical problems at greater depths are plotted in dark grey.

Scapozza et al., 2015), which was not included in our simulations. Although technical problems prevent a detailed analysis of the borehole temperatures until 2010, permafrost conditions are clearly present with an active layer thickness ranging between 4 and 6 m (PERMOS, 2016a). Generally, the simulated values are similar to the observed temperatures; however, a small cold bias can be identified in the model (see Fig. 9). As a result, the modelled active layer is thinner and the penetration depth of the winter cooling is greater than in the observations.

This may have several reasons. Firstly, the mean of the driving GST values of the logger LAP_S15 is colder than the mean of the uppermost temperature sensor in the borehole (Staub et al., 2015). Secondly, the massive ice core influences the ground thermal regime regarding (i) the induced air circulation patterns by blocking the air flow in a central region of the talus between 4 m and approximately 15 m depth, (ii) its different thermal properties from the air and rock material of the simulated talus slope and (iii) the latent heat necessary for phase changes. Finally, due to numerical effectivity, the depth to the bedrock was much lower in the model than in reality (Scapozza et al., 2015), which may have an additional effect on the observed discrepancies.

5.4 Model strengths and weaknesses

Modelling air circulation and thus the convective heat transfer within a talus slope is an important contribution to the understanding of the complex thermal regime of a talus slope in mountainous environments. The strength of this modelling approach lies in the fact that convective heat transfer is ex-

plicitly modelled in two dimensions, and it is a first step to an explicit description of this process in more sophisticated long-term permafrost models where ventilation has so far been neglected or only parameterized (Marmy et al., 2016; Luethi et al., 2016). Weaknesses mainly concern the lack of latent heat effects caused by melting or freezing of ice. The model domain in this study is assumed to be dry and hence there is no ice formation. This allows assessment the influence of the convective heat transfer by air flow in an isolated way but neglects the interaction of water, ice and air. In ice-rich talus slopes this interaction may have an important role but was beyond the scope of this study and should be part of future model improvements. Previous studies on the effect of convective heat transfer in porous media in permafrost environments also neglect the influence of water flow and assume the numeric domain to be dry (Goering and Kumar, 1996; Arenson et al., 2006, 2007; Guodong et al., 2007). The representation of snow is still quite poor. The interactions between the talus slope circulation and snow layer are complex and not yet fully understood. Melt holes due to warm air exits are frequently observed at the top of a talus slope (Morard, 2011) and probably have a significant impact on the air flow path and the air velocity. The pronounced ground cooling in the lower part may also influence the snow cover and some re-freezing of percolating meltwater may take place. Finally, the air block above the talus slope is a very simplified representation of the atmosphere. First of all, a pressure boundary condition could have been applied to link the talus slope to the atmosphere. Air flow at the boundary is not known and would have needed further parameterisations – so this approach was

33

dismissed. Secondly, we assume that the high thermal conductivity of air used in this study to some extent compensates the missing turbulent fluxes, which are prevented by the actual low air conductivity. This may affect the absolute values but allows numerically consistent simulations which represent the underlying process within the talus slope. Modelling the atmospheric air flow explicitly – for example, the effect of wind speed on the intra-talus circulation – would, however, strongly increase the complexity of the model.

6   Conclusions and outlook

A numerical study of convective heat transfer by air flow in a 2-D talus slope has been conducted. The results show that without forced convection a seasonally alternating circulation develops, which leads to a convective heat transfer within the talus and thus to a cooling effect in the lower part of the talus slope. It therefore has a significant influence on the thermal regime in a talus slope. Sensitivity studies with a conduction model show that this cooling can be crucial to maintain the frozen state of the ground during the warm season under warming climate conditions. Furthermore, sensitivity studies, using different atmospheric boundary conditions, were conducted by simulating a closed-to-atmosphere boundary, open-to-atmosphere boundary and seasonally closed-to-atmosphere boundary to represent the seasonal decoupling by a snow cover. The results show that an open-to-atmosphere boundary leads to the most efficient cooling. Compared to a conduction only set-up, a cooling of 0.28 °C (CLO), 0.94 °C (SEA) and 1.19 °C (OPE) was found in the lower part of the talus slope as mean value over the entire 13 years. Further sensitivity studies showed the dependence of strong cooling effects on a high air velocity in the ground as well as on an increase in slope angle. However, the circulation pattern does not change significantly in these cases.

So far, this phenomenon has mainly been documented by field studies (e.g. Delaloye et al., 2003; Gude et al., 2003; Sawada et al., 2003) and the explicit modelling of this process now confirms their findings. For simplicity, we neglected the formation of ice, which may be a reasonable assumption for low-elevation but not for high Alpine talus slopes (Delaloye and Lambiel, 2005; Morard et al., 2010; Hilbich, 2010; Scapozza et al., 2015). Furthermore the infiltration of meltwater and precipitation as well as intra-talus water flows (Luethi et al., 2016), which can lead to advective heat transfer and thus have an influence on the ground thermal regime, are neglected. This will have to be improved in a future study. Future work should therefore aim to model the internal air circulation for a specific site taking into account a more detailed structure like an impermeable ice core to get a better validation and site-specific quantifications of the process. Furthermore, efforts have to be made to understand the complex coupling of snow and air circulation within a talus slope.

The Supplement related to this article is available online at https://doi.org/10.5194/tc-11-1311-2017-supplement.

References

Arenson, L. U. and Sego, D. C.: Considering convective air fluxes in the design of engineered structures in cold regions, in: Proceedings of the 59th Canadian geotechnical conference and the seventh joint CGS/IAH-CNC groundwater specialty conference, 1–4 October 2006, Vancouver, British Columbia, Canada, 1–8, 2006.

Arenson, L. U. and Sego, D. C.: Protection of mine waste tailing ponds using cold air convection, in: Assessment and Remediation of Contaminated Sites in the Arctic and Cold Climates (ARCSACC), edited by: Biggar, K., Cotta, G., Nahir, M., Mullick, A., Buchko, J., Ho, A., and Guigard, S., Edmonton, AB, Canada, 256–264, 2007.

Arenson, L. U., Sego, D. C., and Newman, G.: The use of a convective heat flow model in road designs for Northern regions, in: IEEE EIC Climate Change Conference, 9–12 May 2006, Ottawa, Ontario, Canada, 1–8, 2006.

Arenson, L. U., Pham, H.-N., Klassen, R., and Sego, D. C.: Heat convection in coarse waste-rock piles, in: Proceedings of the 60th Canadian Geotechnical Society (CGS) conference and 8th joint CGS/IAH-CNC groundwater specialty conference, 21–24 October 2007, Ottawa, Ontario, Canada, 1500–1507, 2007.

Balch, E. S.: Glacieres, or Freezing Caverns, Allen Lane & Scott, Philadelphia, USA, 1900.

Cheng, G.: A roadbed cooling approach for the construction of Qinghai–Tibet Railway, Cold Reg. Sci. Technol., 42, 169–176, https://doi.org/10.1016/j.coldregions.2005.01.002, 2005.

Delaloye, R.: Contribution à l'étude du pergélisol de montagne en zone marginale, PhD Thesis, University Fribourg, Fribourg, Switzerland, 2004.

Delaloye, R. and Lambiel, C.: Evidence of winter ascending air circulation throughout talus slopes and rock glaciers situated in the lower belt of alpine discontinuous permafrost (Swiss Alps), Norsk Geogr. Tidsskr., 59, 194–203, https://doi.org/10.1080/00291950510020673, 2005.

Delaloye, R., Reynard, E., and Lambiel, C.: Pergélisol et construction de remontées mécaniques: l'exemple des Lapires (Mont-Gelé, Valais), Frost in der Geotechnik. Mitteilungen der Schweizerischen Gesellschaft für Boden- und Felsmechanik, 141, 103–113, 2001.

Delaloye, R., Reynard, E., Lambiel, C., Marescot, L., and Monnet, R.: Thermal anomaly in a cold scree slope (Creux du Van, Switzerland), in: Proceedings of the Eight International Conference on Permafrost, vol. 2125, 21–25 July 2003, Balkema, Zurich, Switzerland, 2003.

Etzelmüller, B.: Recent Advances in Mountain Permafrost Research, Permafrost Periglac., 24, 99–107, https://doi.org/10.1002/ppp.1772, 2013.

Funk, M. and Hoelzle, M.: A model of potential direct solar radiation for investigating occurrences of mountain permafrost, Permafrost Periglac., 3, 139–142, 1992.

Gądek, B. and Leszkiewicz, J.: Impact of climate warming on the ground surface temperature in the sporadic permafrost zone of the Tatra Mountains, Poland and Slovakia, Cold Reg. Sci. Technol., 79–80, 75–83, https://doi.org/10.1016/j.coldregions.2012.03.006, 2012.

GeoStudio: Air Flow Modeling with AIR/W2012. An Engineering Methodology. September 2013 Edition, GEO-SLOPE International, Ltd., Calgary, Alberta, Canada, 2013a.

GeoStudio: Seepage Modeling with SEEP/W2012. An Engineering Methodology. September 2013 Edition, GEO-SLOPE International, Ltd., Calgary, Alberta, Canada, 2013b.

GeoStudio: Thermal Modeling with TEMP/W2012. An Engineering Methodology. September 2013 Edition, GEO-SLOPE International, Ltd., Calgary, Alberta, Canada, 2013c.

Goering, D. J. and Kumar, P.: Winter-time convection in open-graded embankments, Cold Reg. Sci. Technol., 24, 57–74, https://doi.org/10.1016/0165-232X(95)00011-Y, 1996.

Gorbunov, A. P., Marchenko, S. S., and Seversky, E. V.: The thermal environment of blocky materials in the mountains of Central Asia, Permafrost Periglac., 15, 95–98, https://doi.org/10.1002/ppp.478, 2004.

Gruber, S. and Hoelzle, M.: The cooling effect of coarse blocks revisited: a modeling study of a purely conductive mechanism, in: Proceedings of the Ninth International Conference on Permafrost, 28 June–3 July 2008, Fairbanks, Alaska, USA, 2008.

Gubler, S., Fiddes, J., Keller, M., and Gruber, S.: Scale-dependent measurement and analysis of ground surface temperature variability in alpine terrain, The Cryosphere, 5, 431–443, https://doi.org/10.5194/tc-5-431-2011, 2011.

Gude, M., Hauck, C., Kneisel, C., Krause, S., Molenda, R., Ruzicka, V., and Zacharda, M.: Evaluation of permafrost conditions in non-alpine scree slopes in Central Europe by geophysical methods, EGS-AGU-EUG Joint Assembly, 6–11 April 2003, Nice, France, Vol. 1, p. 8966, 2003.

Guodong, C., Yuanming, L., Zhizhong, S., and Fan, J.: The "thermal semi-conductor" effect of crushed rocks, Permafrost Periglac., 18, 151–160, https://doi.org/10.1002/ppp.575, 2007.

Haeberli, W., Noetzli, J., Arenson, L., Delaloye, R., Gärtner-Roer, I., Gruber, S., Isaksen, K., Kneisel, C., Krautblatter, M., and Phillips, M.: Mountain permafrost: development and challenges of a young research field, J. Glaciol., 56, 1043–1058, https://doi.org/10.3189/002214311796406121, 2010.

Hanson, S. and Hoelzle, M.: The thermal regime of the active layer at the Murtèl rock glacier based on data from 2002, Permafrost Periglac., 15, 273–282, https://doi.org/10.1002/ppp.499, 2004.

Harris, C., Arenson, L., Christiansen, H., Etzelmüller, B., Frauenfelder, R., Gruber, S., Haeberli, W., Hauck, C., Hoelzle, M., Humlum, O., Isaksen, K., Kääb, A., Kern-Lütschg, M., Lehning, M., Matsuoka, N., Murton, J., Nötzli, J., Phillips, M., Ross, N., Seppälä, M., Springman, S., and Vonder Mühll, D.: Permafrost and climate in Europe: monitoring and modelling thermal, geomorphological and geotechnical responses, Earth Sci.Rev., 92, 117–171, 2009.

Harris, S. A. and Pedersen, D. E.: Thermal regimes beneath coarse blocky materials, Permafrost Periglac., 9, 107–120, 1998.

Herz, T., King, L., and Gubler, H.: Microclimate within coarse debris of talus slopes in the alpine periglacial belt and its effect on permafrost, in Proceedings of the Eighth International Conference on Permafrost, 21-25 July 2003, Balkema, Zurich, Switzerland, 383–387, 2003.

Hilbich, C.: Time-lapse refraction seismic tomography for the detection of ground ice degradation, The Cryosphere, 4, 243–259, https://doi.org/10.5194/tc-4-243-2010, 2010.

Hilbich, C., Hauck, C., Hoelzle, M., Scherler, M., Schudel, L., Völksch, I., Vonder Mühll, D., and Mäusbacher, R.: Monitoring mountain permafrost evolution using electrical resistivity tomography: A 7-year study of seasonal, annual, and long-term variations at Schilthorn, Swiss Alps, J. Geophys. Res., 113, F01S90, https://doi.org/10.1029/2007JF000799, 2008.

Juliussen, H. and Humlum, O.: Thermal regime of open-work block fields on the mountains Elgåhogna and Sølen, central-eastern Norway, Permafrost Periglac., 19, 1–18, https://doi.org/10.1002/ppp.607, 2008.

Kneisel, C., Hauck, C., and Vonder Mühll, D.: Permafrost below the Timberline Confirmed and Characterized by Geoelectrical Resistivity Measurements, Bever Valley, Eastern Swiss Alps, Permafrost Periglac., 11, 295–304, https://doi.org/10.1002/1099-1530(200012)11:4<295::AID-PPP353>3.0.CO;2-L, 2000.

Kneisel, C., Emmert, A., Polich, P., Zollinger, B., and Egli, M.: Soil geomorphology and frozen ground conditions at a subalpine talus slope having permafrost in the eastern Swiss Alps, CATENA, 133, 107–118, https://doi.org/10.1016/j.catena.2015.05.005, 2015.

Lambiel, C.: Le pergélisol dans les terrains sédimentaires à forte déclivité: distribution, régime thermique et instabilités, UNIL – Faculté des géosciences et de l'environnement – Institut de géographie, Lausanne, Switzerland, 2006.

Lambiel, C. and Pieracci, K.: Permafrost distribution in talus slopes located within the alpine periglacial belt, Swiss Alps, Permafrost Periglac., 19, 293–304, https://doi.org/10.1002/ppp.624, 2008.

Lebeau, M. and Konrad, J.-M.: Natural convection of compressible and incompressible gases in undeformable porous media under cold climate conditions, Comput. Geotech., 36, 435–445, https://doi.org/10.1016/j.compgeo.2008.04.005, 2009.

Luethi, R., Phillips, M., and Lehning, M.: Estimating non-conductive heat flow leading to intra-permafrost talik formation at Ritigraben rock glacier (Western Swiss Alps), Permafrost Periglac., 28, 183–194, https://doi.org/10.1002/ppp.1911, 2016.

Marmy, A., Rajczak, J., Delaloye, R., Hilbich, C., Hoelzle, M., Kotlarski, S., Lambiel, C., Noetzli, J., Phillips, M., Salzmann, N., Staub, B., and Hauck, C.: Semi-automated calibration method for modelling of mountain permafrost evolution in Switzerland, The Cryosphere, 10, 2693–2719, https://doi.org/10.5194/tc-10-2693-2016, 2016.

Meyer, C., Meyer, U., Pflitsch, A., and Maggi, V.: Analyzing airflow in static ice caves by using the calcFLOW method, The Cryosphere, 10, 879–894, https://doi.org/10.5194/tc-10-879-2016, 2016.

Morard, S.: Effets de la circulation d'air par effet de cheminée dans l'évolution du régime thermique des éboulis froids de basse et moyenne altitude, Université de Fribourg, Switzerland, 2011.

Morard, S., Delaloye, R., and Dorthe, J.: Seasonal thermal regime of a mid-latitude ventilated debris accumulation, in: Proceedings of the Ninth International Conference on Permafrost, 28 June–3 July 2008, Fairbanks, Alaska, USA, vol. 1, 1233–1238, 2008a.

Morard, S., Delaloye, R., and Lambiel, C.: Time-lapse Electrical Resistivity Tomography (ERT) to estimate temperature changes at depth in a low elevation ventilated cold talus slope (Dreveneuse, Swiss Prealps), in: Geophysical Research Abstracts, vol. 10, EGU2008-A-0952, 2008b.

Morard, S., Delaloye, R., and Lambiel, C.: Pluriannual thermal behavior of low elevation cold talus slopes in western Switzerland, Geogr. Helv., 65, 124–134, https://doi.org/10.5194/gh-65-124-2010, 2010.

Mottaghy, D. and Rath, V.: Latent heat effects in subsurface heat transport modelling and their impact on palaeotemperature reconstructions, Geophys. J. Int., 164, 236–245, https://doi.org/10.1111/j.1365-246X.2005.02843.x, 2006.

Noetzli, J., Hilbich, C., Hauck, C., Hoelzle, M., and Gruber, S.: Comparison of simulated 2D temperature profiles with time-lapse electrical resistivity data at the Schilthorn crest, Switzerland, in: Proceedings of the Ninth International Conference on Permafrost, 28 June–3 July 2008, Fairbanks, Alaska, USA, vol. 29, 1293–1298, 2008.

Pei, W., Zhang, M., Lai, Y., Jin, L., and Harbor, J.: Thermal stability analysis of crushed-rock embankments on a slope in permafrost regions, Cold Reg. Sci. Technol., 106, 175–182, https://doi.org/10.1016/j.coldregions.2014.07.005, 2014.

PERMOS: PERMOS Database, Swiss Permafrost Monitoring Network, Fribourg, Switzerland, https://doi.org/10.13093/permos-2016-01, 2016a.

PERMOS: Permafrost in Switzerland 2010/2011 to 2013/2014, edited by: Noetzli, J., Luethi, R., and Staub, B., Glaciological Report (Permafrost) No. 12–15 of the Cryospheric Commission of the Swiss Academy of Sciences, Fribourg, Switzerland, 85 pp., 2016b.

Pham, H.-N., Arenson, L. U., and Sego, D. C.: Numerical analysis of forced and natural convection in waste-rock piles in permafrost environments, in: Proceedings of the Ninth International Conference on Permafrost, 28 June–3 July 2008, Fairbanks, Alaska, USA, 2008.

Phillips, M., Mutter, E. Z., Kern-Luetschg, M., and Lehning, M.: Rapid degradation of ground ice in a ventilated talus slope: Flüela Pass, Swiss Alps, Permafrost Periglac., 20, 1–14, https://doi.org/10.1002/ppp.638, 2009.

Reid, T. D. and Brock, B. W.: An energy-balance model for debris-covered glaciers including heat conduction through the debris layer, J. Glaciol., 56, 903–916, https://doi.org/10.3189/002214310794457218, 2010.

Sawada, Y., Ishikawa, M., and Ono, Y.: Thermal regime of sporadic permafrost in a block slope on Mt. Nishi-Nupukaushinupuri, Hokkaido Island, Northern Japan, Geomorphology, 52, 121–130, https://doi.org/10.1016/S0169-555X(02)00252-0, 2003.

Scapozza, C.: Stratigraphie, morphodynamique, paléoenvironnements des terrains sédimentaires meubles à forte déclivité du domaine périglaciaire alpin, PhD Thesis, University Lausanne, Lausanne, Switzerland, 2013.

Scapozza, C., Baron, L., and Lambiel, C.: Borehole Logging in Alpine Periglacial Talus Slopes (Valais, Swiss Alps), Permafrost and Periglac., 26, 67–83, https://doi.org/10.1002/ppp.1832, 2015.

Schär, C., Vidale, P. L., Lüthi, D., Frei, C., Häberli, C., Liniger, M. A., and Appenzeller, C.: The role of increasing temperature variability in European summer heatwaves, Nature, 427, 332–336, https://doi.org/10.1038/nature02300, 2004.

Scherler, M., Hauck, C., Hoelzle, M., and Salzmann, N.: Modeled sensitivity of two alpine permafrost sites to RCM-based climate scenarios, J. Geophys. Res.-Earth, 118, 780–794, https://doi.org/10.1002/jgrf.20069, 2013.

Scherler, M., Schneider, S., Hoelzle, M., and Hauck, C.: A two-sided approach to estimate heat transfer processes within the active layer of the Murtèl–Corvatsch rock glacier, Earth Surf. Dynam., 2, 141–154, https://doi.org/10.5194/esurf-2-141-2014, 2014.

Schneider, S.: The heterogeneity of mountain permafrost – A field-based analysis of different periglacial materials, PhD Thesis, University of Fribourg, Switzerland, 176 pp., 2014.

Schneider, S., Hoelzle, M., and Hauck, C.: Influence of surface and subsurface heterogeneity on observed borehole temperatures at a mountain permafrost site in the Upper Engadine, Swiss Alps, The Cryosphere, 6, 517–531, https://doi.org/10.5194/tc-6-517-2012, 2012.

Staub, B., Marmy, A., Hauck, C., Hilbich, C., and Delaloye, R.: Ground temperature variations in a talus slope influenced by permafrost: a comparison of field observations and model simulations, Geogr. Helv., 70, 45–62, https://doi.org/10.5194/gh-70-45-2015, 2015.

Stiegler, C., Rode, M., Sass, O., and Otto, J.-C.: An Undercooled Scree Slope Detected by Geophysical Investigations in Spo-

radic Permafrost below 1000 m a.s.l., Central Austria, Permafrost Periglac., 25, 194–207, https://doi.org/10.1002/ppp.1813, 2014.

Tanaka, H. L., Nohara, D., and Yokoi, M.: Numerical simulation of wind hole circulation and summertime ice formation at Ice Valley in Korea and Nakayama in Fukushima, Japan, J. Meteorol. Soc. Jpn., 78, 611–630, 2000.

Tanaka, H. L., Nohara, D., and Byun, H.-R.: Numerical Simulation of Wind Hole Circulation at Ice Valley in Korea Using a Simple 2D Model, J. Meteorol. Soc. Jpn. Ser. II, 84, 1073–1084, https://doi.org/10.2151/jmsj.84.1073, 2006.

Wakonigg, H.: Unterkühlte Schutthalden, Beiträge zur Permafrostforschung in Österreich. Arbeiten aus dem Institut für Geographie der Karl-Franzens-Universität Graz, 33, 209–223, 1996.

Wegmann, M., Gudmundsson, G. H., and Haeberli, W.: Permafrost changes in rock walls and the retreat of Alpine glaciers: a thermal modelling approach, Permafrost Periglac., 9, 23–33, 1998.

Zacharda, M., Gude, M., Kraus, S., Hauck, C., Molenda, R., and Ružička, V.: The relict mite Rhagidia gelida (Acari, Rhagidiidae) as a biological cryoindicator of periglacial microclimate in European highland screes, Arct. Antarct. Alp. Res., 37, 402–408, https://doi.org/10.1657/1523-0430(2005)037[0402:TRMRGA]2.0.CO;2, 2005.

Zacharda, M., Gude, M., and Růžička, V.: Thermal regime of three low elevation scree slopes in central Europe, Permafrost Periglac., 18, 301–308, https://doi.org/10.1002/ppp.598, 2007.

Zhang, M., Lai, Y., Liu, Z., and Gao, Z.: Nonlinear analysis for the cooling effect of Qinghai-Tibetan railway embankment with different structures in permafrost regions, Cold Reg. Sci. Technol., 42, 237–249, https://doi.org/10.1016/j.coldregions.2005.02.003, 2005.

The Cryosphere

Supplement of

Numerical modelling of convective heat transport by air flow in permafrost talus slopes

Jonas Wicky and Christian Hauck

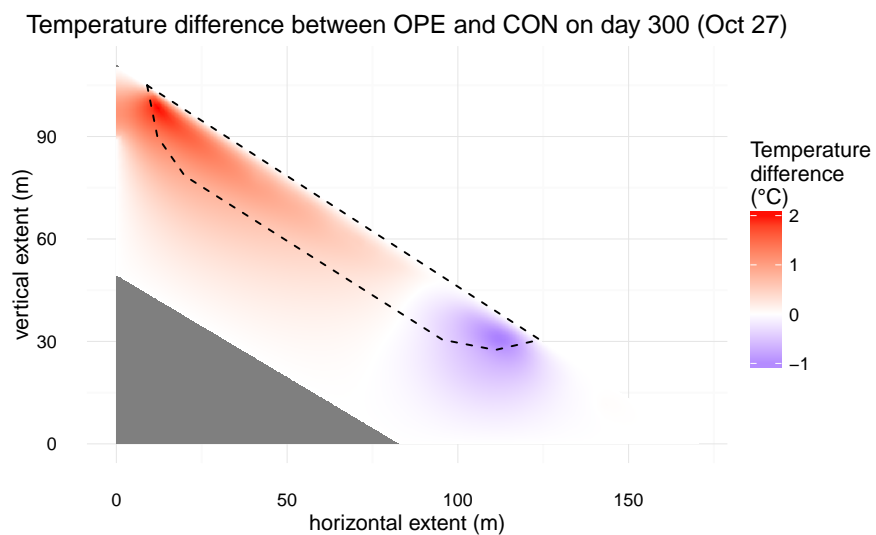*Correspondence to:* Jonas Wicky (jonas.wicky@unifr.ch)

Figure S1. Simulated temperature difference (colours) in the talus slope between the open (OPE) and the conduction only (CON) experiment for day 300 (winter circulation).

5.2 Paper II

Paper II examines the convective heat transfer in the active layer of rock glaciers. The model is set up within the model environment COMSOL Multiphysics 5.3 and solves for heat transfer through conduction as well as for convective air flow within the porous domain described by Darcy's law adopting a Boussinesq approximation for the buoyancy-driven free convection. Murtèl rock glacier below Piz Corvatsch and Schafberg rock glacier above Pontresina in the Engadin, Eastern Swiss Alps are modelled to represent typical yet different examples of alpine rock glaciers. For both, a long-term high-quality dataset exists, and both sites show a long research history. For both of the rock glaciers, borehole data is used for model forcing and validation.

Title: Air Convection in the Active Layer of Rock Glaciers.

Author contributions: Jonas Wicky designed and performed the model calculations and analysed the data, produced all the figures, and wrote the manuscript with substantial inputs from Christian Hauck.

Reference: Wicky, J. and Hauck, C. (2020). Air Convection in the Active Layer of Rock Glaciers. Frontiers in Earth Science 8: 335.

Air Convection in the Active Layer of Rock Glaciers

Jonas Wicky* and Christian Hauck

Department of Geosciences, University of Fribourg, Fribourg, Switzerland

Coarse blocks are an abundant surface cover in mountainous permafrost landscapes. In this coarse blocky layer, air convection occurs and has a significant influence on the ground thermal regime of the underlying permafrost. Besides heat transfer through conduction, free convection of air takes place seasonally and leads to a pronounced ground cooling. Air convection has been observed and described in many field studies but is often neglected or parametrized in permafrost modeling. In the present study, air convection in the active layer of rock glaciers is explicitly modeled through a heat conduction equation coupled with Darcy's law over a two-dimensional geometry. With a series of numerical experiments, we show its effects on the thermal regime of the underlying permafrost. The ground permeability and the thermal gradient in the active layer are the most important parameters for air convection in the ground. On field sites with a high ground permeability (order of magnitude 10^{-6} m^2), convection plays a crucial role and is required to correctly model measured borehole temperatures. The onset of natural convection occurs at critical Rayleigh numbers and is characterized by an increase of the standard deviation of the direction and the vorticity of the airflow field in the active layer. In the numerical solutions, the internal air circulation in the coarse blocky surface layer leads to an efficient ground cooling.

Keywords: rock glacier, convection, active layer, two-dimensional modeling, heat transfer, permafrost

INTRODUCTION

Permafrost, lithospheric material with a temperature below $0°C$ for at least two consecutive years, is found in mountainous regions all over the world. Permafrost as a thermal phenomenon is affected by the recent climate change at a global scale (Biskaborn et al., 2019). Changes in the thermal state of permafrost influence natural hazards, such as rock fall and slope instabilities (Gruber and Haeberli, 2007; Draebing et al., 2017; Myhra et al., 2019). Furthermore, the future contribution of permafrost water resources to the hydrological cycle is debated and may play an important role in some regions (Jones et al., 2018). A thorough understanding of the thermal processes governing the ground thermal regime is thus of great interest. Considerable effort has been undertaken to represent mountain permafrost in numerical models. These model approaches range from (i) statistical approaches to map permafrost (Keller, 1992; Boeckli et al., 2012; Deluigi et al., 2017), (ii) physically based permafrost distribution models (Hoelzle et al., 2001; Stocker-Mittaz et al., 2002; Noetzli and Gruber, 2009; Westermann et al., 2013; Haberkorn et al., 2017) to (iii) process oriented permafrost soil modeling studies (Gruber and Hoelzle, 2008; Scherler et al., 2013, 2014; Marmy et al., 2016; Luethi et al., 2017; Pruessner et al., 2018; Cicoira et al., 2019).

Whereas the energy balance at the surface as well as heat conduction and phase changes in the subsurface are explicitly included in many of the two last (ii & iii) model groups, current approaches of modeling ground temperatures in a permafrost context usually neglect or parametrize air convection processes within the ground. They become especially important in coarse blocky surface and subsurface material, which is abundant in mountainous regions. The role of air convection in the ground is also discussed in unfrozen soils (Weisbrod et al., 2009; Moore et al., 2011; Levintal et al., 2017), but ample field investigations have been done in a permafrost context in different regions (Harris and Pedersen, 1998; Kneisel et al., 2000; Delaloye et al., 2003; Sawada et al., 2003; Hanson and Hoelzle, 2004; Delaloye and Lambiel, 2005; Gubler et al., 2011; Morard et al., 2012; Schneider et al., 2012; Popescu et al., 2017). These studies clearly show that especially in coarse blocky material with a high permeability, convection has a significant influence on the ground thermal regime. Convection in this context generally results in colder ground temperatures and thus a higher favorability for the occurrence of permafrost. Rock glaciers are a characteristic landform in the coarse-grained substrates in mountain permafrost terrain and often used as an indicator of permafrost (Barsch, 1996). They are composed of blocks up to 10 m diameter, block size may vary depending on the site and lithology, and voids filled or supersaturated with ice (Arenson et al., 2002). The active layer, the seasonal thaw layer at the surface, can be several meters thick. On many rock glaciers, the active layer is composed of coarse blocks, where the voids are not sealed by ice and allow for air convection. Different authors discussed this mechanism, either regarding vertical convection (Balch, 1900; Guodong et al., 2007) or two-dimensional advection, also referred to as the "chimney effect" (Wakonigg, 1996). Previous studies modeling ground temperatures in rock glaciers propose a parametrization to represent ground convection, Scherler et al. (2014) use a calibrated seasonal heat source-sink term and Pruessner et al. (2018) use calibrated ventilation parameters, fitted to a specific site. Both studies highlight the importance of convection in the active layer, and encourage more in-depth investigations to characterize ground convection. An explicit physically based modeling of convection is therefore crucial to better understand the ground thermal regime and to improve future estimates of permafrost evolution. With the development and the application of such a model, the uncertainty of a convection parametrization can be reduced and the process itself can be better understood and quantified.

In this study, we show the effect of convection on the ground thermal regime of a rock glacier in a two-dimensional numerical modeling approach. We explicitly model air convection, which allows quantifying the influence of convection. We thereby refer to well approved modeling approaches in engineering sciences, where the passive cooling capacities of crushed rocks were extensively studied (Goering and Kumar, 1996; Arenson and Sego, 2006; Guodong et al., 2007; Pham et al., 2008; Lebeau and Konrad, 2009, 2016; Sun et al., 2010; Darrow and Jensen, 2016) and to an attempt of explicit convection

modeling in a coarse blocky talus slope presented by Wicky and Hauck (2017) with a focus on the simulation of heat advection along a slope. Compared to Wicky and Hauck (2017), the model approach evolved. Pointwise validation and thus a good estimate of the model performance, as well as the quantification of the contribution of ground convection to the ground temperatures, are possible. Switching to the modeling environment COMSOL Multiphysics leads to a purely equation-based modeling approach, which allows the proper formulation of natural convection in a porous media context and thus a meaningful comparison to published studies. Further, the formulation of pressure boundaries is possible; the model represents also ground ice and is, thanks to more sophisticated solvers, more robust and able to handle relatively complicated boundary conditions and geometries. Our study aims to (i) present an explicit two-dimensional model framework within COMSOL for air convection in the porous active layer of rock glaciers, (ii) assess its dependency on driving variables and site properties and (iii) compare its performance for two rock glaciers in the Eastern Swiss Alps with a different thermal behavior.

MODEL DESCRIPTION

We model over a simplified two-dimensional geometry and use forcing data from two different rock glaciers in the Swiss Alps. Of both rock glaciers exist long-time and continuous ground temperature data sets and they have different characteristics that allow a comparison and thus a more in-depth comprehension of the main driving variables in the convection process. We focus on improving the understanding of convection processes on an idealized set up and not to exactly model a specific site. In contrast to most model approaches cited above, no calibration has been done on the model as this may hinder a proper interpretation of the processes afterward. We solve the heat conduction equation coupled with a Darcy equation, including the Boussinesq-Oberbeck approximation to account for density driven buoyancy effects in the airflow within the porous media (*cf* section "Governing Equations"). The aforementioned equations are numerically solved using the finite element method (FEM) with the commercially available software environment COMSOL Multiphysics 5.4.

Governing Equations

The governing equations are described in Nield and Bejan (2017) and COMSOL (2018a). The nomenclature with units can be found in **Appendix A**. Eqs 1 and 2 govern the heat transfer by conduction and convection, where q is the heat flux, Q is a heat source (sink) term (which we do not apply), q_0 the boundary flux, k the (effective) thermal conductivity, C_p the (effective) volumetric heat capacity, ρ the density, V the velocity, T the temperature and t the time.

$$\rho C_p \frac{\partial T}{\partial t} + \rho C_p V \nabla T + \nabla q = Q + q_0 \qquad (1)$$

$$q = -k \nabla T \qquad (2)$$

Airflow in the porous medium is described in Eqs 3 and 4, where Φ is the porosity, Q_m the boundary flux, κ the permeability, μ the dynamic viscosity, g the gravitational acceleration and p the pressure.

$$\frac{\partial}{\partial t} (\Phi \rho) + \nabla (\rho V) = Q_m \tag{3}$$

$$V = -\frac{\kappa}{\mu}(\nabla p - \rho g) \tag{4}$$

In two dimensions, the velocity V is a two-component vector $V = (u, v)$. To characterize the air flow vector field the vorticity ζ, described in Eq. 5 (Wallace and Hobbs, 2006), which is equal to the curl of the two dimensional vector field, and the angle of the flow direction d (Eq. 6) are used in the results section.

$$\zeta = \nabla \times V = \left(\frac{\partial v}{\partial x} - \frac{\partial u}{\partial y}\right) \tag{5}$$

$$d = \tan^{-1}\frac{v}{u} \tag{6}$$

Rayleigh Number

Eq. 7 describes the Rayleigh number as used in this study with C_a the specific heat capacity of air, β the coefficient of thermal expansion, H the vertical dimension of the active layer and ΔT the temperature difference within the active layer.

$$Ra = \frac{\rho^2 C_a \, g \, \beta \, \kappa \, H \, \Delta T}{\mu \, k} \tag{7}$$

The dimensionless Rayleigh (or Rayleigh-Darcy) number Ra describes the potential and the strength of natural convection in a porous media, using the ratio of buoyancy to viscous forces (Kane et al., 2001; Nield and Bejan, 2017). We use this dimensionless number in the results and discussion sections to characterize the convection in the active layer. It has widely been used to analyze natural convection in a permafrost context (Kane et al., 2001; Herz, 2006; Guodong et al., 2007; Wagner et al., 2019).

Ra describes the onset of natural convection when a critical threshold value is reached and thus the buoyancy forces exceed the viscous forces. This threshold is referred as the critical Rayleigh number Ra_{crit} (Kane et al., 2001; Nield and Bejan, 2017). Nield and Bejan (2017) derive theoretical values for Ra_{crit} for an infinitely extended horizontal porous layer heated from below (Horton-Rodgers-Lapwood problem) to be between 3 to $4\pi^2$ depending on the pressure and temperature boundary conditions. In numerical studies on passive cooling in an engineering context the value of $Ra_{crit} = 4\pi^2$ has become established (Goering and Kumar, 1996; Guodong et al., 2007; Pham et al., 2008; Lebeau and Konrad, 2009). Further, studies analyzing temperature data in a permafrost context adopted a critical threshold of ~40 (Juliussen and Humlum, 2008; Wagner et al., 2019). Hence, in the following $Ra_{crit} = 4\pi^2$ (39.42) is used.

Field Sites and Forcing Data

Temperature data measured at the uppermost thermistor in a borehole on Murtèl-Corvatsch (abbr. *COR*) and Schafberg (abbr. *SBE*) rock glacier, both located in the Upper Engadin valley, Eastern Swiss Alps (**Figure 1**), serve as forcing data at the upper boundary of the model. Temperature at lower depths is used for model validation and discussion. The Swiss permafrost monitoring network PERMOS provides the data (Permos, 2019). Both data series have several gaps due to technical failures. To obtain continuous data, a gap filling method using the approach described by Staub et al. (2017) was performed. Gaps up to 5 days were filled with a linear regression, whereas longer gaps were filled with a quantile mapping approach, using data from 61 different ground surface temperature loggers from the Swiss Alps (Permos, 2019). The gap filled temperature data can be found in the **Supplementary Material** section.

Murtèl-Corvatsch rock glacier (coordinates WGS 84 lat/lon 46.42880, 9.82182; front elevation 2,640 m a.s.l.; **Figure 1**) located above Surlej is probably one of the best-studied rock glaciers in the world. A first borehole, which is still operational, was drilled in 1987 (COR0287, Haeberli et al., 1988). Two other boreholes were drilled in 2000 (Vonder Mühll et al., 2003; Arenson et al., 2010), one of which is still operational, but shows signals of possible water infiltration in the casing (Permos, 2019). In 2015 a new borehole COR0315 was drilled close to the 1987 borehole to ensure the continuity of the data series in case of failure of the old borehole COR0287 (Permos, 2019). Geophysical investigations (Vonder Mühll and Haeberli, 1990; Vonder Mühll et al., 2000; Arenson et al., 2002; Maurer and Hauck, 2007; Hilbich et al., 2009) provide a detailed description of the internal structure.

The simulation period at COR extends over the hydrological years 2001–2018. Data from borehole COR0287 is used until January 2016 and from then onward, the thermistor at the same depth from the COR0315 borehole serves as upper boundary. The temperature data from the new borehole matches the old measurements well (Permos, 2019), but shows smoother data close to the surface.

Schafberg rock glacier (coordinates WGS 84 lat/lon 46.49881, 9.92521; front elevation 2,730 m a.s.l., **Figure 1**) is located above Pontresina and has a long research history (Vonder Mühll and Holub, 1992). Two boreholes are operational within the PERMOS network (Permos, 2019). Schafberg rock glacier is a more complex landform with several lobes. The boreholes are not within the same lobes; we use data from the lower borehole 0290, mainly because data is of higher quality and shows less gaps.

The simulation period extends over the hydrological years 2001–2016. The model runs only until 2016 because the SBE site has a data gap of more than a year from mid-July 2017 onward.

MODEL SETUP

Geometry

The geometry is a simplified schematic representation of a rock glacier (**Figure 2**). Three domains are represented by different polygons: the active layer, the rock glacier body and the underlying bedrock. Slope angle and thickness of each domain are chosen according to site characteristics (**Table 1**). The vertical extent is fixed to 150 m to avoid boundary effects. Temperature profiles for comparison to the
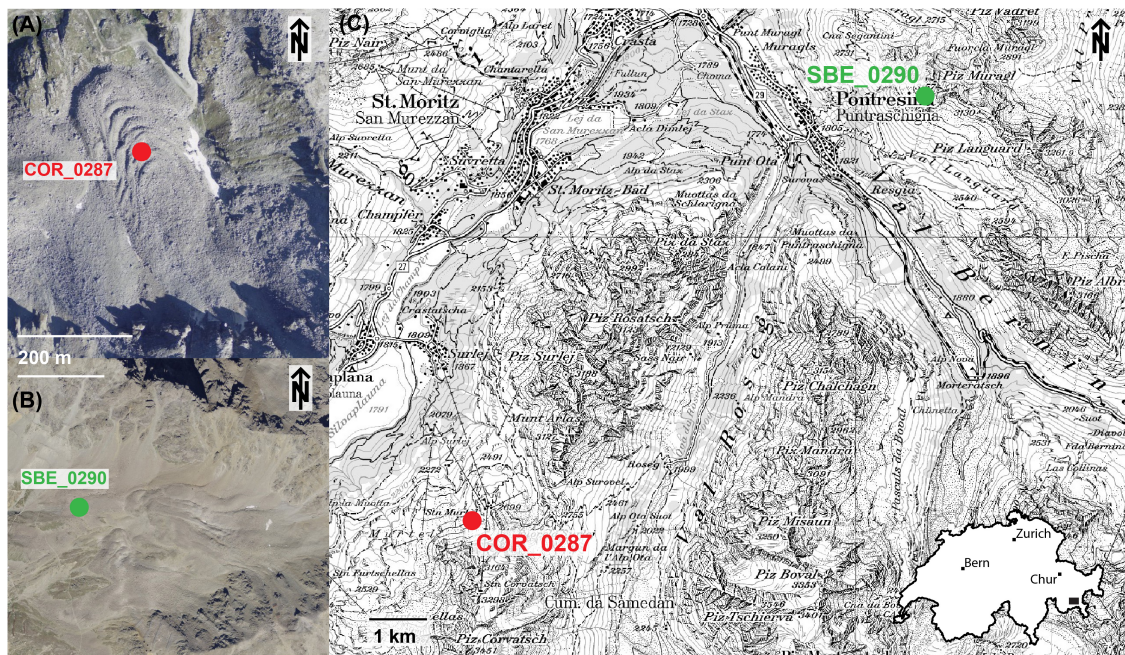
FIGURE 1 | Aerial images of the Corvatsch – Murtel **(A)** and the Schafberg **(B)** rock glacier with the location of the PERMOS boreholes, situated in the Upper Engadin valley, Eastern Swiss Alps **(C)**. Source: Swiss Federal Office of Topography swisstopo.
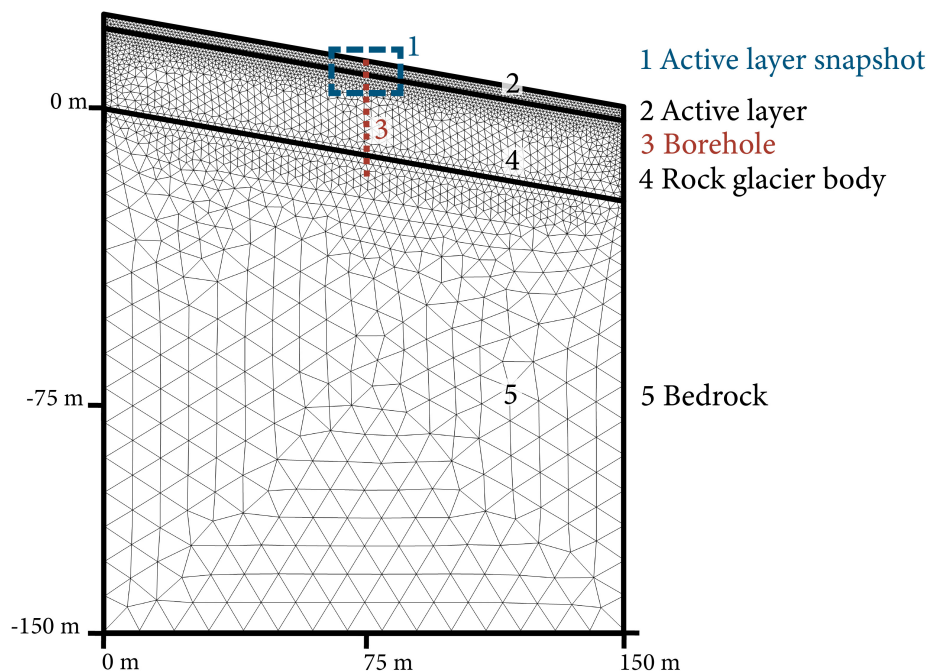

FIGURE 2 | Geometry with the different domains (black) and the meshing. The site respective parameters are given in **Table 1**. The red dotted line (3) indicates the position of the virtual borehole and the blue dashed rectangle (1) the location of the active layer snapshots in the results section (**Figures 6**, **7**).

borehole data are taken in the middle of the geometry. The mesh is composed of triangular elements. In the active layer, the maximum mesh size is of 0.5 m increasing to 11 m at the lower boundary. Mesh dependency tests showed that this setting yields a good representation of the convective process in the active layer, yet numerically stable results and it is a good compromise between accuracy and computational cost.

TABLE 1 | Properties of the geometry for COR and SBE.

	Slope angle (°)	Active layer thickness (m)	Rock glacier thickness (m)
COR	10	4	27
SBE	15	5	25

TABLE 2 | Material properties.

	Active layer (granite/air)	Rock glacier body (ice/water)	Bed rock
Heat capacity ($J kg^{-1} K^{-1}$)	850/temperature dependent	2052/4179	850
Thermal conductivity ($W m^{-1} K^{-1}$)	2.9/temperature dependent	2.31/0.613	2.9
Density ($kg m^{-3}$)	2600/temperature dependent	918/997	2600
Permeability (m^2)	1×10^{-7}, 1×10^{-6}, 3×10^{-6}	0	0
Porosity	0.5	0	0

Material Properties

The physical material properties are shown in **Table 2**. Thermal conductivity, heat capacity and density values are chosen from the COMSOL material library (COMSOL, 2018b) for granite, air and ice respectively water. The physical properties chosen for granite are in the range of previous publications (Noetzli and Gruber, 2009; Pruessner et al., 2018) and correspond also to values published for granite and gneiss by Cermak and Rybach (1982) and Vonder Mühll and Haeberli (1990). No difference is made in the rock material properties for COR and SBE, even though the lithology is different at each of the sites. Because the ranges of thermal properties for COR (mainly granodiorite) and SBE (gneiss) overlap (Cermak and Rybach, 1982; Vonder Mühll and Haeberli, 1990) we prefer to keep model parameters similar when no direct evidence for exact values (laboratory values) are available. Moreover, sensitivity studies (*cf* section "Site Dependence") confirm the findings of Arenson and Sego (2006) that small changes in heat capacity and heat conductivity play a subordinate role in comparison to convective heat transfer. The material properties are thus neither calibrated, nor do we use apparent or measured thermal properties as suggested by other authors (Gruber and Hoelzle, 2008; Schneider et al., 2012).

The active layer is composed of a porous material. The porosity defines the volume ratio of air to granite. Heat conduction is calculated with an effective heat capacity and conductivity obtained through volume averaging. The permeability refers to an intrinsic permeability (Nield and Bejan, 2017), the relevant parameter for convective airflow in the porous media. In a permafrost context, it is not feasible to measure permeability directly on site. The chosen permeability values are in the range of the experimental values of 0.7×10^{-6} m^2 to 3.9×10^{-6} m^2 obtained by Côté et al. (2011) for crushed rock in a permafrost context and can as well be approximated with the Kozeny-Carman equation (Johansen, 1975, *cf* section "Permeability"). Regarding the high sensitivity and uncertainty of permeability, the model solves for three different values: a permeability of 1×10^{-7} m^2, where conduction dominates the heat transfer process, as well as values of 1×10^{-6} m^2 and 3×10^{-6} m^2, which are in the range given by Côté et al. (2011) to represent the convective effects. Heat capacity and thermal conductivity for air are temperature dependent and updated at each time step (COMSOL, 2018b). The air density is pressure and temperature dependent, described by the ideal gas law, which is a prerequisite to represent natural convection effects.

The rock glacier body is composed of ice and considers phase change. Borehole geophysics at COR report a very high ice content of up to 100% (Haeberli et al., 1988), whereas at SBE lower values are reported reaching 80% in the main part (Vonder Mühll and Holub, 1992). Heat transfer in the rock glacier body is

governed only by conduction and the porosity is assumed to be zero. The representation of phase change in a numerical model potentially leads to very high temperature gradients on a small spatial scale and is therefore prone to numerical instabilities. To mitigate these numerical instabilities and allow for coherent results, two measures are taken: (i) we apply a freezing function with a freezing interval dT around the phase change temperature of 0°C, where the material properties linearly change and the latent heat is added to the heat capacity (COMSOL, 2018b) and (ii) the latent heat is linearly ramped up over the whole rock glacier domain to reach the latent heat of fusion of ice of 333.5 kJ at the base of the rock glacier. The freezing interval dT has a high influence on the numerical stability and the computational cost and was therefore optimized through numerical tests. At COR a uniform dT of 1 K is applied in all model runs. At SBE, the boundary data is less smooth and thus dT is adapted accordingly and set to 0.3, 0.8, and 2 K for the respective permeability of 1×10^{-7} m^2, 1×10^{-6} m^2 and 3×10^{-6} m^2.

In the model set up for both sites, the underlying bedrock is composed of granite, where conduction is assumed the dominant heat transfer process. Hence, the model solves in the bedrock only for heat conduction (Eqs 1 and 2) for a non-porous medium.

Boundary Conditions

The upper thermal boundary is of Dirichlet type with a temperature series measured at the uppermost thermistor of the respective borehole (*cf* section "Field Sites and Forcing Data"; Permos, 2019). The uppermost thermistor is located at a depth of 0.55 m at COR for the borehole COR0287 and at 0.5 m for the new borehole COR0315. For SBE, the uppermost thermistor is at a depth of 0 m. The simulation period extends over the hydrological years 2000–2018 for COR and 2000–2016 for SBE. The lower thermal boundary is of Neumann type with a constant geothermal heat flux of 0.03 W m^{-2} (Scherler et al., 2013) for both sites. The sidewalls are insulated. Pressure conditions at the upper model boundary are set to atmospheric, which is represented by an altitude dependent zero pressure head. Sidewalls and bottom boundaries do not allow for any airflow.

The boundary data is available as daily values. Therefore, time steps are constrained to the maximum length of one day. The

solver internally defines the optimal time step size through an adaptive time stepping scheme to favor numerical convergence (COMSOL, 2018a).

Initial Conditions

To obtain proper initial conditions we applied a two-step procedure. First, we perform a steady-state spin up. The lower thermal boundary is prescribed by the geothermal heat flux of 0.03 W m^{-2}, whereas the upper boundary is the mean of the site-respective complete temperature data measurements. In a second step, the results of the steady-state run serve as initial conditions for a 30-years transient spin up run. The lower boundary in the transient spin up is yet again a constant geothermal heat flux, whereas the upper boundary consists of the daily median temperature from the site-respective temperature data series, repeated over the years. Numerical tests showed that with this setting a quasi-equilibrium state is reached after 30 years. This temperature field then serves as initial condition for the transient model runs. Previous modeling studies show vast ranges of spin-up times from decades (Scherler et al., 2013; Marmy et al., 2016) to several hundred years (Darrow and Jensen, 2016). Whereby this spin up period is also often used for calibration, it serves in our case only to obtain stable initial conditions. Other authors (e.g., Pruessner et al., 2018) also use measured temperatures as initial conditions. In the context of this study, we prefer using the borehole data at depth only for validation and not to precondition the model.

RESULTS

For COR, the simulation period extends over 18 hydrological years from 2001 to 2018; whereas at SBE the simulation period extends over 16 hydrological years, from 2001 to 2016. For both sites, a spin up (section "Initial Conditions") was performed. Then, based on these initial conditions, three model runs per site with three different permeability values were conducted. The permeability values range from 1×10^{-7} m^2, where conduction dominates the heat transfer regime, to 3×10^{-6} m^2, where convection is shown to have a high influence on the ground thermal regime.

Temperature

Figures 3, **4** show the temperature evolution in a virtual borehole in the middle of the model domain (**Figure 2**) in comparison with measured borehole data at COR and SBE respectively for four typical depths: (A) in the active layer (COR 2.55 m, SBE 3.2 m), (B) just below the active layer (4.55 m, 7.2 m), (C) at roughly 10 m depth (9.55 m, 9.2 m) and (D) at roughly 20 m depth (21.56 m, 21.2 m), where the zero annual amplitude is reached. Simulation results with all three modeled permeability values are represented in **Figures 3**, **4**. The differences in temperature at depth respective to the permeability are well visible. The higher the permeability, the higher also the influence of convection in the active layer on the ground temperatures. With increasing permeability, the temperature amplitude increases at all depths and ground temperatures are

lower. Regardless of the fit to the measured data, the strong ground cooling induced by convection is evident in both modeled temperature series.

For COR, the highest permeability of 3×10^{-6} m^2 value yields the best agreement with observations, whereas at SBE a lower permeability of 1×10^{-6} m^2 shows the best agreement with the measured data. This is shown in **Figure 5**, where the differences between modeled and measured temperatures are plotted. Note that the two peaks in the years 2003/04 at SBE in **Figure 5D** (as also **Figure 4D**) are probably due to technical problems in the measurements, as well as the noisy data in the years 2009–2012 at a depth of 21.56 m at COR (**Figures 3D**, **5B**). Both sites show discrepancies within the active layer. As dry conditions are assumed in the active layer in the model, no phase change takes place and the zero curtain, the period where temperature stays at 0°C due to latent heat exchange, cannot be represented. This effect is more pronounced at SBE. It is also important to note that the temperatures at SBE are in general closer to the melting point and thus much more affected by latent heat effects. As the freezing function has an interval dT of at least 0.3 K, modeled temperatures within this range differ from measured data. This is most visible at a depth of 21.2 m at SBE, where the temperatures for higher permeability values are dampened by the latent heat due to a higher dT and show therefore no increase.

Convection Regime

Distinct circulation patterns can be observed in the active layer depending on the permeability and the forcing temperature (**Figure 6**). The circulation shows a clear seasonality. Summertime is characterized by a gentle gravitational down flow with low vorticity. Conduction dominates the thermal regime. Temperature propagates right-angled to the surface through the active layer. Wintertime convection is more complex and highly depending on the material properties and the thermal gradient (respective the Rayleigh number – *cf* section "Air Flow Field and Rayleigh Number"). Two different situations can occur – for a low permeability and small thermal gradients in the active layer, a gentle density driven up-flow of air takes place within the active layer (**Figure 6A**). Its influence on the thermal regime is comparably small and conduction is the dominant heat transfer process. However, if thermal gradient and permeability are high enough (and thus the critical Rayleigh number is reached, Eq. 7; **Table 3**) the onset of free convection can be observed. Multicellular vertical convection, sometimes also referred to as Rayleigh-Bénard convection (Guodong et al., 2007; Nield and Bejan, 2017), takes place in the active layer. The multicellular convection leads to an efficient propagation of cold temperatures into the ground (**Figure 6B**). As this buoyancy driven multicellular convection occurs only in winter when low air temperatures are present, a highly permeable active layer acts as a thermal filter. When the thermal gradient in the active layer is negative, the cooling is enhanced due to convective heat transfer. With a positive temperature gradient in the active layer, conduction is the dominant process, yet not very effective due to the high air content in the active layer and the corresponding low thermal conductivity. Ground temperatures
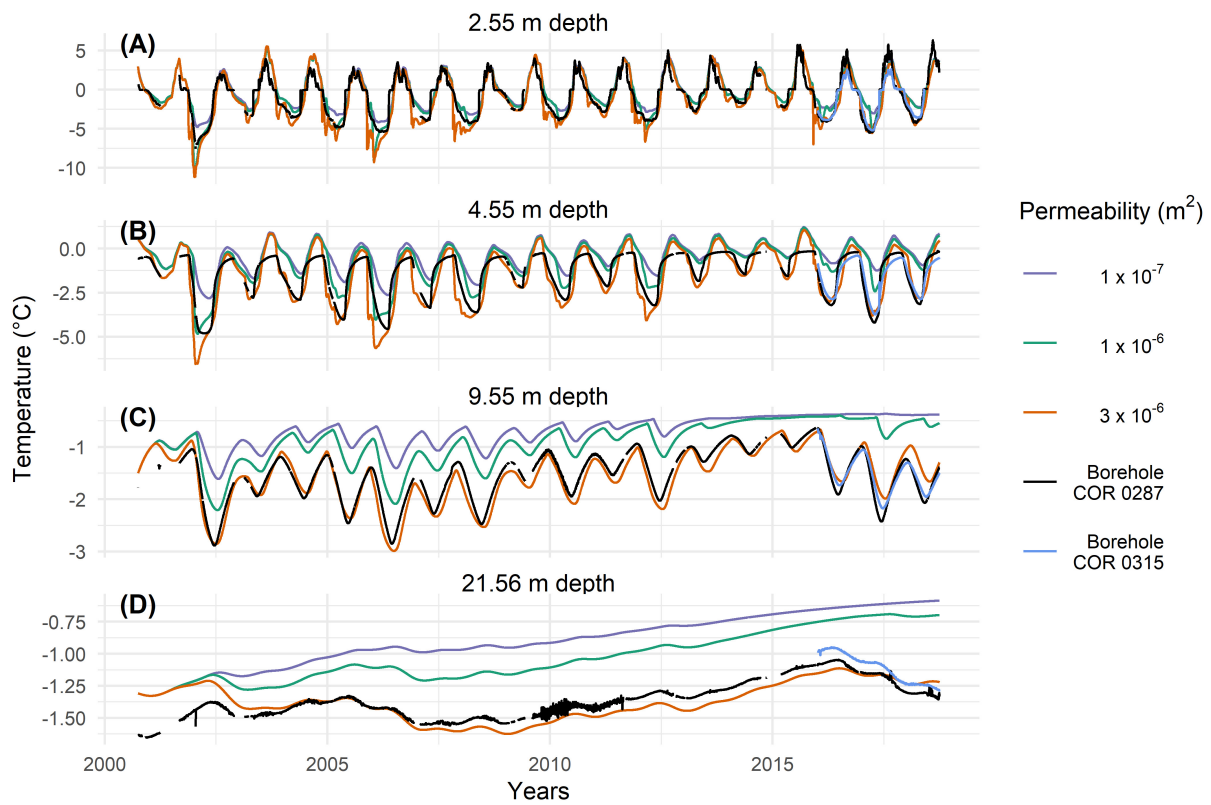
FIGURE 3 | Modeled temperatures at COR for different permeability at different depths of 2.55 m **(A)**, 4.55 m **(B)**, 9.55 m **(C)**, and 21.56 m **(D)** in a virtual borehole in the middle of the model domain (see **Figure 1**). Measured temperatures in the borehole are shown in black for the COR0287 borehole and blue for the COR0315 borehole (only from 2015 onward).

can be substantially lower due to this ground cooling than without convection effects.

Air Flow Field and Rayleigh Number

Figure 7 shows the evolution of the Rayleigh number Ra (Eq. 7) with time and a sum up of the days per hydrological year, where the critical Rayleigh number Ra_{crit} of $4\pi^2$ is reached (**Figures 7A,B,G,H** respectively). In **Table 3**, the smallest modeled temperature gradients are listed for which $Ra > Ra_{crit}$ for each site and permeability. These temperature gradients are thus the respective minimum thresholds for the onset of convection for each site and permeability observed in the active layer. Furthermore, two additional characteristics of the airflow vector field in the porous active layer are determined. To avoid boundary effects, data for the central 20 m of the domain (**Figure 2**) is used. The standard deviation of the direction of the airflow d (Eq. 6, **Figures 7C,D**) is used to characterize the type of circulation regime. A high standard deviation of d stands for a multicellular convection, whereas a low standard deviation indicates a down flow parallel to the surface (**Figures 7C,D**). This measure is independent of the strength of the airflow and can be interpreted as an on/off value for multicellular convection. In addition, the magnitude of the vorticity ζ (Eq. 5, **Figure 7E,F**) of the airflow vector field is shown. In contrast to the standard deviation of d, this measure depends on the strength of the

circulation. **Figure 7** shows monthly rolling means of standard deviation of d and of the magnitude of the vorticity ζ to facilitate the interpretation.

The governing parameters of Ra are independent from the modeled airflow vector field (Eq. 7). At Ra values well below Ra_{crit} no convection cells form, the vorticity ζ is relatively low and the standard deviation of d is always low. This is the case for a low permeability of 1×10^{-7} m². With higher permeability values also an increase of Ra can be observed, either reaching Ra_{crit} in some years (for 1×10^{-6} m²) or in every year (for 3×10^{-6} m²). The results suggest that approximately a weeklong period above Ra_{crit} is needed to pass to a convection dominated heat transfer regime. This is reflected in a high standard deviation of d and in an increase in the magnitude of vorticity ζ. The higher Ra, the higher is also the vorticity magnitude und thus the stronger the air convection in the active layer. A general pattern can be observed in the onset and the duration of convection in **Figure 7** for all years. **Figure 8** shows an excerpt for the hydrological years 2015/2016 of **Figure 7** for COR to describe the observed convection pattern. The onset of convection is characterized by an increase in the standard deviation of d (**Figure 8B**). Multicellular convection (**Figure 6B**) then takes place during the winter season, until Ra drops to zero and the convection regime switches to a summer situation of uniform gravitational down flow (**Figures 6C,D**), characterized by a low
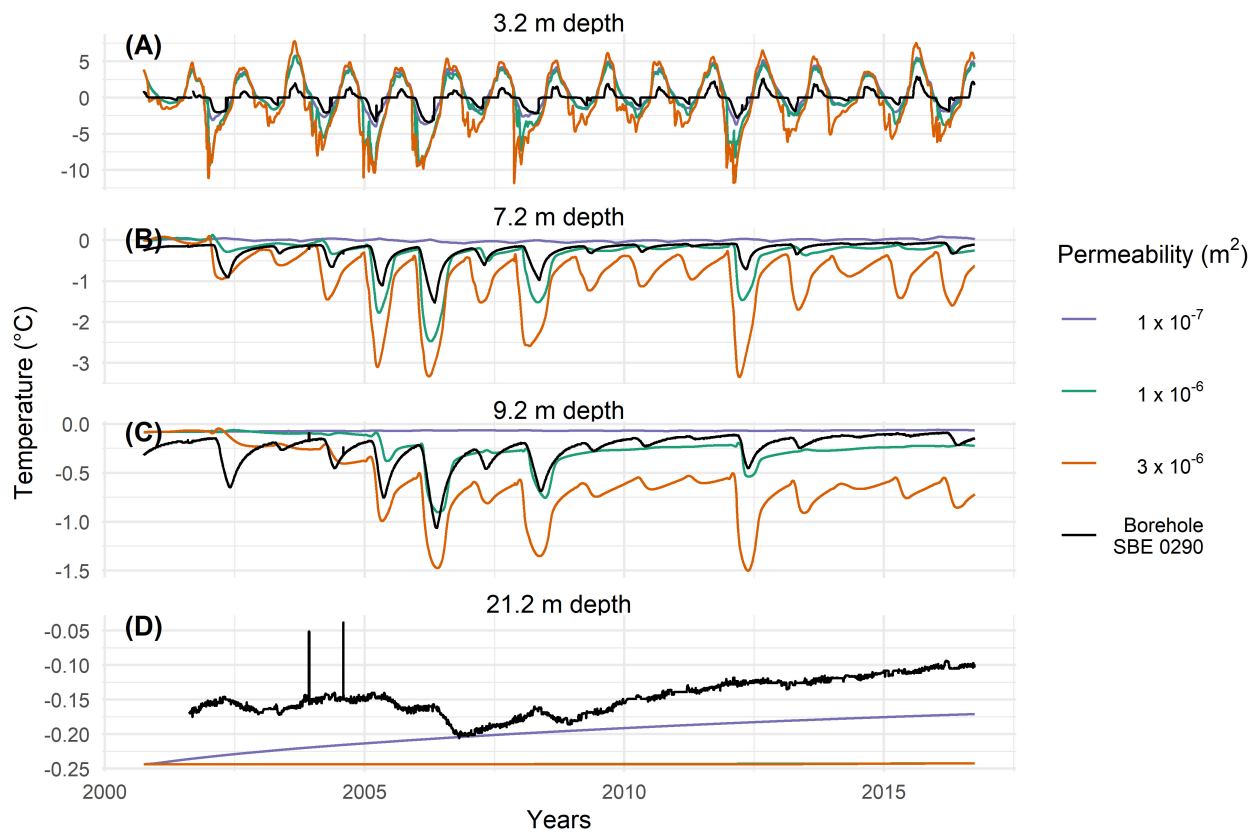
FIGURE 4 | Modeled temperatures at SBE for different permeability at different depths of 3.2 m **(A)**, 7.2 m **(B)**, 9.2 m **(C)**, and 21.2 m **(D)** in a virtual borehole in the middle of the model domain (see **Figure 1**). Measured temperatures in the borehole are shown in black for the SBE0290 borehole. In panel **(D)** the orange line covers the green line.

standard deviation of d. An approximately weeklong period of $Ra > Ra_{crit}$ leads to the onset of convection. In years without multicellular convection, the sum of days with $Ra > Ra_{crit}$ is always less than six, regardless of permeability values and site. For a permeability of 3×10^{-6} m^2, multicellular convection occurs in 2015 and 2016, whereas in 2016 the autumn cooling is especially prominent and characterized by high Ra and multiple shorter periods of multicellular convection (**Figure 8**). For a permeability of 1×10^{-6} m^2, no multicellular convection takes place in 2015 because $Ra < Ra_{crit}$. Multicellular convection occurs in 2016 but the onset is delayed compared to a situation with a higher permeability and does not occur in autumn. At a low permeability of 1×10^{-7} m^2, multicellular convection never takes place because $Ra << Ra_{crit}$ and conduction dominates the heat transfer.

DISCUSSION

Convection

An indicator for the importance of convection is the resulting cooling. Comparing yearly mean temperatures at a depth of approximately 10 m for the simulations with low (1×10^{-7} m^2) and high permeability (3×10^{-6} m^2) at both sites, we find that the mean temperatures of the last modeled year at COR (SBE) are 0.93°C (0.64°C) colder at a depth of 9.55 m (9.2 m) for the high permeability case than for the low permeability case, where no convection is present. Albeit these values seem relatively low compared to reported values from specifically designed engineering structures, where the underlying temperatures decreased up to several degrees Celsius (Arenson and Sego, 2006), and to low elevation talus slopes, where permafrost occurrences with surrounding mean annual air temperature of up to 5°C were reported (Kneisel et al., 2000; Delaloye et al., 2003), the simulations show that active layer convection has a significant influence on the thermal regime of permafrost. Especially in the European Alps, where permafrost temperatures are often close to 0°C (Permos, 2019), the cooling trough convection is essential to maintain permafrost conditions. Furthermore, active layer convection has also an influence on the assumed distribution of permafrost. Discontinuous permafrost is known to have heterogeneous distribution patterns, highly influenced by the ground cover (Harris and Pedersen, 1998; Gubler et al., 2011; Schneider et al., 2012; Harrington and Hayashi, 2019) and the results from this study underline the importance of this influence. Care has therefore to be taken in generalizing measured temperatures in the context of permafrost mapping, as ground temperatures are highly
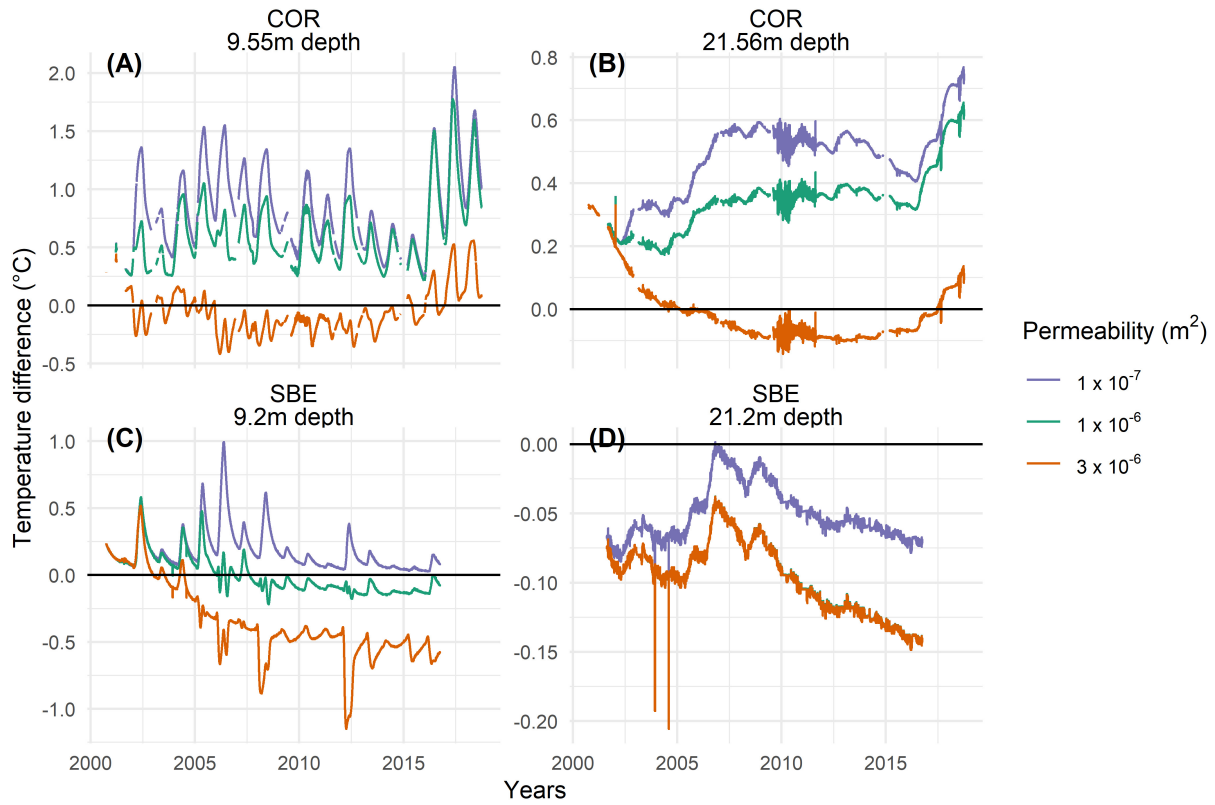
FIGURE 5 | Temperature difference (observed minus modeled) at two different depths of approximately 10 m **(A,C)** and 20 m **(B,D)** for COR **(A,B)** and SBE **(C,D)**. The black zero-line indicates a perfect match with the measured temperature at the borehole COR0287 and SBE0290 respectively. The color lines represent the difference from the modeled to the measured temperatures for different permeability values. In panel **(D)** the orange line covers the green line.
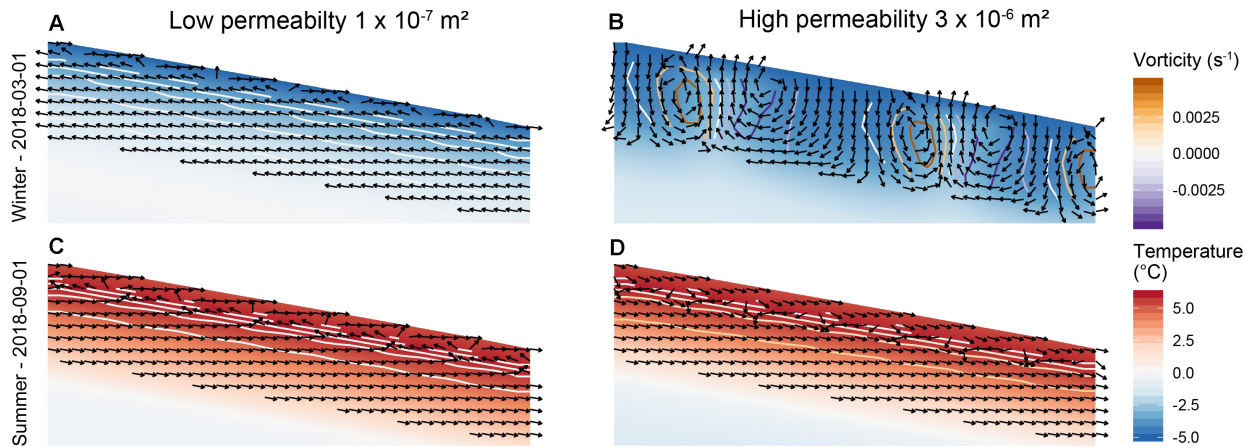

FIGURE 6 | Typical winter **(A,B)** and summer **(C,D)** circulation in the active layer of the Murtel-Corvatsch rock glacier for a low permeability of 1×10^{-7} m^2 **(A,C)** and a high permeability of 3×10^{-6} m^2 **(B,D)**. The color scheme indicates the temperatures, the colored contours the vorticity and the black arrows indicate the direction of airflow field. Note the multicellular convection pattern in panel **(B)**, where the vorticity is positive (negative) for counter-clockwise (clockwise) circulating cells.

dependent on the ground cover and the corresponding active layer permeability.

The temperature gradients shown in **Table 3** are taken from the modeling results. Solving Eq. 7 for ΔT with

$Ra = Ra_{\mathrm{crit}}$, assuming 0°C as reference temperature for the material properties, yields similar values. The difference between the two sites is due to the difference in active layer thickness as Ra is linearly depending on it. When assuming all other

TABLE 3 | Critical temperature gradients in the active layer corresponding to Ra_{crit}.

Permeability (m²)	COR	SBE
1×10^{-6}	-0.99 K m^{-1}	-0.62 K m^{-1}
3×10^{-6}	-0.32 K m^{-1}	-0.22 K m^{-1}

material properties constant, the temperature gradient is the main driver of Ra and can easily be estimated through borehole data. This allows thus for a simple estimation of the probability of free convection effects in the active layer, which occurs when the critical temperature gradient is surpassed. Herz (2006) discussed the temperature gradients required for the onset of free convection in the active layer of an Alpine rock glacier. Field measurements yield values of -0.64 K m^{-1} at the base of the active layer, which is in agreement with the findings of this study.

The time scale of the study allows investigating the yearly behavior and the, relative to the available data, long-term effects of convection in the active layer on the ground thermal regime. The boundary data are daily values. Hence, our model does not represent intra-daily temperature or convection cycles. Convective air flow has already been measured in field-based studies on shorter time-scales (Morard and Delaloye, 2008; Panz, 2008), where intra-daily cycles are described as well. The airflow and temperature measurements of Panz (2008) took place in the uppermost meter of the active layer at COR and are thus much more influenced by the intra-daily temperature cycle, leading to higher temperature gradients. For this reason, and because of relatively high permeability values (*cf* section "Permeability"), the Ra values in the present study are about one order of magnitude smaller compared to Panz (2008). Nevertheless, the seasonal cycles observed by Panz (2008) agree well with the modeled convection patterns described in section "Air Flow Field and Rayleigh Number."

Site Dependence

The comparison between modeled and measured temperatures (**Figure 5**) shows that the importance of convection is site dependent. At COR only the highest permeability shows a good agreement with the measured data. The active layer convection is therefore an important process, which is a necessary condition for accurate modeling of the measured temperatures. The influence of this convection at depths below the active layer is, as already shown by Scherler et al. (2014), still high. The active layer at COR is composed of big blocks without fine material which supports the assumption of a high permeability. At SBE, the permeability of 3×10^{-6} m² is overestimating the convective cooling effect at this site. Nevertheless, the results show that permeability still has an influence on the ground thermal regime and a permeability of 1×10^{-6} m² reproduces the measured wintertime cooling. The active layer at SBE is composed of smaller blocks and fine material is visible at the surface. Furthermore, water seems to play a more important role in the active layer of SBE than in COR, as the measured active layer temperatures show a distinct zero curtain. The occurrence of water in the active layer of SBE was also reported by other studies (e.g., Kenner et al., 2019). Water in

the active layer can, at least seasonally, reduce the circulation of air and lower the influence of air convection in the active layer. Furthermore, **Figure 7** shows that convection occurs more often at 1×10^{-6} m² at SBE compared to COR. The temperature at the boundary at SBE is measured closer to the surface than at COR and shows thus a higher amplitude which leads to an increased temperature gradient within the active layer. Further, a smaller temperature gradient within the active layer (**Table 3**) leads to Ra_{crit}, as SBE has a thicker active layer, also favoring the onset of free convection.

To generalize our findings to other sites and landforms, it is important to consider the site dependence beyond the differences of the two studied sites, which are shortly discussed in the following. We focus on variations in (i) the material properties, i.e., mainly the thermal properties and the permeability, (ii) the geometry, characterized by a slope angle and eventual spatial heterogeneities and (iii) the potential importance of neglected processes, like energy exchange related to moist air or ponding meltwater.

The influence of changing thermal material properties (i) on the final simulation results due to a different lithology is rather small. A sensitivity study at COR with a permeability of 1×10^{-6} m² showed for example that with a change in thermal conductivity of +7% (−7%), the mean temperature of the last modeled year at COR shows a temperature difference of +0.04°C (−0.05°C) at a depth of 10 m. This is negligible compared to the convective cooling effect of 0.93°C (section "Convection"). Further, the permeability is shown to have a big influence and is site specific, but as discussed in section "Permeability" hard to determine. A direct and reliable link between permeability and the material found at/within the surface cover is still not possible and needs further empirical work.

Regarding the geometry (ii), the slope angle has an influence on the convection patterns. With an increasing slope, advection, meaning the lateral component of the convective heat flux, becomes more important within the landform (Guodong et al., 2007; Wicky and Hauck, 2017). The gravitational gradient leads to an advective cooling in the lower part of the rock glacier. Geoelectrical measurements on COR, but also on other rock glaciers and talus slopes, also suggest such a pattern, with the highest resistivity values and therefore higher ice contents toward the front (Hilbich et al., 2009). Further, the heterogeneity of the active layer is at some sites also characterized by unevenly distributed liquid water (e.g., Halla et al., unpublished).

At sites with a high water content in the active layer, processes related to latent heat exchange and heat advection through percolating water gain in importance (iii). Nevertheless, Scherler et al. (2014) showed that the latent heat exchange due to seasonal melting and refreezing of the active layer can be equal and result in a net-zero balance over a year. Moore et al. (2011) showed that in ventilated fractures in an Alpine context, the heat input of melt water is negligible compared to cooling effects of free air convection. Furthermore, water plays also a role in gaseous state, i.e., within the air-filled voids. Changes in temperature lead to changes in relative humidity and thus lead to condensation, evaporation or sublimation of water in the active layer. Field evidence (Harris and Pedersen, 1998; Hanson and Hoelzle, 2004;
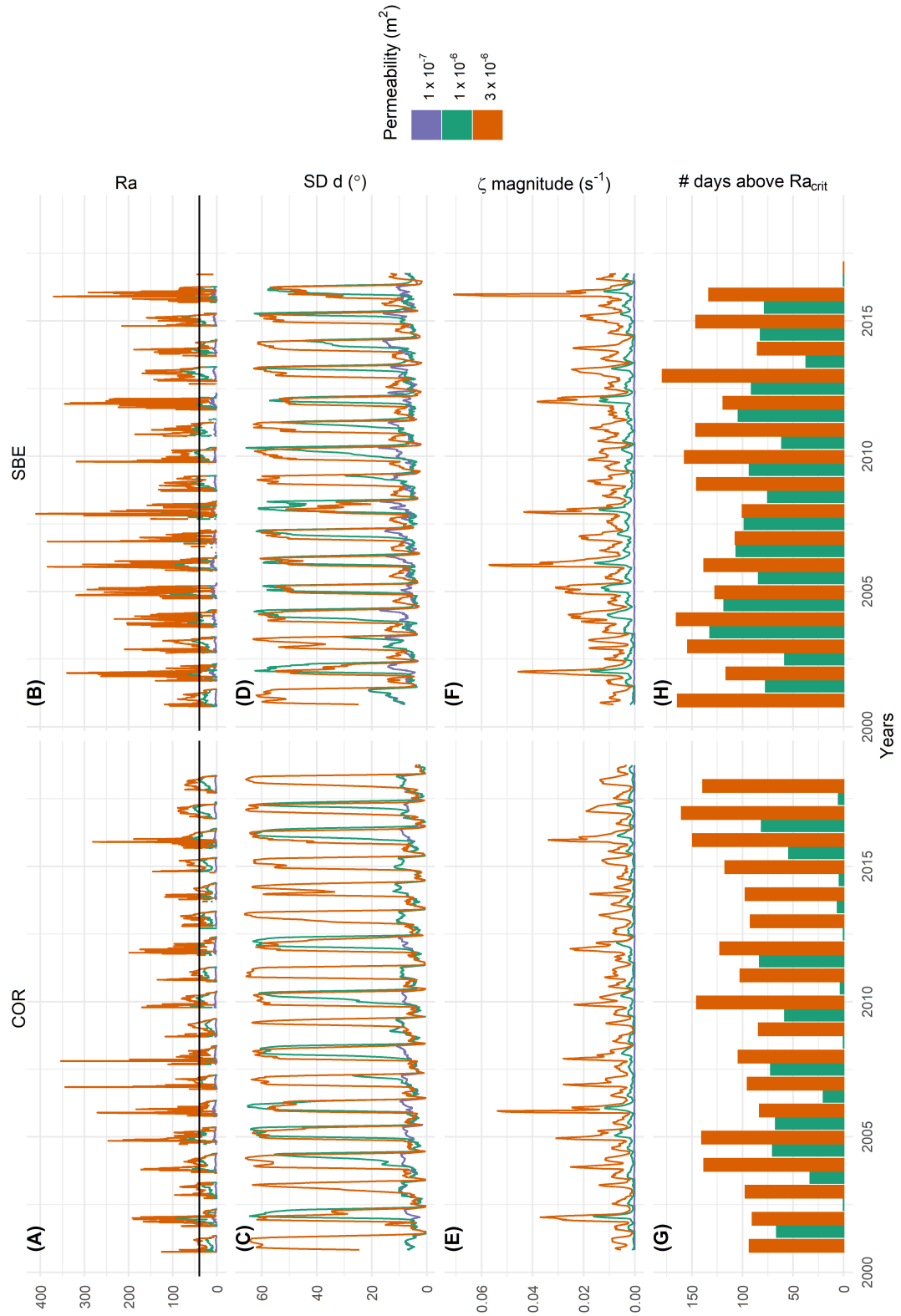
FIGURE 7 | (A,B) Rayleigh number *Ra* with *Ra*_{crit} in black, **(C,D)** monthly rolling mean of the standard deviation of the airflow direction *d*, **(E,F)** monthly rolling mean of the magnitude of the vorticity ζ and **(G,E)** the number of days above a critical Rayleigh number within the hydrological year for COR **(A,C,E,G)** and SBE **(B,D,F,H)** for three different permeability values, represented by different colors. The magnitude of ζ and the standard deviation of *d* are calculated over the airflow vector field shown in **Figure 6**, respectively **Figure 1**.
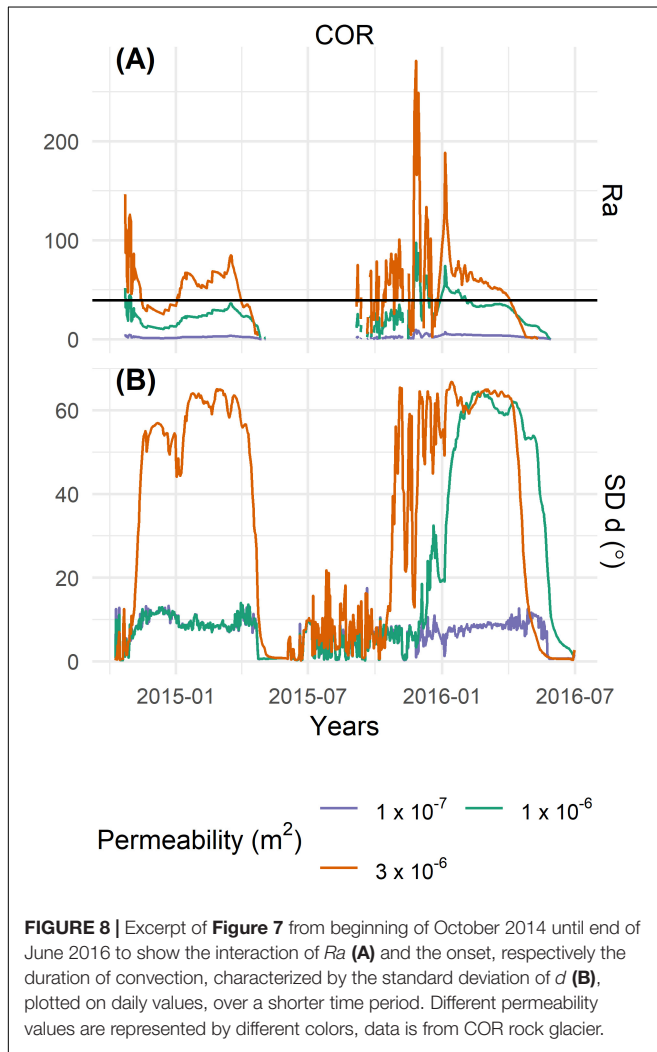
FIGURE 8 | Excerpt of **Figure 7** from beginning of October 2014 until end of June 2016 to show the interaction of *Ra* **(A)** and the onset, respectively the duration of convection, characterized by the standard deviation of *d* **(B)**, plotted on daily values, over a shorter time period. Different permeability values are represented by different colors, data is from COR rock glacier.

Herz, 2006) and modeling studies (Scherler et al., 2014; Pruessner et al., 2018) state that these processes play a secondary role in the energy balance of a coarse blocky active layer and that the cooling effect induced by free convection prevails. Nevertheless, more *in situ* measurements in active layers of rock glaciers would be beneficial to quantify this effect in more detail.

Permeability

One of the key parameters is the intrinsic permeability of the porous active layer. **Table 4** provides a brief literature overview of relevant permeability values in the context of this study without any claim to be exhaustive. The range of reported values differs by more than one order of magnitude. The Rayleigh number is especially sensitive to the chosen permeability as it is linearly depending on it – changes in order of magnitude in other material properties would not be physically justifiable. In **Table 4**, it is important to note that for values below 3×10^{-7} m^2 natural convection does not occur in models in the context of coarse permafrost substrate, which agrees well with our study. Further, many authors rely upon the Kozeny-Carman equation (Eq. 8) with diameter of particles d_p (Johansen, 1975;

Nield and Bejan, 2017):

$$\kappa = \frac{\Phi^3}{5 \left(\frac{6}{d_p}\right)^2 (1 - \Phi)^2} \tag{8}$$

The aforementioned relation was developed and validated for comparatively small particle sizes (e.g., sand) in a packing of perfect spheres (Johansen, 1975; Côté et al., 2011). It is often not valid for non-spherical particles, broad range of particle diameters and consolidated media, nevertheless because of the simple applicability it is widely used (Nield and Bejan, 2017). Côté et al. (2011) showed with experimental data that the Kozeny – Carman equation overestimates the permeability for bigger particle sizes (e.g., crushed rocks) by a factor of about 4.25. Published values for permeability in the context of active layer convection for rock glaciers (**Table 4**; Herz, 2006; Panz, 2008; Wagner et al., 2019) are based on the Kozeny-Carman equation with no further validation and seem thus to be overestimating the permeability. It is also important to note that modeling studies normally use values in the order of 10^{-7}-10^{-6} m^2, whereas higher permeability values order of 10^{-5}-10^{-4} m^2 are only used in the analysis of field data (**Table 4**). This is in agreement with our study, where the best results were obtained for permeability values in the order of magnitude of 10^{-6} m^2, confirming the experimental values of Côté et al. (2011).

In summary, we recommend that in future attempts of analyzing the convection regime of the active layer of rock glaciers, the Kozeny-Carman equation should be used with caution. Because of a lack of experimental and field data, reliable estimations of the permeability in the active layer of rock glaciers are so far not possible. However, analogies to crushed rock from an engineering context serve as a good indicator and allow a consistent modeling of the process.

Independent of the permeability values, this porous media modeling approach inherently homogenizes the active layer. Borehole geophysics generally only provide limited information about the composition of the active layer of rock glaciers (Haeberli et al., 1988; Vonder Mühll and Holub, 1992; Arenson et al., 2002), geophysics draw a relatively homogenous pattern in terms of the electrical resistivity (Hilbich et al., 2009) and more recent findings suggest that the air content and thus the permeability decreases toward the bottom of the active layer (Mollaret et al., 2020). However, at different sites there is also geophysical evidence for heterogeneous active layers, often depending on 3D topography and differential water infiltration patterns (Scapozza et al., 2015; Halla et al., unpublished). For COR the assumption of a homogenous active layer is less of a simplification than for SBE. The blocks at COR are relatively big (0.4 m up to several meters), the water percolates quickly, the surface is almost always dry (Hanson and Hoelzle, 2004) and geophysical measurements do not show signs of water in the active layer (Hilbich et al., 2009; Mollaret et al., 2020). At SBE less information is available. A previous study reports the presence of water in the active layer (Kenner et al., 2019) and the freezing process is visible in the temperature data of the active layer (**Figure 4A**, *cf* section "Site Dependence"). The presence of water fills the pores and prevents convective circulation of air.

TABLE 4 | Literature values for intrinsic permeability.

Permeability (m^2)	References	Context	Comment
1.5–3.9 × 10^{-6}	Côté et al., 2011	Coarse rock fills; permafrost engineering	Laboratory set-up, with (indirect) measurements
6.32 × 10^{-7}	Goering and Kumar, 1996	Road embankment modeling in permafrost	Refers to Nield and Bejan (2017) for Φ = 0.4 and average rock diameter of 3 cm
6.32 × 10^{-7}	Guodong et al., 2007	Road embankment modeling in permafrost	Typical diameter of 22 cm
8.89 × 10^{-5} 9.88 × 10^{-6}	Herz, 2006	Ritigraben rock glacier, close to surface and within the AL	Kozeny-Carman equation with typical diameter of 30 cm, respectively 10 cm
0.97 × 10^{-6}	Johansen, 1975	Free convection in crushed rocks	Experimetal setup – Kozeny-Carman equation, particle size 2–8 cm
5 × 10^{-7} 4.5–6.9 × 10^{-7}	Lebeau and Konrad, 2009, 2016	Modeling of a road embankment	Apparent permeability values due to non-Darcy effects
1.6 × 10^{-7}, 6.5 × 10^{-7} 1.3 × 10^{-6}, 2.4 × 10^{-6}	Levintal et al., 2017	Natural convection in porous non-permafrost soils	Kozeny-Carman with spherical particles of 1, 2, 3, 4 cm diameter
6.69 × 10^{-5} 2.68 × 10^{-4}	Panz, 2008	Corvatsch-Murtèl rock glacier, close to surface and within the AL	Refers to Herz (2006), Kozeny-Carman equation; typical diameter of 20 cm, respectively 40 cm
1 × 10^{-8}, 3 × 10^{-8} 1 × 10^{-7}, 3 × 10^{-7}	Pham et al., 2008	Numerical modeling of mine waste in permafrost environment	Parameter study – Significant convection (Ra_{crit} reached) only with 3 × 10^{-7} m^2
2.28 × 10^{-6} 4.38 × 10^{-6} 5.46 × 10^{-6}	Sun et al., 2010	Road embankment modeling in permafrost	Fair-Hatch (~ Kozeny-Carman) for particle size 4-6 cm, 6-8 cm and 8-10 cm respectively
1.21 × 10^{-4}	Wagner et al., 2019	Temperature data analysis on an alpine rock glacier	Refers to Herz (2006), Kozeny-Carman equation; typical diameter 35 cm

The model performs thus also less well at SBE. Deeper knowledge of the active layer composition, especially at its base, would be of benefit and could then be included in the model set up. Still, it is also important to avoid modeling artefacts originating from a very complex active layer set up without means for validation.

Boundary Conditions

The temperature boundary condition at the upper model boundary is prescribed by the uppermost thermistor of the borehole. By this, the thermal effect of a temporally variable snow cover is represented in the boundary data. The disadvantage of this approach is that it depends on the measured temperature data below the snow cover, and would need an additional snow model/energy balance approach to use meteorological data as a boundary condition. Further, a casing protects the thermistor chain measuring temperature in the borehole. Convection occurs therefore not directly at the thermistors, but additional temperature measurements showed that the disturbances caused by the casing are negligible (Vonder Mühll and Haeberli, 1990).

The temperature boundary condition is constant in space per time step. Spatially distributed temperature dataset on rock glaciers are rare and not available for the modeled sites over many years. This does not pose a problem, when comparing modeled data to measured data on a point scale, but it could influence the interpretation of spatial temperature patterns.

Compared to other modeling approaches of convection in permafrost (see Goering and Kumar, 1996; Guodong et al., 2007) we use real measured temperature data as upper thermal boundary condition. This is essential to compare the modeled data to the measured borehole data for a

better understanding of the behavior of the ground thermal regime. Still, this has also some drawbacks. The naturally occurring extensive temperature changes on short timescales inherently cause numerical instabilities in the model. To cope with these instabilities, in an addition to an adaptive time stepping scheme and extensive mesh tests, we dampened the effects of latent heat (*cf* section "Boundary Conditions") and chose the computationally effective and stable Darcy approach with an Oberbeck-Boussinesq approximation and thus incompressible flow.

Modeling porous media air convection in a permafrost context with a Darcy approach including the Oberbeck-Boussinesq approximation can be seen as the state of the art in this domain and is by far the most used approach (e.g., Goering and Kumar, 1996; Pham et al., 2008; Lebeau and Konrad, 2009; Sun et al., 2010; Darrow and Jensen, 2016). However, recent studies on thermal modeling of road embankments show that accounting for compressible flow (Lebeau and Konrad, 2009), radiation and non-Darcy effects (Lebeau and Konrad, 2016) influences the results. The modeling approaches of Lebeau and Konrad (2009, 2016) are applied to a smaller setting with harmonic boundary conditions and relatively low permeability in the order of ∼5 × 10^{-7} m^2 (**Table 4**). The increase of non-linearity accounting for compressible flow, radiation and non-Darcy effects, in our setting with real boundary data, relatively high permeability and phase change, is numerically more challenging and computationally more expensive. Nevertheless, their studies also show that the difference to a Darcy model adopting the Oberbeck-Boussinesq approximation is negligible on the scales we are addressing in our study. Lebeau and Konrad (2016) show

that non-Darcy effects, such as the inertial drag described by the Forchheimer term, have the potential to reduce the intrinsic permeability by 6%. Radiative effects lead to a slight increase in summer temperatures (Lebeau and Konrad, 2016), which in our case, with the possibility of validation, means that the convective cooling is rather underestimated. Accounting for compressibility has also subordinate influence on the results. The absolute error of Oberbeck-Boussinesq approximation compared to an approach with compressibility does not exceed 6% in the tests of Lebeau and Konrad (2009). Further, the assumption of a local thermal equilibrium in the porous media is made, meaning that the solid and the liquid phase have the same temperature. This is common to all so far cited studies of thermal modeling in crushed rocks. Concerning local thermal non-equilibrium (LTNE) models in a general permafrost context, only very little work has been carried out so far (e.g., Heinze, 2020). The uncertainty of the additional parameters and the additional computational cost needed outweigh the benefit to the presented modeling approach. Regarding the relatively small influence of the above effects, we prefer to run a simpler but stable model, which allows for using real measured boundary conditions and a higher permeability while accepting the potentially small resulting error.

CONCLUSION AND OUTLOOK

We developed and applied a model approach, which, in addition to conduction, also explicitly models convection on a two-dimensional domain of a schematic rock glacier. Convection is modeled in a porous media with a Darcy approach, adopting the Oberbeck-Boussinesq approximation to account for natural convection. Datasets from two different rock glaciers in the Swiss Alps were used to exemplary characterize the different convection regimes and the effects of active layer convection on ground temperatures. Our findings show that:

1. Natural convection in a coarse blocky active layer has a major influence on the thermal regime of the active layer and the underlying permafrost body, even at depth of the zero annual amplitude.
2. Borehole temperatures are in good agreement with the modeling results – convection is needed to represent the measured temperatures at both sites, albeit not to the same degree.
3. The cooling potential mainly depends on the permeability and the thermal gradient within the active layer, which is also described by the Rayleigh number.

In future research, the permeability in coarse blocky alpine permafrost should be further addressed, either with attempts of *in situ* or indirect measurements or with laboratory experiments. Furthermore, in a modeling perspective, our findings should be integrated in long-term permafrost models to enhance parametrizations of convective heat transfer and improve future temperature and ground ice content projections.

DATA AVAILABILITY STATEMENT

The boundary datasets generated for this study are included in the article/**Supplementary Material**. The model files can be obtained through the corresponding author.

AUTHOR CONTRIBUTIONS

JW designed and performed the model calculations and analyzed the data, produced all the figures, and wrote the manuscript with substantial inputs from CH. Both authors contributed to the article and approved the submitted version.

FUNDING

ACKNOWLEDGMENTS

SUPPLEMENTARY MATERIAL

The Supplementary Material for this article can be found online at: https://www.frontiersin.org/articles/10.3389/feart. 2020.00335/full#supplementary-material

REFERENCES

Arenson, L., Hoelzle, M., and Springman, S. (2002). Borehole deformation measurements and internal structure of some rock glaciers in Switzerland. *Permafr. Periglac. Process.* 13, 117–135. doi: 10.1002/ppp.414

Arenson, L. U., Hauck, C., Hilbich, C., Seward, L., Yamamoto, Y., and Springman, S. M. (2010). "Sub-surface heterogeneities in the Murtèl-Corvatsch rock glacier, Switzerland," in *Proceedings of the Sixth Canadian Permafrost Conference*, Vol. 12–16, Calgary, AL, 1494–1500.

Arenson, L. U., and Sego, D. C. (2006). "Considering convective air fluxes in the design of engineered structures in cold regions", in *Proceedings of the Fifty Nineteenth Conference*, Vancouver, BC.

Balch, E. S. (1900). *Glacieres, or Freezing Caverns*. Philadelphia: Allen Lane & Scott.

Barsch, D. (1996). *Rockglaciers?: Indicators for the Present and Former Geoecology in High Mountain Environments*. Berlin: Springer.

Biskaborn, B. K., Smith, S. L., Noetzli, J., Matthes, H., Vieira, G., Streletskiy, D. A., et al. (2019). Permafrost is warming at a global scale. *Nat. Commun.* 10, 1–11. doi: 10.1038/s41467-018-08240-8244

Boeckli, L., Brenning, A., Gruber, S., and Noetzli, J. (2012). A statistical approach to modelling permafrost distribution in the European Alps or similar mountain ranges. *Cryosph* 6, 125–140. doi: 10.5194/tc-6-125-2012

Cermak, V., and Rybach, L. (1982). "Thermal properties: thermal conductivity and specific heat of minerals and rocks," in *Landolt-Bornstein Zahlenwerte und Funktionen aus Naturwissenschaften und Technik, Neue Serie*, ed. G. Angensteiner (Berlin: Springer Verlag), 305–343.

Cicoira, A., Beutel, J., Faillettaz, J., Gärtner-Roer, I., and Vieli, A. (2019). Resolving the influence of temperature forcing through heat conduction on rock glacier dynamics: a numerical modelling approach. *Cryosph* 13, 927–942. doi: 10.5194/tc-13-927-2019

COMSOL (2018a). *COMSOL Multiphysics Reference Manual*. Burlington, MA: COMSOL.

COMSOL (2018b). *Heat Transfer Module. Users Guide*. Burlington, MA: COMSOL.

Côté, J., Fillion, M. H., and Konrad, J. M. (2011). Intrinsic permeability of materials ranging from sand to rock-fill using natural air convection tests. *Can. Geotech. J.* 48, 679–690. doi: 10.1139/t10-097

Darrow, M. M., and Jensen, D. D. (2016). Modeling the performance of an air convection embankment (ACE) with thermal berm over ice-rich permafrost, Lost Chicken Creek, Alaska. *Cold Reg. Sci. Technol.* 130, 43–58. doi: 10.1016/j.coldregions.2016.07.012

Delaloye, R., and Lambiel, C. (2005). Evidence of winter ascending air circulation throughout talus slopes and rock glaciers situated in the lower belt of alpine discontinuous permafrost (Swiss Alps). *Nor. Geogr. Tidsskr.* 59, 194–203. doi: 10.1080/00291950510020673

Delaloye, R., Reynard, E., Lambiel, C., Marescot, L., and Monnet, R. (2003). Thermal anomaly in a cold scree slope (Creux du Van. Switzerland). *Proc. Eighth Int. Conf. Permafr.* 2003, 175–180.

Deluigi, N., Lambiel, C., and Kanevski, M. (2017). Data-driven mapping of the potential mountain permafrost distribution. *Sci. Total Environ.* 590–591, 370–380. doi: 10.1016/j.scitotenv.2017.02.041

Draebing, D., Krautblatter, M., and Hoffmann, T. (2017). Thermo-cryogenic controls of fracture kinematics in permafrost rockwalls. *Geophys. Res. Lett.* 44, 3535–3544. doi: 10.1002/2016GL072050

Goering, D. J., and Kumar, P. (1996). Winter-time convection in open-graded embankments. *Cold Reg. Sci. Technol.* 24, 57–74. doi: 10.1016/0165-232X(95)00011-Y

Gruber, S., and Haeberli, W. (2007). Permafrost in steep bedrock slopes and its temperatures-related destabilization following climate change. *J. Geophys. Res. Earth Surf.* 112, 1–10. doi: 10.1029/2006JF000547

Gruber, S., and Hoelzle, M. (2008). "The cooling effect of coarse blocks revisited," in *9th International Conference on Permafrost, Institute of Norther Engineering*, Vol. 1, eds D. L. Kane and K. M. Hinkel Fairbanks, AK: University of Alaska Fairbanks, 557–561.

Gubler, S., Fiddes, J., Keller, M., and Gruber, S. (2011). Scale-dependent measurement and analysis of ground surface temperature variability in alpine terrain. *Cryosph* 5, 431–443. doi: 10.5194/tc-5-431-2011

Guodong, C., Yuanming, L., Zhizhong, S., and Fan, J. (2007). The 'thermal semi-conductor' effect of crushed rocks. *Permafr. Periglac. Process.* 18, 151–160. doi: 10.1002/ppp.575

Haberkorn, A., Wever, N., Hoelzle, M., Phillips, M., Kenner, R., Bavay, M., et al. (2017). Distributed snow and rock temperature modelling in steep rock walls using Alpine3D. *Cryosph* 11, 585–607. doi: 10.5194/tc-11-585-2017

Haeberli, W., Hunder, J., Keusen, H.-R., Pika, J., and Röthlisberger, H. (1988). Core drilling through rock-glacier permafrost. *Proc. Fifth Int. Conf. Permafr.* 2, 937–942.

Hanson, S., and Hoelzle, M. (2004). The thermal regime of the active layer at the Murtèl rock glacier based on data from 2002. *Permafr. Periglac. Process.* 15, 273–282. doi: 10.1002/ppp.499

Harrington, J. S., and Hayashi, M. (2019). Application of distributed temperature sensing for mountain permafrost mapping. *Permafr. Periglac. Process.* 30, 113–120. doi: 10.1002/ppp.1997

Harris, S. A., and Pedersen, D. E. (1998). Thermal regimes beneath coarse blocky materials. *Permafr. Periglac. Process.* 9, 107–120. doi: 10.1002/(SICI)1099-1530(199804/06)9:2<107::AID-PPP277>3.0.CO;2-G

Heinze, T. (2020). Possible effect of flow velocity on thawing rock-water-ice systems under local thermal non-equilibrium conditions. *Cold Reg. Sci. Technol.* 170:102940. doi: 10.1016/j.coldregions.2019.102940

Herz, T. (2006). *Das Mikroklima Grobblockiger Schutthalden der Alpinen Periglazialstufe und seine Auswirkungen auf Energieaustauschprozesse zwischen Atmosphäre und Lithosphäre*. PhD Thesis, Justus-Liebig-Universität Gießen, Giessen.

Hilbich, C., Marescot, L., Hauck, C., Loke, M. H., and Mäusbacher, R. (2009). Applicability of electrical resistivity tomography monitoring to coarse blocky and ice-rich permafrost landforms. *Permafr. Periglac. Process.* 20, 269–284. doi: 10.1002/ppp.652

Hoelzle, M., Mittaz, C., Etzelmüller, B., and Haeberli, W. (2001). Surface energy fluxes and distribution models of permafrost in European mountain areas: an overview of current developments. *Permafr. Periglac. Process.* 12, 53–68. doi: 10.1002/ppp.385

Johansen, O. (1975). *Thermal Conductivity of Soils*. PhD Thesis, University of Trondheim, Trondheim.

Jones, D. B., Harrison, S., Anderson, K., and Betts, R. A. (2018). Mountain rock glaciers contain globally significant water stores. *Sci. Rep.* 8, 1–10. doi: 10.1038/s41598-018-21244-w

Juliussen, H., and Humlum, O. (2008). Thermal regime of openwork block fields on the mountains Elgåhogna and Sølen, central-eastern Norway. *Permafr. Periglac. Process.* 19, 1–18. doi: 10.1002/ppp.607

Kane, D. L., Hinkel, K. M., Goering, D. J., Hinzman, L. D., and Outcalt, S. I. (2001). Non-conductive heat transfer associated with frozen soils. *Glob. Planet. Change* 29, 275–292. doi: 10.1016/S0921-8181(01)00095-99

Keller, F. (1992). Automated mapping of mountain permafrost using the program PERMAKART within the geographical information system ARC/INFO. *Permafr. Periglac. Process.* 3, 133–138. doi: 10.1002/ppp.3430030210

Kenner, R., Pruessner, L., Beutel, J., Limpach, P., and Phillips, M. (2019). How rock glacier hydrology, deformation velocities and ground temperatures interact: examples from the Swiss Alps. *Permafr. Periglac. Process.* 31, 12–14. doi: 10.1002/ppp.2023

Kneisel, C., Hauck, C., and Mühll, D. V. (2000). Permafrost below the Timberline confirmed and characterized by geoelectrical resistivity measurements, Bever Valley, eastern Swiss Alps. *Permafr. Periglac. Process.* 11, 295–304. doi: 10.1002/1099-1530(200012)11:4<295::AID-PPP353>3.0.CO;2-L

Lebeau, M., and Konrad, J. M. (2009). Natural convection of compressible and incompressible gases in undeformable porous media under cold climate conditions. *Comput. Geotech.* 36, 435–445. doi: 10.1016/j.compgeo.2008.04.005

Lebeau, M., and Konrad, J. M. (2016). Non-Darcy flow and thermal radiation in convective embankment modeling. *Comput. Geotech.* 73, 91–99. doi: 10.1016/j.compgeo.2015.11.016

Levintal, E., Dragila, M. I., Kamai, T., and Weisbrod, N. (2017). Free and forced gas convection in highly permeable, dry porous media. *Agric. For. Meteorol.* 232, 469–478. doi: 10.1016/j.agrformet.2016.10.001

Luethi, R., Phillips, M., and Lehning, M. (2017). Estimating Non-conductive heat flow leading to intra-permafrost talik formation at the ritigraben rock glacier (Western Swiss Alps). *Permafr. Periglac. Process.* 28, 183–194. doi: 10.1002/ppp.1911

Marmy, A., Rajczak, J., Delaloye, R., Hilbich, C., Hoelzle, M., Kotlarski, S., et al. (2016). Semi-automated calibration method for modelling of mountain permafrost evolution in Switzerland. *Cryosph* 10, 2693–2719. doi: 10.5194/tc-10-2693-2016

Maurer, H., and Hauck, C. (2007). Geophysical imaging of alpine rock glaciers. *J. Glaciol.* 53, 110–120. doi: 10.3189/172756507781833893

Mollaret, C., Wagner, F. M., Hilbich, C., Scapozza, C., and Hauck, C. (2020). Petrophysical joint inversion applied to alpine permafrost field sites to image subsurface Ice, Water, Air, and Rock Contents. *Front. Earth Sci.* 8:85. doi: 10.3389/feart.2020.00085

Moore, J. R., Gischig, V., Katterbach, M., and Loew, S. (2011). Air circulation in deep fractures and the temperature field of an alpine rock slope. *Earth Surf. Process. Landforms* 36, 1985–1996. doi: 10.1002/esp.2217

Morard, S., Delaloye, R., and Lambiel, C. (2012). Pluriannual thermal behavior of low elevation cold talus slopes in western Switzerland. *Geogr. Helv.* 65, 124–134. doi: 10.5194/gh-65-124-2010

Morard, S., and Delaloye, R. (2008). Airflow velocity measurements in ventilated porous debris accumulations. *Swiss Geosci. Meet.* 192–193.

Myhra, K. S., Westermann, S., and Etzelmüller, B. (2019). Modeling conductive heat flow between steep rock walls and talus slopes – thermal processes and

geomorphological implications. *Front. Earth Sci.* 7:192. doi: 10.3389/feart.2019.00192

Nield, D. A., and Bejan, A. (2017). *Convection in Porous Media*. Cham: Springer.

Noetzli, J., and Gruber, S. (2009). Transient thermal effects in Alpine permafrost. *Cryosph* 3, 85–99. doi: 10.5194/tc-3-85-2009

Panz, M. (2008). *Analyse von Austauschprozessen in der Auftauschicht des Blockgletschers Murtèl-Corvatsch, Oberengadin*. Master Thesis, Ruhr Universität, Germany.

Permos (2019). *PERMOS Database*. Fribourg: Swiss Permafrost Monitoring Network.

Pham, H., Arenson, L. U., and Sego, D. C. (2008). Numerical analysis of forced and natural convection in waste-rock piles in permafrost environments. *Proc. Ninth Int. Conf. Permafr.* 28, 1411–1416.

Popescu, R., Vespremeanu-Stroe, A., Onaca, A., Vasile, M., Cruceru, N., and Pop, O. (2017). Low-altitude permafrost research in an overcooled talus slope–rock glacier system in the Romanian Carpathians (Detunata Goală Apuseni Mountains). *Geomorphology* 295, 840–854. doi: 10.1016/j.geomorph.2017.07.029

Pruessner, L., Phillips, M., Farinotti, D., Hoelzle, M., and Lehning, M. (2018). Near-surface ventilation as a key for modeling the thermal regime of coarse blocky rock glaciers. *Permafr. Periglac. Process.* 29, 152–163. doi: 10.1002/ppp.1978

Sawada, Y., Ishikawa, M., and Ono, Y. (2003). Thermal regime of sporadic permafrost in a block slope on Mt. Nishi-Nupukaushinupuri, Hokkaido Island, Northern Japan. *Geomorphology* 52, 121–130.

Scapozza, C., Baron, L., and Lambiel, C. (2015). Borehole logging in Alpine periglacial talus slopes (Valais, Swiss Alps). *Permafr. Periglac. Process.* 26, 67–83. doi: 10.1002/ppp.1832

Scherler, M., Hauck, C., Hoelzle, M., and Salzmann, N. (2013). Modeled sensitivity of two alpine permafrost sites to RCM-based climate scenarios. *J. Geophys. Res. Earth Surf.* 118, 780–794. doi: 10.1002/jgrf.20069

Scherler, M., Schneider, S., Hoelzle, M., and Hauck, C. (2014). A two-sided approach to estimate heat transfer processes within the active layer of the Murtèl-Corvatsch rock glacier. *Earth Surf. Dyn.* 2, 141–154. doi: 10.5194/esurf-2-141-2014

Schneider, S., Hoelzle, M., and Hauck, C. (2012). Influence of surface and subsurface heterogeneity on observed borehole temperatures at a mountain permafrost site in the Upper Engadine. *Swiss Alps. Cryosph.* 6, 517–531. doi: 10.5194/tc-6-517-2012

Staub, B., Hasler, A., Noetzli, J., and Delaloye, R. (2017). Gap-Filling algorithm for ground surface temperature data measured in permafrost and periglacial environments. *Permafr. Periglac. Process.* 28, 275–285. doi: 10.1002/ppp.1913

Stocker-Mittaz, C., Hoelzle, M., and Haeberli, W. (2002). Modelling alpine permafrost distribution based on energy-balance data: a first step. *Permafr. Periglac. Process.* 13, 271–282. doi: 10.1002/ppp.426

Sun, B., Yang, L., Liu, Q., and Xu, X. (2010). Numerical modelling for crushed rock layer thickness of highway embankments in permafrost regions of the Qinghai-Tibet Plateau. *Eng. Geol.* 114, 181–190. doi: 10.1016/j.enggeo.2010.04.014

Vonder Mühll, D., and Haeberli, W. (1990). Thermal characteristics of the permafrost within an active rock glacier (Murtel/Corvatsch, Grisons, Swiss Alps). *J. Glaciol.* 36, 151–158.

Vonder Mühll, D. S., Arenson, L. U., and Springman, S. M. (2003). "Temperature conditions in two Alpine rock glaciers," in *Proceedings of the Eighth International Conference on Permafrost*, Zürich, 1195–1200.

Vonder Mühll, D. S., Hauck, C., and Lehmann, F. (2000). Verification of geophysical models in Alpine permafrost using borehole information. *Ann. Glaciol.* 31, 300–306. doi: 10.3189/172756400781820057

Vonder Mühll, D. S., and Holub, P. (1992). Borehole logging in alpine permafrost, upper Engadin, Swiss Alps. *Permafr. Periglac. Process.* 3, 125–132. doi: 10.1002/ppp.3430030209

Wagner, T., Pauritsch, M., Mayaud, C., Kellerer-Pirklbauer, A., Thalheim, F., and Winkler, G. (2019). Controlling factors of microclimate in blocky surface layers of two nearby relict rock glaciers (Niedere Tauern Range, Austria). *Geogr. Ann. Ser. A, Phys. Geogr.* 101, 310–333. doi: 10.1080/04353676.2019.1670950

Wakonigg, H. (1996). Unterkühlte Schutthalden. *Arb. aus dem Inst. für Geogr. der Karl Franzens Universität Graz* 33, 209–223.

Wallace, J. M., and Hobbs, P. V. (2006). *Atmospheric Science*. Amsterdam: Elsevier.

Weisbrod, N., Dragila, M. I., Nachshon, U., and Pillersdorf, M. (2009). Falling through the cracks: the role of fractures in Earth-atmosphere gas exchange. *Geophys. Res. Lett.* 36, 1–5. doi: 10.1029/2008GL036096

Westermann, S., Schuler, T. V., Gisnås, K., and Etzelmüller, B. (2013). Transient thermal modeling of permafrost conditions in Southern Norway. *Cryosph* 7, 719–739. doi: 10.5194/tc-7-719-2013

Wicky, J., and Hauck, C. (2017). Numerical modelling of convective heat transport by air flow in permafrost talus slopes. *Cryosph* 11, 1311–1325. doi: 10.5194/tc-11-1311-2017

APPENDIX A

TABLE | Nomenclature.

C_a	Specific heat capacity of air (J kg^{-1} K^{-1})
C_p	Volumetric heat capacity (J m^{-3} K^{-1})
d	Angle of the flow direction (°)
d_p	Particle diameter (m)
dT	Freezing interval (K)
g	Gravitational acceleration (m s^{-2})
H	Vertical dimension (m)
k	Thermal conductivity (W m^{-1} K^{-1})
p	Pressure (Pa)
q	Heat flux (W m^{-2})
Q	Heat source (sink) (W m^{-2})
q_0	Heat boundary flux (W m^{-2})
Q_m	Boundary flux (kg m^{-2} s^{-1})
Ra	Rayleigh number
Ra_crit	Critical Rayleigh number
T	Temperature (K)
t	Time (s)
u	Horizontal velocity component (m s^{-1})
V	Velocity (m s^{-1})
v	Vertical velocity component (m s^{-1})
x	Cartesian coordinate (m)
y	Cartesian coordinate (m)
β	Coefficient of thermal expansion (K^{-1})
ζ	Vorticity (s^{-1})
κ	Permeability (m^2)
μ	Dynamic viscosity (Pa s)
ρ	Density (kg m^{-3})
Φ	Porosity

Paper III deals yet again with talus slopes but provides an insight into the thermal regime of a low elevation cold talus slope through numerical modelling. The model is solved in the COMSOL Multiphysics 5.6 environment and solves for conduction and convection through airflow in the porous medium, described by the laws of Fourier and Darcy. From the Dreveneuse site, located in the Valais Prealps, GST data is used as a boundary, borehole temperature data for validation and further geophysical data is integrated to improve the representation of soil heterogeneity.

Title: Modelling the link between air convection and the formation of short-term permafrost in low altitude cold talus slopes.

Author contributions: Jonas Wicky designed and performed the model calculations, analysed the data, produced all the corresponding figures, and wrote the main part of the manuscript with inputs from Christian Hauck. Christin Hilbich and Christian Hauck performed and analysed the geophysical measurements, produced the corresponding figure und contributed substantially in writing the corresponding section. Reynald Delaloye provided the monitoring data and his knowledge on the site which contributed to a consistent manuscript.

Reference: Wicky, J., Hilbich, C., Delaloye, R. and Hauck, C. (in prep.). Modelling the link between air convection and the formation of short-term permafrost in low altitude cold talus slopes. Submission to *Permafrost and periglacial Processes* foreseen.

Modelling the link between air convection and the occurrence of short-term permafrost in a low altitude cold talus slope

Jonas Wicky , Christin Hilbich , Reynald Delaloye , and Christian Hauck

Abstract

We extend a numerical modelling approach developed to explicitly model convective heat transfer in periglacial landforms to represent the ground thermal regime of low altitude cold talus slopes. Our model solves for heat conduction and accounts explicitly for air convection adopting a Darcy term with a Boussinesq approximation for air circulation in the porous ground. Numerical model experiments with forcing data from the low altitude talus slope Dreveneuse in the Valais Pre-Alps, which showed the occurrence of two short-term permafrost periods over the last 17 years, confirm that air convection is the key to forming and maintaining ground ice. In the model, the porous talus slope is underlain by a layer of water-bearing morainic material, where ground ice forms due to air convection. In years, where the gradient between air temperature and talus temperature is sufficiently large to result in increased cooling, the ground ice lasts for more than a year. It is only by considering convection that the model is able to represent the occurrences of ground ice respectively permafrost, which is in correspondence with the observations on-site. These findings are insofar important, as they confirm that ground ice can be formed and maintained in landforms with a MAAT $> 0°C$ if ground air convection is present combined with the presence of water. Further, the model proved its capacity to reproduce the spatio-temporal occurrence of short-term permafrost in a low elevation talus slope.

Keywords talus slope, convection, numerical modelling, periglacial landform, permafrost

1 Introduction

Due to their exceptional climatic behaviour, low altitude talus slopes have long research history. Ground temperatures at the base of such talus slopes are colder than in the surroundings creating a local ground microclimate that is characterized by colder mean temperatures and lower temperature variability. This has an effect on the local flora and fauna, as these low altitude sites serve as a refuge for different species in flora and fauna (Zacharda et al., 2005; Millar, Westfall, & Delany, 2016; Lendemer, Edenborn, Harris, et al., 2009). Moreover, the existence of ground ice has been proven (Kneisel, Hauck, & Mühll, 2000), which favours the occurrence of azonal permafrost (Delaloye, Reynard,

Lambiel, Marescot, & Monnet, 2003). Although their thermal behaviour has been extensively studied through field analysis with temperature measurements, geophysical investigations and geomorphic research (Popescu et al., 2017; Sawada, Ishikawa, & Ono, 2003; Hauck & Kneisel, 2008; Morard, Delaloye, & Lambiel, 2010; Zacharda, Gude, & Růžička, 2007; Gude et al., 2003; Stiegler, Rode, Sass, & Otto, 2014), attempts of a representation in a numerical modelling framework are sparse (Tanaka, Nohara, & Yokoi, 2000). In a recent modelling approach, (Wicky & Hauck, 2017) and (Wicky & Hauck, 2020) developed a model that explicitly accounts for air convection in the ground in the context of coarse blocky alpine permafrost. The results showed that ground air convection is a crucial process governing the ground thermal regime and that the model is able to represent it well. Compared to a talus slope within the altitudinal belt of mountain permafrost, convection influences not only the distribution of permafrost (Lambiel & Pieracci, 2008; Scapozza, Lambiel, Baron, Marescot, & Reynard, 2011) but is key to the occurrence of permafrost in low altitude talus slopes. The MAAT can be several degrees above the freezing point and still year-round ground temperatures at or below 0°C can be observed (Delaloye et al., 2003; Morard et al., 2010). Moreover, the dynamics of the ground ice occurrence and distribution are quite high in a low altitude talus slope (Morard et al., 2010) and cannot be explained by the incorporation of avalanche snow deposits, as postulated by (Kenner et al., 2017) for a particular alpine talus slope.

To represent the specific thermal behaviour of a low altitude talus slope, our model approach (Wicky & Hauck, 2020, 2017) was further developed in the (i) geometry, (ii) subsurface heterogeneity, (iii) boundary conditions and the (iv) incorporated processes. The two-dimensional geometry (i) represents the slope profile, accounting for changes in slope angle and is not only schematic. The subsurface heterogeneities (ii) are approximated through the integration of geophysical data, whereby in the previous publications porous media was always homogeneous. Regarding the boundary conditions (iii), temperature measurements from different locations along the surface profile are integrated and the boundary is therefore not constant over space anymore. This provides a more realistic representation of the model forcing. Furthermore, the model is able to account for more processes (iv), as the aggregation and melting of ice in porous sediments below the talus, respecting the latent heat exchange, and the representation of an observed seasonal asymmetry in the airflow intensity.

We use data from the Dreveneuse site, which is located below the timberline in the Swiss Prealps and showed the occurrence of permafrost over some years only in the recent past (Morard et al., 2010; PERMOS, 2019). The research site offers a broad and high-quality data set that can be efficiently used to constrain numerical modelling. The aim is to answer the following questions: To what extent is the model able to explain the exceptionally cold thermal behaviour observed in the measured data through convection? How can ground ice be formed and how can the dynamics of

occurrence and extent be characterized?

2   Study site

2.1   Description

The Dreveneuse study site is located in the Valais Prealps (Switzerland) above the Rhone valley on its western flank (coordinates WGS 84 lat/lon 46.27344/6.88959). The slope stretches from 1560 m.a.s.l. to 1650 m.a.s.l, the slope angle rises from about 30° at the base of the talus to 40° at the top and is oriented to E/ENE. The mean annual air temperature MAAT is around 5 °C (Morard et al., 2010). The lowest part is covered by dwarf spruces (mainly *Picea abies*) and mosses, the middle part is covered with mixed forest, whereas the upper part is almost free of vegetation and the limestone blocks appear at the surface. The Dreveneuse low altitude talus slope has been extensively studied on a geomorphic field-based approach combined with temperature, anemometer and geophysical measurements (Morard et al., 2010; Delaloye & Lambiel, 2007; Delaloye, 2004; Lambiel, 2006), geophysical ERT monitoring (Mollaret et al., 2019) and soil moisture characteristics (Pellet & Hauck, 2016). Dreveneuse was part of the Swiss permafrost monitoring network (PERMOS) to represent low-elevation permafrost sites but was later withdrawn from the network because of the absence of permafrost conditions since 2012. A comprehensive overview of the data and site history is given in (PERMOS, 2019).

2.2   Temperature data

Ground Surface temperature (GST) monitoring data is from GST loggers distributed along an altitudinal profile over the site (Fig. 1), the loggers with the ID 10, 11, 13 and 14 are used in this study as boundary data (Fig. 4, section 3.4). Logger 12 is dismissed because the data gaps are of too long duration. Logger 15 lies beneath bare blocks, where the energy balance is strongly influenced by the incoming radiation. Therefore, the boundary temperature in the uppermost section is also prescribed by logger 14. The ground temperature data used for validation (section 3.8) is monitored in two boreholes drilled in 2004 (PERMOS, 2019). Borehole DRE_0104 is reaching a depth of 14.5m in the middle part, the underlying morainic material is reached at a depth of roughly 10 m (Morard et al., 2010). Borehole DRE_0204 in the lower part is reaching a depth of 4.8 m (see Figs. 1 and 4), where the porous accumulation is 4 m thick (Morard, 2011). Data is available on request through either the PERMOS network or R. Delaloye directly (Co-Author and Site PI).
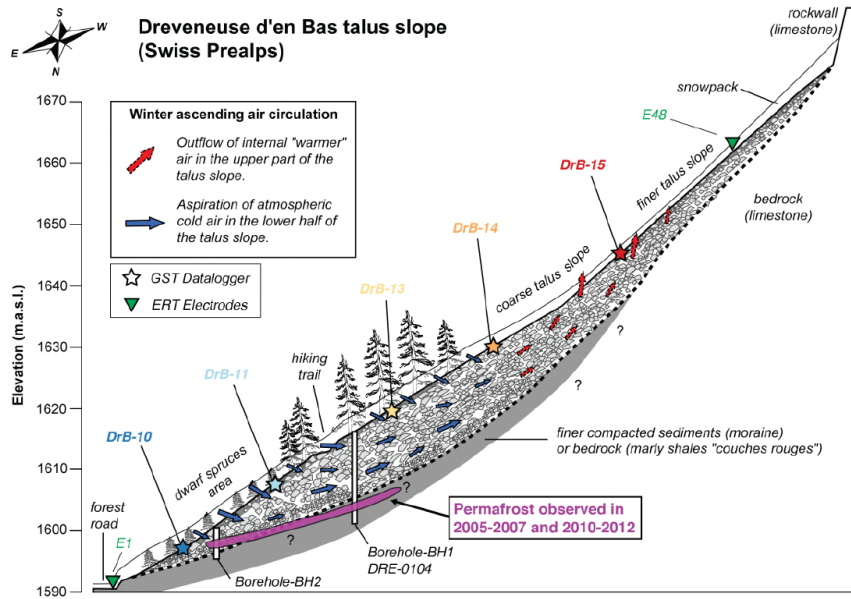
Figure 1: Overview sketch of the Dreveneuse site with the location of temperature loggers, boreholes and the ERT-electrodes of the geoelectrical profile as well as the winter air circulation situation. Published in (PERMOS, 2019) and (Morard, 2011).

2.3 Geophysical surveys

Geophysical surveying at the Dreveneuse site was started in 2007 to characterise the talus slope, but also to monitor potential changes in the subsurface composition related to thermal changes (Morard, 2011). Initial ERT surveying revealed a clearly visible resistive anomaly in the central part of the slope (> 50 kΩ m, Fig. 2 A), which is typical for coarse blocky material and often found in low-altitude and alpine talus slopes (Mollaret et al., 2019; Gude et al., 2003; Kneisel et al., 2000; Hilbich, 2010). The thickness of this resistive layer is around 10-15 m with a more conductive layer (~3 kΩ m) on top and decreasing resistivities below.

Collocated refraction seismic tomographic measurements from autumn 2020 (Fig. 2 B) reveal overall low (< 1500 m s^{-1}) P-wave velocities in the region of the resistive anomaly which indicate a low probability of substantial ground ice occurrences. Comparable RST surveys at higher altitudes in alpine talus slopes usually show much higher P-wave velocities, which can be interpreted as ice-rich permafrost occurrences (e.g. at the Lapires talus slope, (Hilbich, 2010)). The absence of P-wave velocities > 2000 m s^{-1} in the region of the resistive anomaly (cf. Fig 2 A) would therefore indicate that no larger ice content volumes have been present in 2020 in the talus slope Dreveneuse.

A geophysical argument in favour of the former presence of small ground ice volumes until 2015 has been shown and discussed in (PERMOS, 2019) and (Mollaret et al., 2019), i.e. the continuous decrease of mean specific electrical
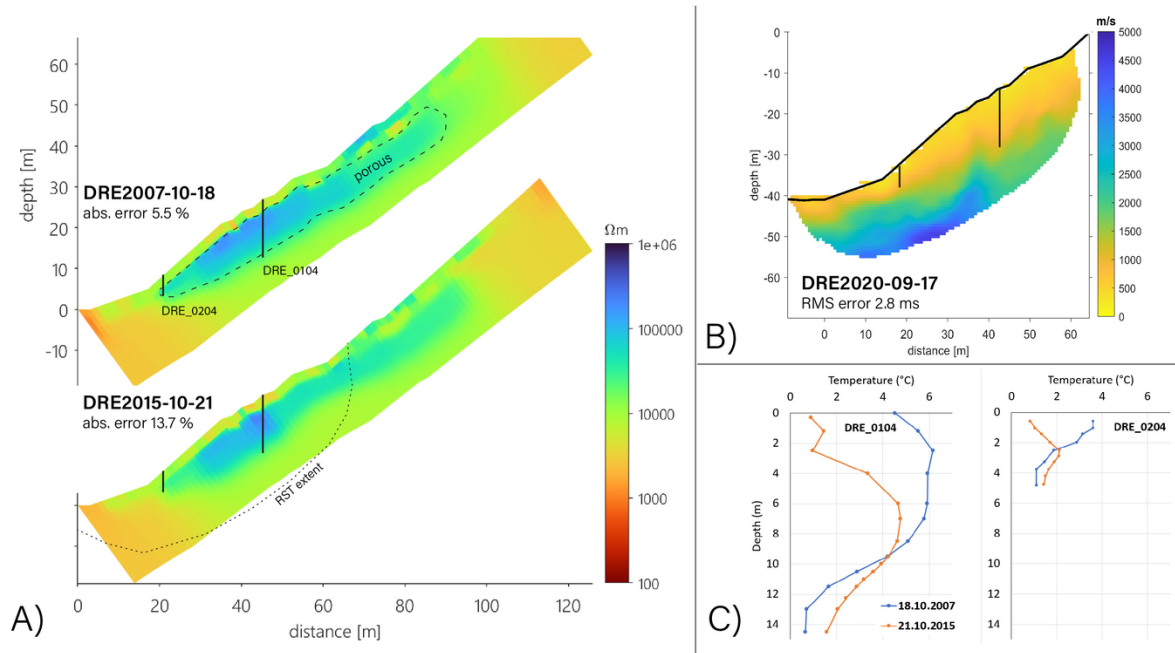
Figure 2: (A) ERT inversion results for two measurements along the talus slope in October 2007 and 2015. The black vertical lines mark the upper (DRE_0104) and lower (DRE_0204) borehole. (B) RST inversion results (extent marked in lower panel of A) from September 2020 along the same measurement line. (C) Borehole temperature measurements for the two measurement dates shown in (A).

resistivity at around 10 m depth between 2007 and 2015. Borehole temperatures in the two boreholes suggest warming at larger depths during this period and continuously negative temperatures were only present from 2005 to 2007 and for a short period in 2011/12 (see section 4.1). However, the continuous decrease in resistivity between 2007 and 2013 (Mollaret et al., 2019) and the geometrical change of the shape of the resistive anomaly between 2007 and 2015, which is still present afterwards (Fig. 2 A) could also be interpreted as evidence for still ongoing permafrost degradation or at least warming ground conditions. This is, however, in contrast with the measured borehole temperatures, which indicate the absence of ground ice from 2015 onwards (section 4.1). The interpretation of the geophysical measurements thus leaves open the question of whether small ground ice occurrences (and hence permafrost) still existed in 2015 and whether the (point-scale) borehole temperature data can be considered representative in this respect.

2.4   Seasonal heat transfer cycle

Heat transfer by conduction, as described by (Fourier, 1822), is the main heat transfer mechanism in frozen soils. However, further non-conductive heat transfer processes need also to be taken into consideration (Kane, Hinkel, Goering, Hinzman, & Outcalt, 2001). Heat can further be transferred through radiation and convection. Especially in substrates

with high permeability, heat transfer through convection plays an important role. Convection can be described as heat transfer through a moving fluid. Natural convection in a flat porous ground occurs vertically and results in convection cells (Rayleigh-Bénard circulation), which is also often referred to as the Horton-Rogers-Lapwood problem for a porous medium heated from below (Horton & Rogers, 1945; Lapwood, 1948). In mountain slopes, convection develops also a lateral component due to gravity resulting in heat transfer along the slope (Guodong, Yuanming, Zhizhong, & Fan, 2007). This is also often referred to as advection. Advection is very pronounced in talus slopes and is referred to as the *chimney effect*, described by (Wakonigg, 1996).

The convective air circulation is driven by the temperature gradient between the talus (interior) temperature and the air (exterior) temperature, leading to a seasonally reversing internal air circulation. During winter, the temperature within the talus is warmer than the exterior temperature. Due to the density difference between warm and cold air, a buoyancy-driven ascending air courant develops and is released in the upper part of the talus. Snowmelt holes with hoar formations can sometimes be observed at the warm air exits. The upper part of the talus often shows round melt patterns of air expulsion, especially during very cold periods, and is earlier snow-free. As the release of warm air in the upper part of the talus leads to an underpressure in the lower part of the talus, the cold outside air is even aspirated through a think snow cover, either through snow funnels or through the snow as a porous medium (Morard, 2011). During summer, the circulation reverses. When the air temperature is higher than the talus temperature, cold air sinks down within the talus and is expulsed at its base. The cold air expulsion can easily be observed on the field on warm summer days.

Fig. 3 shows ground temperatures at depth in the borehole DRE_0104 during an intensive cooling period from mid-January to mid-February 2011. The temperature drop is propagated to lower depths not only through conduction. In particular, at a depth of 8.5 m and 9.5 m, the advection of cold air is visible and demonstrates the strong influence of convective heat transfer on the ground thermal regime of the talus slope.

3 Model description

3.1 Governing equations

The governing equations are described in (Wicky & Hauck, 2020). Heat transfer by conduction and convection is described by equations 1 and 2, where q is the heat flux, Q is the storage term, q_0 the boundary flux, k the (effective) thermal conductivity, C_p the (effective) volumetric heat capacity, ρ the density, V the velocity, T the temperature and t
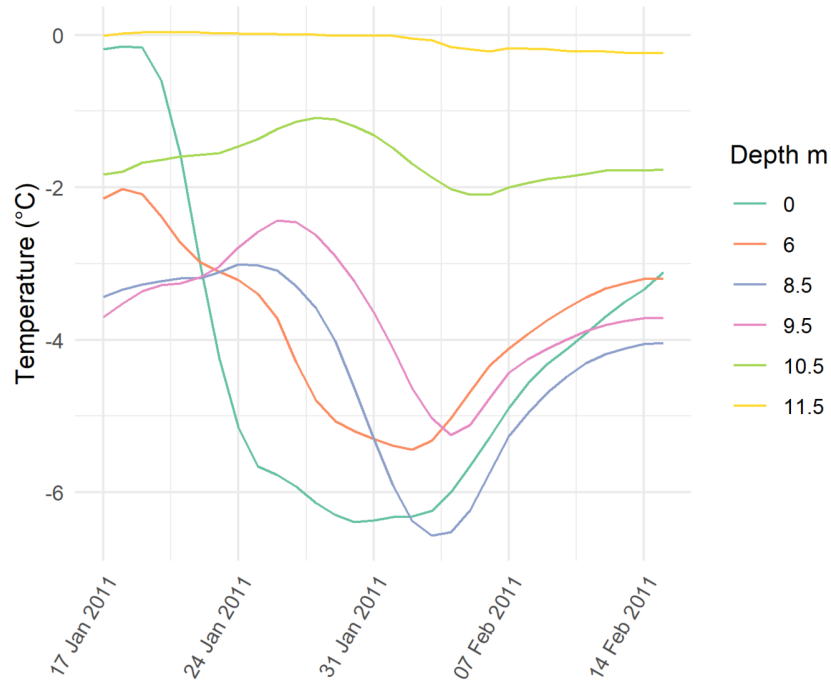
Figure 3: Ground temperatures at different depths in borehole DRE_0104 during an intensive cooling period in January/February 2011. Especially at a depth of 8.5 m, the non-conductive heat transfer is clearly visible.

the time.

$$rC_p\frac{\partial T}{\partial t} + rC_p V \nabla T + \nabla q = Q + q_0 \tag{1}$$

$$q = -k\nabla T \tag{2}$$

The airflow in the porous domain is described by Darcy's law expressed in equations 3 and 4, where Φ is the porosity, Q_m the boundary flux, κ the permeability, μ the dynamic viscosity, g the gravitational acceleration and p the pressure. Note the ρg term in equation 4 - the Boussinesq approximation accounting for density changes in the air and thus for natural convection effects.

$$\frac{\partial}{\partial t}(\phi\rho) + \nabla(\rho V) = Q_m \tag{3}$$

$$V = -\frac{\kappa}{\mu}(\nabla p - \rho g) \tag{4}$$

3.2 Geometry

The geometry consists of three regions. These regions are constrained by (i) geophysical measurements showing the different entities of the subsurface and (ii) by the boreholes on-site which indicates that in the middle part of the talus, consolidated sediments, probably morainic deposits, lie at a depth of roughly 10 m (Morard et al., 2010). Fig. 4 shows the extent of the numerical domain with the three sub-domains representing the bedrock, the porous talus and the underlying morainic material (Table 1).

Figure 4: Model geometry with 3 domains: porous talus slope (1), a layer of morainic material (2) and bedrock (3), and the meshing. The boreholes DRE_0104 (DRE_0204) are indicated with a purple (pink) line, the line length is according to the borehole depth. The GST loggers defining the forcing at the upper boundary are indicated in green.

3.3 Material properties

3.3.1 Thermal properties

The thermal properties of the solid part, corresponding to the talus debris, are constant and set to values for Alpine limestone (Čermák & Rybach, 1982) with thermal conductivity k of 2.09 W m^{-1} K^{-1}, specific heat capacity C_p of 800 J kg^{-1} K^{-1} and density ρ of 2700 kg m^{-3}. The thermal properties of the air (C_p, k, ρ) in the porous part of the talus

(domain 1, Fig. 4) are set to standard literature values as a function of temperature (COMSOL, 2021). The same applies to the thermal properties of water and ice (C_p, k, ρ) in the morainic material (domain 2, Fig. 4). The change of phase between water and ice accounts for latent heat. The latent energy of freezing (or melting) is represented by a corresponding increase in heat capacity in a transition interval around the phase change temperature of 0°C of [-0.5°C, 0.5°C], where also the thermal properties linearly change. Both, the talus and the underlying morainic material are porous media. The porosity of the morainic material is homogeneous and set to 0.2, whereas the talus porosity is linked to the measured normalized resistivity nR (cf 3.3.2). The thermal properties of the porous domains are obtained through volume averaging.

Do-main	Description	Material	Conduc-tion	Convec-tion	Poros-ity	Phase change	Mesh element size
1	Bedrock	Limestone	x	-	-	-	0.39 m - 8.71 m
2	Porous talus	Limestone, Air	x	x	0.5 * nR	-	0.0 m - 0.87 m
3	Morianic sediment	Limestone, Water	x	-	0.2	Water / Ice	0.39 m - 8.71 m

Table 1: Summary of the main properties of each domain, depicted in Fig. 4.

3.3.2 Permeability

Airflow in the porous domain is described by Darcy's law where the most important parameter describing the flow is the ground permeability. The permeability is often obtained through empirical relationships, whereby the Kozeny-Carman (K-C) equation is probably the most used one (Nield & Bejan, 2017). It defines the permeability as :

$$\kappa = \frac{\phi^3}{5 \, S_p^2 \, (1-\phi)^2} \tag{5}$$

Where S_p is the specific surface area, which is the surface area per unit volume and can also be described with the typical particle diameter d_p (Johansen, 1975):

$$S_p = \frac{6}{d_p} \tag{6}$$

However, the K-C relation has been developed with perfect spheres of equal sizes packed in a bed for d_p in the range of mm. For sand, (Johansen, 1975) finds that d_p is either the harmonic mean or d_{10}, the diameter which 90% of the particles exceed. For bigger particle sizes, laboratory measurements have been done (Côté, Fillion, & Konrad,

2011; Rieksts, Hoff, Scibilia, & Côté, 2019), as the permeability can not be measured on-site. They reveal that the K-C relation is likely to overestimate the permeability in crushed rocks. Furthermore, they derive permeability values of around 0.5 - 3.9 * 10^{-6} m^2 for the crushed rocks laboratory experiments, which is consistently integrated into numerical modelling studies on the passive cooling capacities of road embankments (Lebeau & Konrad, 2009). The probable ranges of permeability for an alpine permafrost context have been extensively discussed in (Wicky & Hauck, 2020), and model simulations herein were consequently conducted with different permeability values.

3.3.3 Sub-surface heterogeneity

To account for the spatial heterogeneity of the subsurface, we integrate data from geophysical measurements - more precisely electrical resistivities. At DRE, electrical resistivity tomography (ERT) was performed regularly to monitor the resistivity on-site (section 2.3). We use a single high-quality measurement from 2015-10-21 (Fig. 2 A) to account for spatial patterns of the heterogeneity in the subsurface. High permeability soils (in a comparatively dry state) tend to show lower conductivity values thus having a higher resistivity. This allows to link the permeability to the electrical resistivity measurements as follows (Lesmes & Friedman, 2005):

$$\kappa = \frac{1}{a \, F \, S_p^2} \tag{7}$$

where a is a dimensionless shape factor (ranging from 1.7-3) and F is the electrical formation factor, described by Archie's law as follows (Lesmes & Friedman, 2005):

$$F = \frac{R_t}{R_w} \tag{8}$$

where R_w is the resistivity of the fluid phase and R_t is the total resistivity. However, (Lesmes & Friedman, 2005) note that S_p is far more sensitive than F. As it is not possible to perform any permeability measurements (respective measurements of S_p) on-site, we decided to use the permeability values κ of 1 * 10^{-7} m^2, 1 * 10^{-6} m^2 and 3 * 10^{-6} m^2 that were proven to be adequate for modelling of air convection in coarse blocky alpine permafrost in (Wicky & Hauck, 2020) and that are within the range of proposed values from the literature, whether from laboratory values (Rieksts et al., 2019; Côté et al., 2011) or from modelling studies (Lebeau & Konrad, 2009; Guodong et al., 2007). Eq. 7 describes that the permeability is scaled by F, which in turn is defined by the measured resistivity (Eq. 8), assuming that R_w is constant. We thus normalize measured values of R_t on a logarithmic scale to a scale from 0-1 (Eq. 9) as

follows:

$$nR = \frac{\log(R_t)}{\max(\log(R_t))} \tag{9}$$

Where R_t is the total resistivity measured on the field, and nR the resulting scaling factor (Fig. 5), which is then multiplied with the porosity ϕ of 0.5 at each node and the respective permeability value κ of $1 * 10^{-7}$ m^2, $1 * 10^{-6}$ m^2 and $3 * 10^{-6}$ m^2. The permeability values represent a low permeability with conduction dominated regime, a mid-high permeability and a permeability, where convection is of high importance.
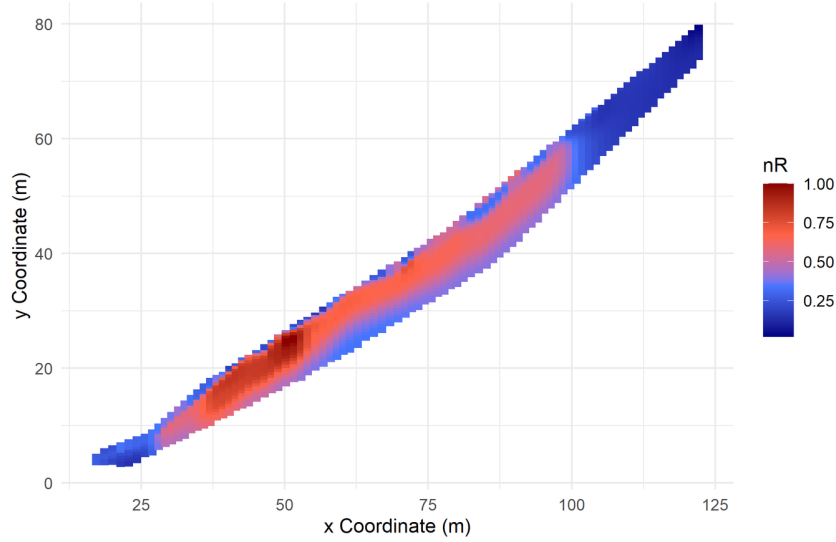

Figure 5: Values of nR.

3.3.4 Seasonal asymmetry

Ground temperature mapping showed an asymmetry between the summer air expulsion area and the winter air aspiration area (Delaloye, 2004). Further, roughly two times higher air velocities were observed during the winter aspiration phase (Morard et al., 2010; Delaloye & Lambiel, 2007) than during the summer expulsion phase, indicating that air convection is more effective during the winter. The exact physical process explaining this spatio-temporal asymmetry is not fully known, but it appears that the summer and winter circulation does not use the same flow paths. This is

taken into account by the implementation of a seasonal switch in permeability. At each time step, the mean temperature of the porous talus (domain 2) is calculated. If the mean talus temperature is lower than the mean air temperature measured on-site at the meteorological station at the corresponding time step, the permeability is switched to $1 * 10^{-7}$ m^2. When the gradient inverses and thus the mean talus temperature is higher than the outside temperature, the three above mentioned permeability values are applied. The sensitivity of this switch is further discussed in section 5.2.

3.4 Boundary conditions

The upper thermal boundary condition is of Dirichlet type and is described by measured GST. The loggers with the ID 10, 11, 13, 14 are used for the simulation of the hydrological years 2006-2018 (cf. Fig. 4). The GST forcing data set is almost complete, except for logger 11 for the hydrological year 2014 where data is replaced by measurements from the year 2013, which shows a quite similar meteorological behaviour. Gap filling algorithms over such an extended period are not very trustworthy and therefore we choose this option. The loggers are placed according to their GPS measured elevation along the upper boundary (Fig. 4). Then, daily altitudinal temperature gradients are calculated to yield the temperature boundary condition for each surface node using a linear interpolation between the four different GST loggers at the upper boundary. Below (above) GST logger 10 (14), the temperature of the corresponding logger is prescribed.

The lower thermal boundary is of Neuman type and is described by a constant geothermal heat flux of 0.03 W m^{-2}. The sidewalls are isolated. Pressure at the upper boundary is set to atmospheric using an altitude-dependent pressure head boundary condition ($p = \rho g \left(-y\right)$), sidewalls and bottom do not allow for any flow.

3.5 Initial conditions

The initial conditions of the transient model run using data from the hydrological years of 2006-2018 are obtained through a two-step spinup procedure. The first step consists of a steady-state model run, where the lower boundary is prescribed by the constant geothermal heat flux and the upper boundary is a temperature with a constant gradient of 0.1 °C m^{-1}, starting at 0°C at the lowermost node. The gradient is chosen to assure that this steady-state run provides stable initial conditions to a transient spin-up. The bottom boundary of the transient spin-up is yet again the geothermal heat flux. The upper thermal boundary is defined by data of the year 2005 from all GST loggers, repeatably applied for a spin-up time of ten years. Numerical tests show that quasi-equilibrium is reached with 10 years of spin-up and that repeating the first modelled year (2005) provides stable initial conditions and a smooth transition to transient model simulation, even though 2005 is a comparatively cold year. The spinup procedure showed a quite high influence on the

235 results and has to be handled with care, especially since the initial ice content has the potential to influence the model

236 results substantially due to the latent heat reservoir.

3.6 Time-stepping

238 The time-stepping follows the adaptive time-stepping scheme proposed by the COMSOL Multiphysics (COMSOL,

239 2021) solver. The maximum time step size is one day in order to make sure that each data point from the boundary

240 data is modelled.

3.7 Mesh size

242 The mesh is composed of triangular elements and consists of a total of 11'137 nodes. The element size is decreasing

243 with depth, the range of mesh size is indicated in Tab. 1. The relatively fine mesh in domain two allows for an accurate

244 representation of the airflow. Mesh tests showed that the applied configuration is a good compromise between accuracy

245 and computational effort, whereby a coarser mesh tends to be less accurate and a finer meshing leads to a higher

246 computational cost and at some point to deteriorating results.

3.8 Validation data

248 Data for validation is used from two boreholes on site, which are still operational. The validation data is thus com-

249 pletely independent from the forcing data. We use ground temperature data which is measured in the two boreholes

250 DRE_0104 and DRE_0204 (cf section 2.3) at depth and aggregated to daily means to compare measured and modelled

251 data. For the borehole DRE_0104 data is missing from 2013-02-27 to 2014-07-16 and for DRE_0204 data was only

252 available until 2016.

4 Results

4.1 Borehole temperatures

255 Fig. 6 and 7 show the modelled temperature at different depths in two virtual boreholes for permeability values of

256 $1 * 10^{-7}$ m^2, $1 * 10^{-6}$ m^2 and $3 * 10^{-6}$ m^2, indicated with different colours. The validation data from the boreholes

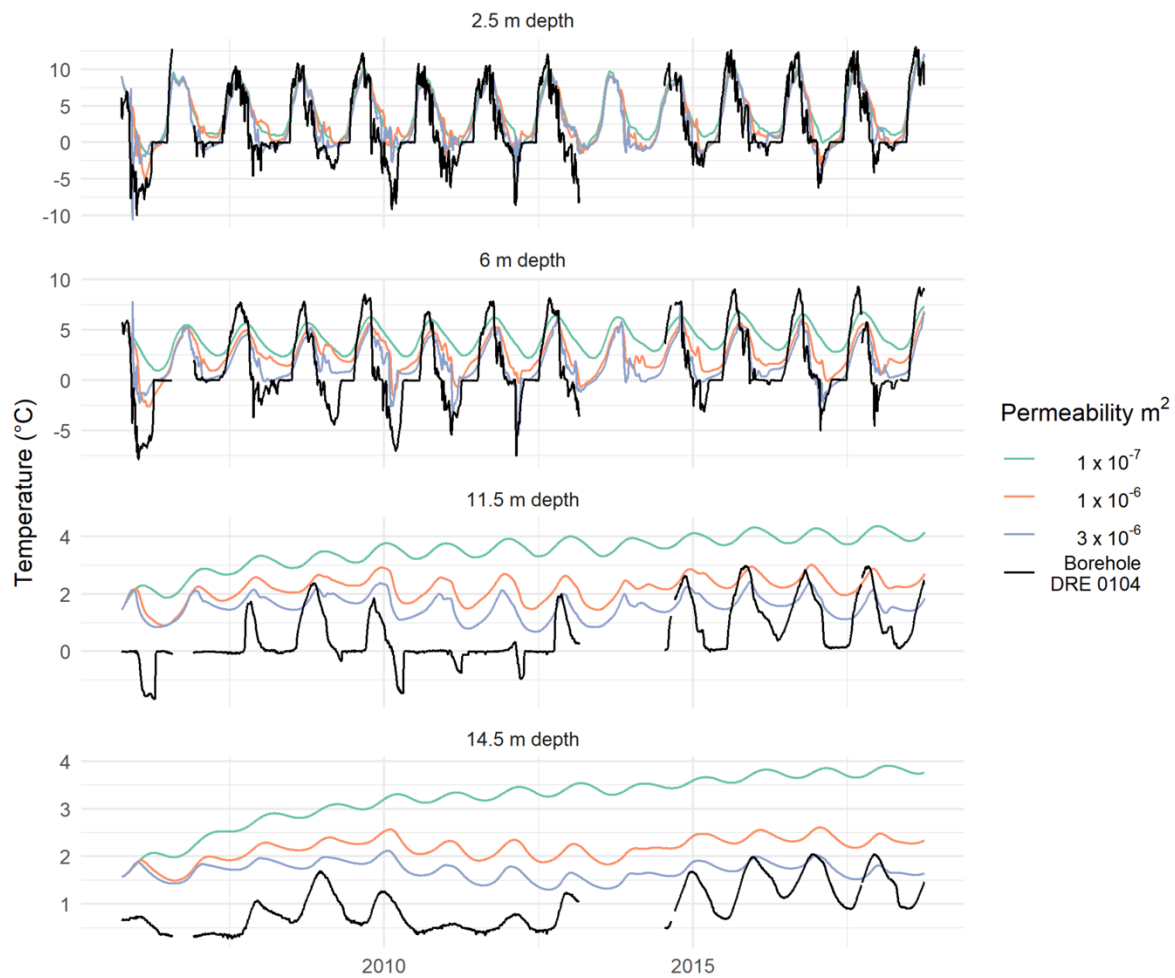257 DRE_0104 and DRE_0204 is plotted in black.

Figure 6: Modelled and measured temperatures at different depths in a virtual borehole at the location corresponding to the DRE_0104 borehole (Fig. 4). The colours represent different ground permeability values in the porous talus (Domain 2). The black line indicates the measured data at the borehole DRE_0104.

At the upper borehole DRE_0104 (Fig. 6), it is important to note that the lowest permeability value yields far too warm temperatures. Convective heat transfer is needed to reach the measured temperatures. Permeability values of 1 * 10^{-6} m^2 and 3 * 10^{-6} m^2 lead to results in the range of the measured temperatures. It is important to consider that ice aggregation is not modelled in the porous talus and therefore latent heat effects cannot be represented. This is an issue at depths of 2.5 and 6 meters, where the zero curtain periods are not represented. At depths lower than 10 m, the virtual borehole reaches morainic, water-saturated substrate but the modelled temperatures are too high to aggregate ice at the virtual borehole. Lower down in the model, ice aggregates (Fig. 8) and allows to represent the observed periods of permafrost.

In the lower borehole DRE_0204 (Fig. 7) the missing integration of latent heat is as well apparent. In comparison to the upper borehole, ice aggregates also in the porous talus in the lower borehole. This escapes the model because the talus is modelled as always dry. Still, the temperature amplitude, if not masked by latent heat effects, is well captured representing the colder microclimate at the base of the talus slope.
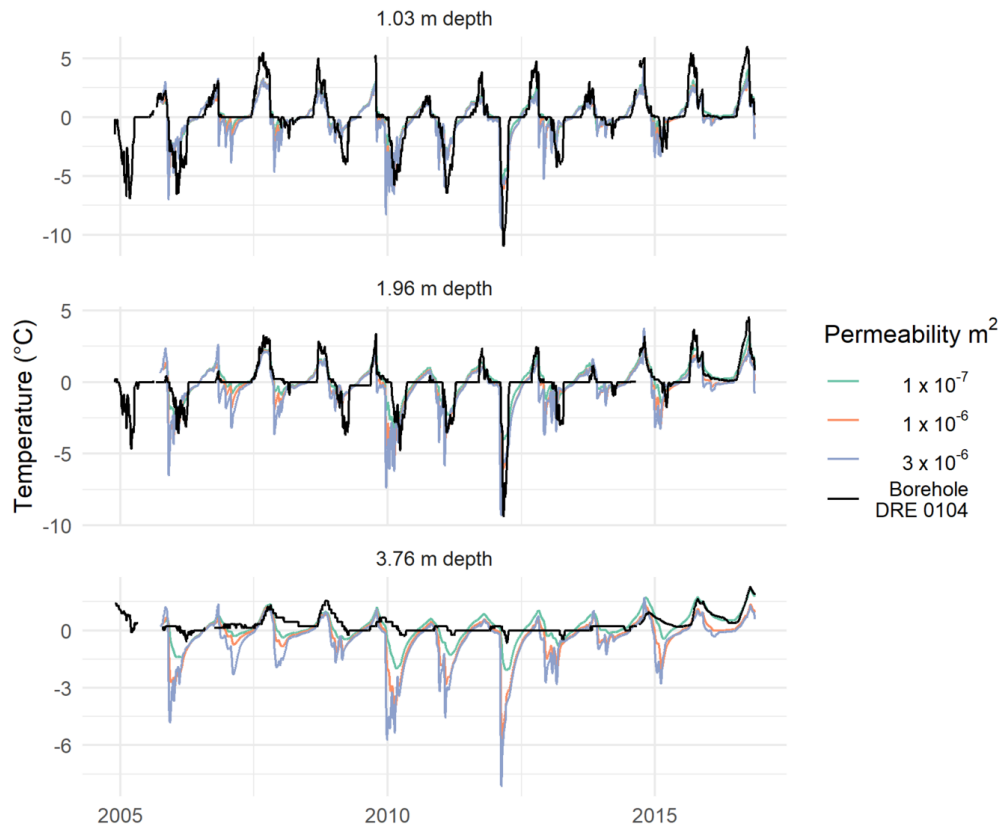

Figure 7: Modelled and measured temperatures at different depths in a virtual borehole at the location of DRE_0204 borehole. The colors represent different permeability values in the porous domain 2, the black line inidcate the measured data.

4.2 Temperature and air flow field

Fig. 8 & 9 show a 2D profile plot with airflow vectors. Fig. 8 shows the circulation and temperature at the end of September just before the cooling starts again (2012-09-30). The frozen part is restricted to the lower part of the talus, where the model is able to aggregate ground ice in the morainic material. This coincides with the findings from (Morard et al., 2010), schematically illustrated in Fig. 1. The circulation is a uniform gravitational downflow

due to the descending cold air inside the talus. Fig. 9 shows a situation at the end of January (2012-01-30) where the convective ascending air circulation is best established. It can be observed that an upwards convective flux takes place due to the relatively warmer air in the talus. The location of the cells is thereby somewhat influenced through the location of the GST Loggers and the related change in temperature gradient along the slope. It can also be seen, that the frozen part in the bottom is a remnant from the previous year. The (re-)freezing of the morainic material starts about mid-February for a permeability value of $1 * 10^{-6}$ m^2. A higher permeability leads to stronger and earlier (re-)freezing of the morainic layer and more pronounced convection cells.

Figure 8: Temperature field (colour) and airflow vector field (black arrows) at 2012-09-30 for a permeability value of $1 * 10^{-6}$ m^2. Note the light blue zero degrees isotherm contour, showing the extent of the frozen domain at the end of the summer, just before the cold fall temperatures start to cool the talus.

4.3 Permafrost occurence

Fig. 10 A and B show the extent of the frozen area in domain 3 (Fig. 4), the morainic material below the porous talus slope. If parts of the model domain stay frozen for two or more years, this can be interpreted as the occurrence of (short-term) permafrost. The size of this frozen area depends on the permeability value of the porous talus above (Fig. 10 A) and on the porosity (Fig. 10 B), which corresponds to the water (respectively ice) content in domain 3. It can be noted that the permeability value is a decisive parameter for the presence or absence of permafrost conditions in the simulation. A low permeability value of $1 * 10^{-7}$ m^2 yields almost no freezing in the morainic material underlying the talus slope. The mid-permeability value of $1 * 10^{-6}$ m^2 leads to an occurrence of short-term permafrost, meaning
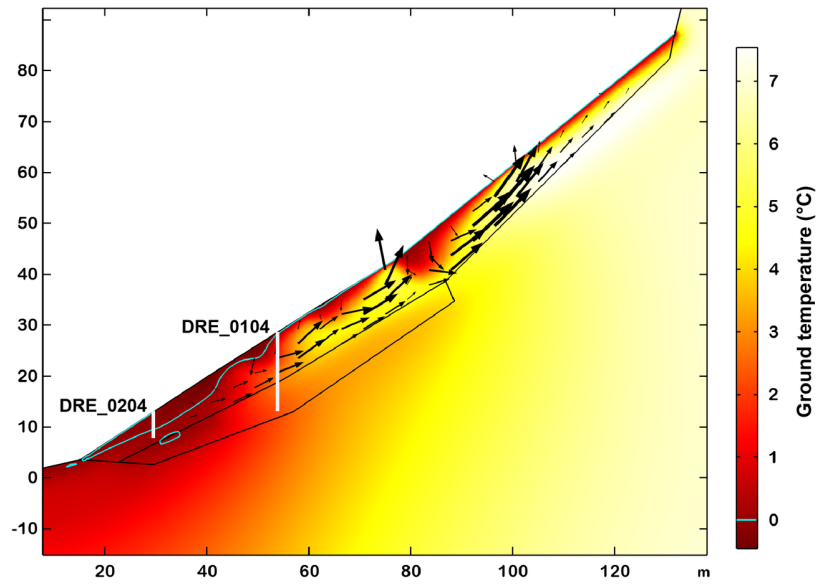
74

Figure 9: Temperature field (colour) and airflow vector field (black arrows) at 2012-01-30 for a permeability value of $1 * 10^{-6}$ m^2. Note the light blue zero degrees isotherm contour. A winter cooling situation, showing predominantly upwards convective flow.
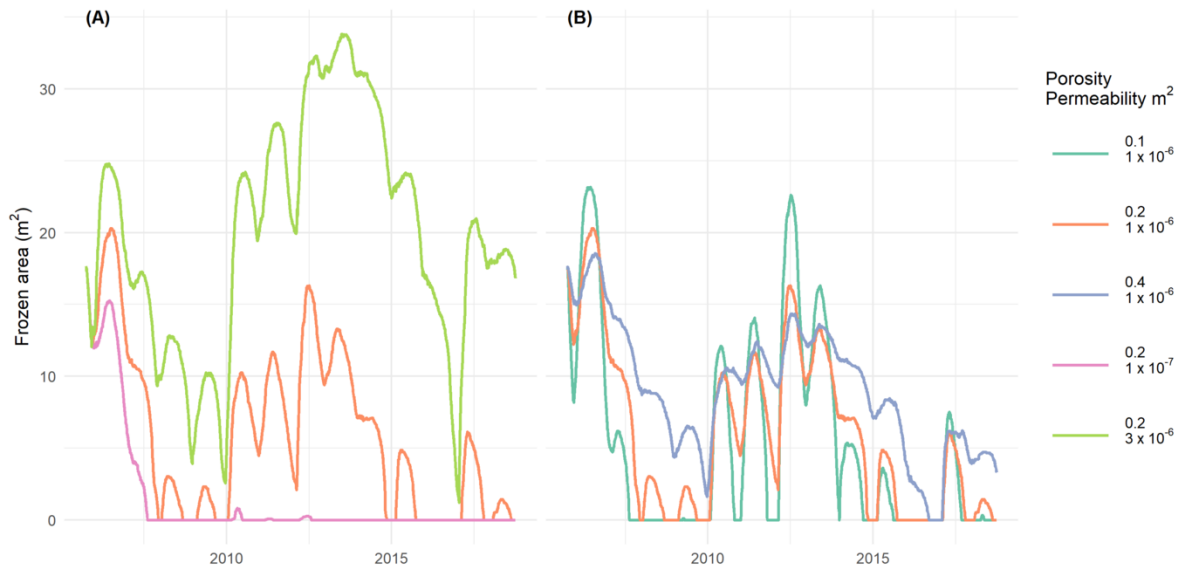

Figure 10: Frozen area (m^2) in the morainic material beneath the talus (domain 2). The two panels illustrate the sensitivity on different permeability values (A) and on different porosity (B) in domain 2 and thus water/ice content in domain 2. The colour lines indicate the respective parameter combination.

frozen conditions in the morainic material for more than a year, which appears and disappears. The timing of the occurrence of this short term permafrost corresponds to the periods of freezing observed in the borehole DRE_0104 at

a depth of 11.5m (Fig. 6). This is also the depth, where the freezing takes part in the model, whereby it is observed more downslope (Fig. 8 and 10). The virtual borehole, from which the data is shown in Fig. 6, does capture the frozen part. Further, a high ground permeability value of $3 * 10^{-6}$ m^2 yields a continuous existence of permafrost in the morainic domain below the talus (Fig. 10 A).

4.4   Sensitivity

Besides the sensitivity on the permeability values, which is an integral part of the model approach and presented along with the results, two more process-related sensitivities are presented in this section. First, the influence of preferential flow paths and the resulting seasonal difference in permeability and second, the water content in the sub-talus morainic layer which influences the extent and the sustainability of the frozen part of the talus. Fig. 11 shows a reduced data set of a model run, where the summer switch is not active and thus the permeability is the same throughout the whole year. Consequently, convective airflow acts in the same way as in winter, and the modelled temperatures are far too warm from the beginning onwards (the spinup is performed with the same constant permeability) and never reach temperatures that are close to the observations. The exact process leading to this asymmetry in summer and winter convection is not fully known yet but the high sensitivity in the model gives further evidence of its existence. The causes and effects are discussed in section 5.2.

A further sensitive parameter is the water content in the morainic material below the porous talus slope. The borehole only indicates the existence of such material. Further, the occurrence of permafrost coupled with a long zero curtain at this depth in the borehole suggest the existence of ground ice and therefore the presence of water. Fig. 10 B shows the sensitivity of the results to the porosity of the morainic layer beneath the porous talus and corresponds thus to the water content. This is summarized in Fig. 12, showing the minimal, maximal and mean extent of the frozen surface according to the relative permeability and porosity. It is important to note that a higher water content leads to more stable permafrost conditions. The strong cooling in the lower part of the talus can be more efficiently stored as a form of latent heat, whereas a lower water content may lead to a bigger extent of permafrost but is temporally less stable as the reservoir of latent heat is smaller.
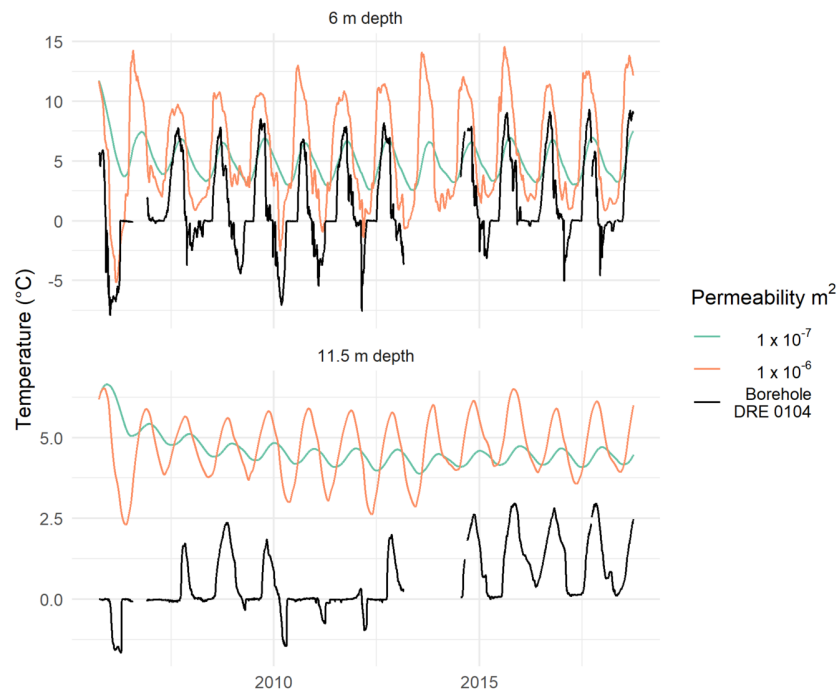
Figure 11: Comparison of measured and modelled data without the summer switch in permeability - the modelled values are far to warm.
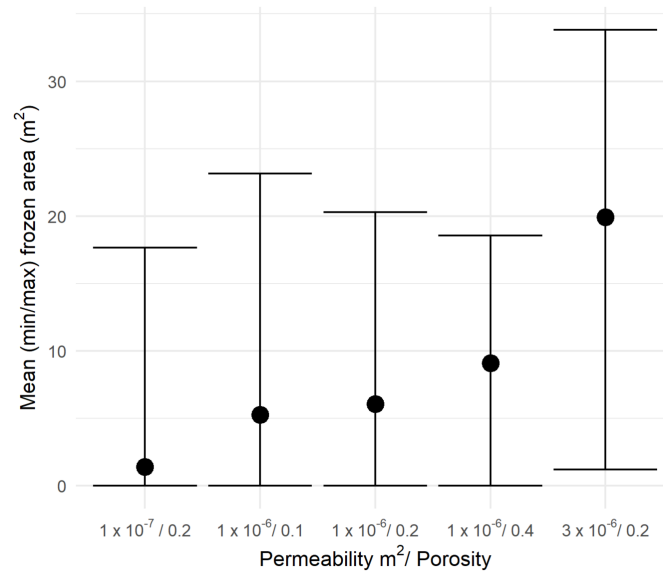

Figure 12: Mean (black dot), minimal and maximal (range indicated through bars) extent of the frozen surface summarizing the data shown in Fig. 10 A and B. The parameter combination is indicated on the x-axis.

5   Discussion

5.1   Short term permafrost

Convection has the potential to cool the ground to an extent that permafrost appears which can also vanish in the following years. The complex interaction of thermal gradient (between atmospheric boundary temperature and talus temperature), permeability and groundwater (respectively ice) content can lead to the occurrence of permafrost. The validation data exist only point-wise at the borehole locations and our model approach, even solving for the full physical process, is yet still quite conceptual in many aspects. We therefore cannot conclude which permeability values are best to represent the whole modelling domain and to exactly what extent in time and space we can expect permafrost conditions. But, and almost more importantly, the results clearly show that convection can indeed build up ground ice and thus permafrost conditions, which may persist for some years in the ground, whereas a low-permeability model run does not build up any ground ice.

Regarding the interpretation of permafrost dynamics, the temporal and spatial variability of permafrost occurrence is of relevance. Although aggregation of ice due to convective cooling can be studied best at the lower margin of the permafrost extent, it is very likely that it is of importance at any site with a highly permeable ground. At low altitude sites with a relatively low ground ice content, the model results, supported by observational data, indicate that permafrost degradation is reversible and represents a quite direct response to current cold climatic conditions. The long-term trend is rather described by the frequency of occurrence, which decreased as no permafrost was observed in the last decade. Therefore, the occurrence of short-term permafrost periods can also be interpreted as a phase of transition towards non-permafrost conditions. The high temporal dynamics makes it harder to observe a clear long-term trend as it can be seen in temperature measurements in ice-rich permafrost landforms such as e.g. the Murtèl rock glacier (PERMOS, 2019).

The distribution of permafrost and thus also the methods of prediction of permafrost distribution are affected by this convective process. At the lower margin of permafrost, as observed at Dreveneuse, convective cooling is the tipping point for the existence of permafrost. It can be assumed that also at Alpine sites at higher elevation convection plays a crucial role in the distribution and the sustainability of permafrost. (Kenner, Noetzli, Hoelzle, Raetzo, & Phillips, 2019) differentiate between ice-poor permafrost, which is mainly the result of the atmospheric forcing, and ice-rich permafrost as a result of mass wasting processes incorporating snow and ice into the landform. This explains why massive ground ice is often found at the base of a slope. Our results confirm that it is likely to find eventual ground ice at the base of the slope but also highlight the importance of convection in this context. Unconsolidated

debris originating from mass wasting processes are highly permeable porous media favouring the occurrence of air convection in the ground, having the potential to control the occurrence and extent of permafrost, at least at its lower margin.

5.2 Permeability switch

In order to explain the overestimated temperatures in the model (Fig. 11), numerous different modelling experiments were carried out. The most promising one is the one we finally implemented - a summer switch of the convective circulation by reducing the permeability when the outside temperature is warmer than the talus temperature. Other approaches, such as the cut-off of high summer temperatures, which could potentially be the result of radiation effects at the surface, were dismissed. They did not lead to satisfying modelling results in terms of fit to the validation data.

The exact physical explanation of this summer switch is still lacking, but it is mentioned in the literature (Rist, Philips, & Auerswald, 2003; Delaloye, 2004; Lambiel, 2006; Schwindt, 2013). Higher air velocities were measured during the autumn aspiration phase than during the summer expulsion phase (Delaloye & Lambiel, 2007). The asymmetry of winter and summer circulation has also been observed and described in caves (Faimon & Lang, 2013), although their interpretation is strongly linked to the cave shape and can not directly be transferred to a talus slope. Further, at Dreveneuse specifically, the areas of the lowest winter and summer temperatures do not match, showing that there is an asymmetry in the convective airflow (Delaloye, 2004; Lambiel, 2006). It can thus be assumed, that winter and summer air circulation do not use the same flow paths. These temporal differences in flow paths are not represented in the model but approximated by a change in permeability. They can be explained by the nature of the flow, which is directed to the atmosphere when ascending, and due to gravity towards the ground when descending. In addition, cold air expulsion can be observed punctually at the base of the talus, whereas cold air aspiration seems to be more diffuse (Schwindt, 2013). Further, ground heterogeneities that are not captured by the electrical resistivity tomogram, seasonal cycles in snow cover and ice content within the talus and vegetation influence the ground permeability or the surface boundary condition, at times on a seasonal scale, by sealing or just altering pore space structures locally.

It can further be assumed that this parametrization through a permeability switch is not of relevance for landforms with a slope angle $< 15°$. During the summer, only advective unicellular downwards flow takes place in the talus and is thus affected by this parametrization. (Bories & Combarnous, 1973) showed in an experimental study, which was later reworked by (Guodong et al., 2007) in engineering sciences, that the temperature field from a flat and a sloping layer differs only from an angle of ˜ 15° on. This is corresponding to (Wicky & Hauck, 2020), where natural multicellular air convection during winter has been shown to be fundamental to the understanding of the ground thermal regime of

374 rock glaciers.

5.3 Latent heat

376 Latent heat is represented in the model in the morainic layer only, where freezing of water takes place and latent
377 heat can be stored and released. This influences the temperature gradients, especially during summer. A prolonged
378 zero-curtain period during the release of latent heat influences the temperature gradient and leads thus to stronger
379 internal air circulation. In this regards the model has also some major shortcomings as water is only present in this
380 morainic layer, all other domains are assumed to be dry. No ice can be built up within the talus, whereas the borehole
381 data show a seasonal ice formation in the talus. It is of a small extent and does not persist throughout the year in
382 the talus at the borehole DRE_0104, whereas temperatures lower borehole DRE_0204 in the porous domain remained
383 at or below 0°C for more than one year (Fig. 7). In a talus that is ice-free during summer, the energy balance of
384 latent heat within the talus is net-zero over a year. Therefore, neglecting latent heat within the talus has only an
385 influence on the convection strength, as the thermal gradient between interior (talus) temperature and exterior (air)
386 temperature depends on the potential existence of ice. (Sawada et al., 2003) observed the refreezing of meltwater
387 and identified this, besides winter air convection, as the main driving factor of the local cold microclimate of low-
388 elevation talus permafrost. But they also stated that the meltwater does not come from the snow on-site but is supplied
389 from groundwater, which is the way the water is represented in the presented model approach. Further, the presented
390 approach neglects the incoming convective heat flux of meltwater and liquid precipitation. A previous study from an
391 Alpine site concludes that air convection is of much higher importance for the ground thermal regime than the heat
392 input of meltwater (Moore, Gischig, Katterbach, & Loew, 2011), but attention has to be drawn to that issue in future
393 studies. To our knowledge, air convection in the porous ground has so far never been modelled with three phases - rock
394 matrix, water and air on a two-dimensional spatial scale. From a modelling perspective, it is technically challenging
395 to incorporate such convective water flows, as the boundary conditions are very hard to define because they are not
396 fully known (e.g. melt rates, interaction with groundwater, flow paths of water etc.). Moreover, running a numerically
397 stable model with three phases with the actual model setup is not yet feasible.

6 Conclusion

399 We applied a physically-based numerical model approach in order to better understand and assess the influence of
400 convective cooling in a low altitude cold talus slope. The numerical model solves for conduction and also explicitly
401 models convention with a Darcy approach in porous media. The following main conclusions can be drawn:

- The model approach reproduces the observed seasonally reversing air circulation as a result of the density difference of cold and warm air, leading to a buoyancy-driven convective flow within the talus. The seasonal reversal of the convective flow leads to a pronounced cooling of the lower part of the talus slope.

- Permafrost, respectively ground ice, can be formed and maintained in sedimentary material beneath a porous talus slope thanks to convective cooling. This is in line with the conclusions drawn from the interpretation of observational data and is now confirmed by the possibility to represent the process in a physics-based model.

- The model results show that the spatio-temporal dynamics of the ground ice depend on the forcing at the upper boundary, the permeability of the porous talus and thus the strength of the convective heat transfer as well as on the water content in the ground.

- The stronger air circulation in the cooling phase needs to be parameterized, the full physical process is not known yet.

- The ground heterogeneity was successfully approximated from geoelectrical data.

Data availability statement

The model file and the corresponding boundary data that support the findings of this study are openly available in figshare at http://doi.org/10.6084/m9.figshare.16793218. The borehole data is available through the PERMOS data repository at http://dx.doi.org/10.13093/permos-2016-01.

Acknowledgments

References

Bories, S. A., & Combarnous, M. A. (1973, jan). Natural convection in a sloping porous layer. *Journal of Fluid Mechanics*, *57*(1), 63–79. Retrieved from https://doi.org/10.1017%2Fs0022112073001023 doi: 10.1017/s0022112073001023

Čermák, V., & Rybach, L. (1982). Thermal conductivity and specific heat of minerals and r ocks. *Landolt-Börnstein: Numerical Data and Functional Relationships in Science and Technology, New Series, Group V (Geophysics and Space Research), Volume Ia,(Physical Properties of Rocks), edited by G. Angenheister, Springer, Berlin-Heidelberg*, 305–343.

COMSOL. (2021). *COMSOL Reference Manual*. COMSOL Muliphysics AB Sweden.

Côté, J., Fillion, M.-H., & Konrad, J.-M. (2011, may). Intrinsic permeability of materials ranging from sand to rock-fill using natural air convection tests. *Canadian Geotechnical Journal*, *48*(5), 679–690. Retrieved from https://doi.org/10.1139%2Ft10-097 doi: 10.1139/t10-097

Delaloye, R. (2004). *Contribution à l'étude du pergélisol de montagne en zone marginale*. Thèse de doctorat: Université de Fribourg.

Delaloye, R., & Lambiel, C. (2007). Drilling in a low elevation cold talus slope (Dreveneuse, Swiss Prealps). In *Egu geophysical research abstracts, vol. 9*.

Delaloye, R., Reynard, E., Lambiel, C., Marescot, L., & Monnet, R. (2003). Thermal anomaly in a cold scree slope (Creux du Van, Switzerland). In *Proceedings of the 8th international conference on permafrost* (Vol. 2125, pp. 175–180).

Faimon, J., & Lang, M. (2013, may). Variances in airflows during different ventilation modes in a dynamic U-shaped cave. *International Journal of Speleology*, *42*(2), 115–122. Retrieved from https://doi.org/10.5038%2F1827-806x.42.2.3 doi: 10.5038/1827-806x.42.2.3

Fourier, J. B. J. (1822). *Théorie Analytique de la Chaleur*. F. Didot, Paris.

Gude, M., Dietrich, S., Mäusbacher, R., Hauck, C., Molenda, R., Ruzicka, V., & Zacharda, M. (2003). Probable occurrence of sporadic permafrost in non-alpine scree slopes in central Europe. In *Proceedings 8th international conference on permafrost* (Vol. 1, pp. 331–336).

Guodong, C., Yuanming, L., Zhizhong, S., & Fan, J. (2007). The 'thermal semi-conductor' effect of crushed rocks. *Permafrost and Periglacial Processes*, *18*(2), 151–160. Retrieved from https://doi.org/10.1002%2Fppp.575 doi: 10.1002/ppp.575

Hauck, C., & Kneisel, C. (2008). Quantifying the ice content in low-altitude scree slopes using geophysical methods. In C. Hauck & C. Kneisel (Eds.), *Applied geophysics in periglacial environments* (pp. 153–164). Cambridge University Press. Retrieved from https://doi.org/10.1017%2Fcbo9780511535628.011 doi: 10.1017/cbo9780511535628.011

Hilbich, C. (2010). Time-lapse refraction seismic tomography for the detection of ground ice degradation. *The Cryosphere*, *4*(3), 243–259. doi: 10.5194/tc-4-243-2010

Horton, C. W., & Rogers, F. T. (1945, jun). Convection Currents in a Porous Medium. *Journal of Applied Physics*, *16*(6), 367–370. Retrieved from https://doi.org/10.1063%2F1.1707601 doi: 10.1063/1.1707601

Johansen, O. (1975). *Thermal Conductivity of soils* (Unpublished doctoral dissertation). Trondheim, Group for Thermal Analysis of Frost in the Ground, Institute for Kjoleteknikk. CREEL Draft Translation 637.

Kane, D. L., Hinkel, K. M., Goering, D. J., Hinzman, L. D., & Outcalt, S. I. (2001, jun). Non-conductive heat transfer associated with frozen soils. *Global and Planetary Change*, *29*(3-4), 275–292. Retrieved from https://doi.org/10.1016%2Fs0921-8181%2801%2900095-9 doi: 10.1016/s0921-8181(01)00095-9

Kenner, R., Noetzli, J., Hoelzle, M., Raetzo, H., & Phillips, M. (2019, jul). Distinguishing ice-rich and ice-poor permafrost to map ground temperatures and ground ice occurrence in the Swiss Alps. *The Cryosphere*, *13*(7), 1925–1941. Retrieved from https://doi.org/10.5194%2Ftc-13-1925-2019 doi: 10.5194/tc-13-1925-2019

Kenner, R., Phillips, M., Hauck, C., Hilbich, C., Mulsow, C., Bühler, Y., . . . Buchroithner, M. (2017, aug). New insights on permafrost genesis and conservation in talus slopes based on observations at Flüelapass Eastern Switzerland. *Geomorphology*, *290*, 101–113. Retrieved from https://doi.org/10.1016%2Fj.geomorph.2017.04.011 doi: 10.1016/j.geomorph.2017.04.011

Kneisel, C., Hauck, C., & Mühll, D. V. (2000). Permafrost below the timberline confirmed and characterized by geoelectrical resistivity measurements, Bever Valley, eastern Swiss Alps. *Permafrost and Periglacial Processes*, *11*(4), 295–304.

Lambiel, C. (2006). *Le pergélisol dans les terrains sédimentaires à forte déclivité: distribution, régime thermique et instabilités*. Thèse de doctorat: Université de Lausanne.

Lambiel, C., & Pieracci, K. (2008, jul). Permafrost distribution in talus slopes located within the alpine periglacial belt Swiss Alps. *Permafrost and Periglacial Processes*, *19*(3), 293–304. Retrieved from https://doi.org/10.1002%2Fppp.624 doi: 10.1002/ppp.624

Lapwood, E. R. (1948, oct). Convection of a fluid in a porous medium. *Mathematical Proceedings of the Cambridge Philosophical Society*, *44*(4), 508–521. Retrieved from https://doi.org/10.1017%2Fs030500410002452x doi: 10.1017/s030500410002452x

Lebeau, M., & Konrad, J.-M. (2009, apr). Natural convection of compressible and incompressible gases in undeformable porous media under cold climate conditions. *Computers and Geotechnics*, *36*(3), 435–445. Retrieved from https://doi.org/10.1016%2Fj.compgeo.2008.04.005 doi: 10.1016/j.compgeo.2008.04.005

Lendemer, J. C., Edenborn, H. M., Harris, R. C., et al. (2009). Contributions to the lichen flora of Pennsylvania: Notes on the lichens of a remarkable talus slope in Huntingdon County. *Opuscula Philolichenum*, *6*, 125–136.

Lesmes, D. P., & Friedman, S. P. (2005). Relationships between the electrical and hydrogeological properties of rocks and soils. In *Hydrogeophysics* (pp. 87–128). Springer.

Millar, C. I., Westfall, R. D., & Delany, D. L. (2016). Thermal components of American pika habitat—how does a small lagomorph encounter climate? *Arctic, Antarctic, and Alpine Research*, *48*(2), 327–343.

Mollaret, C., Hilbich, C., Pellet, C., Flores-Orozco, A., Delaloye, R., & Hauck, C. (2019, sep). Mountain permafrost degradation documented through a network of permanent electrical resistivity tomography sites. *The Cryosphere*, *13*(10), 2557–2578. Retrieved from https://doi.org/10.5194%2Ftc-13-2557-2019 doi: 10.5194/tc-13-2557-2019

Moore, J. R., Gischig, V., Katterbach, M., & Loew, S. (2011, oct). Air circulation in deep fractures and the temperature field of an alpine rock slope. *Earth Surface Processes and Landforms*, *36*(15), 1985–1996. Retrieved from https://doi.org/10.1002%2Fesp.2217 doi: 10.1002/esp.2217

Morard, S. (2011). *Effets de la circulation d'air par effet de cheminée dans l'évolution du régime thermique des éboulis froids de basse et moyenne altitude*. Thèse de doctorat: Université de Fribourg.

Morard, S., Delaloye, R., & Lambiel, C. (2010, jun). Pluriannual thermal behavior of low elevation cold talus slopes in western Switzerland. *Geographica Helvetica*, *65*(2), 124–134. Retrieved from https://doi.org/10.5194%2Fgh-65-124-2010 doi: 10.5194/gh-65-124-2010

Nield, D. A., & Bejan, A. (2017). *Convection in Porous Media*. Springer International Publishing. Retrieved from https://doi.org/10.1007%2F978-3-319-49562-0 doi: 10.1007/978-3-319-49562-0

Pellet, C., & Hauck, C. (2016). Monitoring soil moisture from middle to high elevation in Switzerland: Set-up and first results from the SOMOMOUNT. *Hydrol. Earth Syst. Sci.*, *21*. Retrieved from https://doi.org/10.5194%2Fhess-2016-474 doi: 10.5194/hess-2016-474

PERMOS. (2019). *Permafrost in Switzerland 2014/2015 to 2017/2018, Glaciological Report Permafrost No. 16–19*. Cryospheric Commission of the Swiss Academy of Sciences.

Popescu, R., Vespremeanu-Stroe, A., Onaca, A., Vasile, M., Cruceru, N., & Pop, O. (2017, oct). Low-altitude permafrost research in an overcooled talus slope–rock glacier system in the Romanian Carpathians (Detunata Goală Apuseni Mountains). *Geomorphology*, *295*, 840–854. Retrieved from https://doi.org/10.1016%2Fj.geomorph.2017.07.029 doi: 10.1016/j.geomorph.2017.07.029

Rieksts, K., Hoff, I., Scibilia, E., & Côté, J. (2019, jun). Modelling the Nu-Ra relationship to establish the intrinsic permeability of coarse open-graded materials from natural air convection tests in a 1m3 cell. *International Journal of Heat and Mass Transfer*, *135*, 925–934. Retrieved from https://doi.org/10.1016%2Fj.ijheatmasstransfer.2019.01.034 doi: 10.1016/j.ijheatmasstransfer.2019.01.034

Rist, A., Philips, M., & Auerswald, K. (2003). Undercooled scree slopes covered with stunted dwarf trees in Switzerland–abiotic factors to characterize the phenomenon. In *Proceedings of the 8th international conference on permafrost, zurich* (pp. 135–136).

Sawada, Y., Ishikawa, M., & Ono, Y. (2003, may). Thermal regime of sporadic permafrost in a block slope on Mt.

Nishi-Nupukaushinupuri Hokkaido Island, Northern Japan. *Geomorphology*, *52*(1-2), 121–130. Retrieved from https://doi.org/10.1016%2Fs0169-555x%2802%2900252-0 doi: 10.1016/s0169-555x(02)00252-0

Scapozza, C., Lambiel, C., Baron, L., Marescot, L., & Reynard, E. (2011, sep). Internal structure and permafrost distribution in two alpine periglacial talus slopes Valais, Swiss Alps. *Geomorphology*, *132*(3-4), 208–221. Retrieved from https://doi.org/10.1016%2Fj.geomorph.2011.05.010 doi: 10.1016/j.geomorph.2011 .05.010

Schwindt, D. (2013). *Permafrost in ventilated talus slopes below the timberline: A multi-methodological study on the ground thermal regime and its impact on the temporal variability and spatial heterogeneity of permafrost at three sites in the Swiss Alps* (Unpublished doctoral dissertation). Bayerischen Julius-Maximilians-Universität Würzburg.

Stiegler, C., Rode, M., Sass, O., & Otto, J.-C. (2014, jul). An Undercooled Scree Slope Detected by Geophysical Investigations in Sporadic Permafrost below 1000 M ASL Central Austria. *Permafrost and Periglacial Processes*, *25*(3), 194–207. Retrieved from https://doi.org/10.1002%2Fppp.1813 doi: 10.1002/ppp.1813

Tanaka, H. L., Nohara, D., & Yokoi, M. (2000). Numerical Simulation of Wind Hole Circulation and Summertime Ice Formation at Ice Valley in Korea and Nakayama in Fukushima Japan. *Journal of the Meteorological Society of Japan. Ser. II*, *78*(5), 611–630. Retrieved from https://doi.org/10.2151%2Fjmsj1965.78.5_611 doi: 10.2151/jmsj1965.78.5_611

Wakonigg, H. (1996). Unterkühlte Schutthalden. *Arbeiten aus dem Institut für Geographie der Karl-Franzens Universität, Graz*, *33*.

Wicky, J., & Hauck, C. (2017, jun). Numerical modelling of convective heat transport by air flow in permafrost talus slopes. *The Cryosphere*, *11*(3), 1311–1325. Retrieved from https://doi.org/10.5194%2Ftc-11-1311 -2017 doi: 10.5194/tc-11-1311-2017

Wicky, J., & Hauck, C. (2020, aug). Air Convection in the Active Layer of Rock Glaciers. *Frontiers in Earth Science*, *8*. Retrieved from https://doi.org/10.3389%2Ffeart.2020.00335 doi: 10.3389/feart.2020.00335

Zacharda, M., Gude, M., Kraus, S., Hauck, C., Molenda, R., & Ržička, V. (2005). The relict mite Rhagidia gelida (Acari, Rhagidiidae) as a biological cryoindicator of periglacial microclimate in European highland screes. *Arctic, antarctic, and alpine research*, *37*(3), 402–408.

Zacharda, M., Gude, M., & Růžička, V. (2007). Thermal regime of three low elevation scree slopes in central Europe. *Permafrost and Periglacial Processes*, *18*(3), 301–308. Retrieved from https://doi.org/10.1002%2Fppp .598 doi: 10.1002/ppp.598

6 Unpublished work

6.1 Influence of slope angle and permeability on the circulation pattern

The model developed to represent the Lapires talus slope in GeoStudio was transferred to COMSOL. The aim was not to remodel the Lapires case as in paper I, but to extend the study. In addition to the change of the model environment, which serves for verification, special attention was paid to the influence of the slope angle. COMSOL has the advantage that the permeability values can be linked to the literature values and further that an atmospheric pressure boundary is applicable (cf section 3.4.3, Table 1). The computations are also much faster and allow thus for a broad combination of parameters. The model was run with the geometry shown in Figure 2 for slope angles of 0, 5, 10, 15, 20, 25, 30 and 40 degrees and permeability values of $1 * 10^{-7}$, $5 * 10^{-7}$, $1 * 10^{-6}$, $9.88 * 10^{-6}$ and $8.89 * 10^{-5}\,m^2$. The three lower permeability values are in the range of values used in engineering model application (Lebeau and Konrad, 2009; Pham et al., 2008), the two larger permeability values were proposed by Herz (2006) in the context of alpine permafrost. To allow a stable transient modelling, the upper thermal boundary condition is the median from a ground surface temperature time series from the hydrological year 2000-2016 from logger 15 at Lapires talus slope (PERMOS, 2019) and not daily measured values as in paper I. The lower thermal boundary is the same as in paper I: constant at +0.6 °C, the temperature measured in the Lapires borehole at a depth of 39 m.
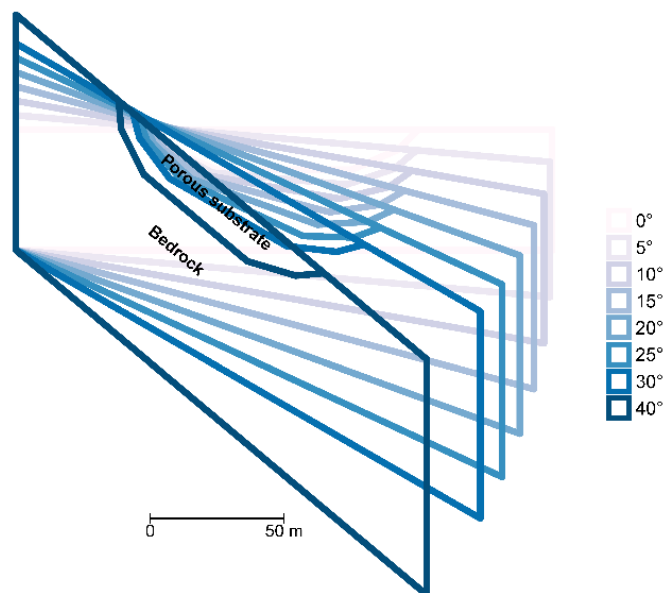

Figure 2 Geometries of the Lapires talus in the COMSOL model approach with different slope angles.

The results are summarised in Figure 3 and were presented at the Swiss Geoscience Meeting 2017 (Wicky and Hauck, 2017a). Three distinct circulation patterns develop for the different combinations of slope angle and permeability. A seasonally reversing circulation can be observed with low permeability, multicellular convection can be seen in the transition to a unicellular down flow, which corresponds to a then free atmospheric flow. The flow patterns observed on field-scale correspond to the flow patterns that were observed in engineering structures (Guodong et al., 2007; Zhang et al., 2009). Paper II tackles these questions again with a more theoretical approach introducing *Ra*, which to some extent exactly explains these circulation patterns. The relationship of *Ra* and slope angle is further discussed in section 7.2.
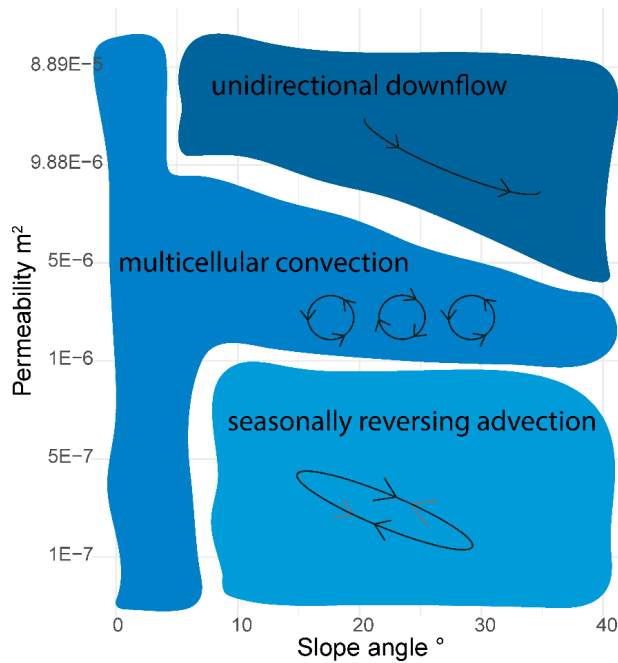
Figure 3 Sketch of different circulation patterns relative to slope angle and permeability.

6.2 Sensitivity of active layer thickness and slope angle

In the context of rock glaciers, the sensitivity on the slope angle and the active layer thickness were modelled, too. The sensitivity of modelled ground temperatures to the two key elements of the geometry of a rock glacier are outlined here. The model setup is described in paper II, boundary data is from the Murtèl rock glacier and the permeability value of the active layer is $1 * 10^{-6}$ m^2. The changes are in the geometrical setup. The model was run with a slope angle of 0, 5, 10, 15 and 20 degrees (Figure 4) and the active layer was chosen to be 2, 4 and 6 m thick (Figure 4 shows a 4 m thick active layer).

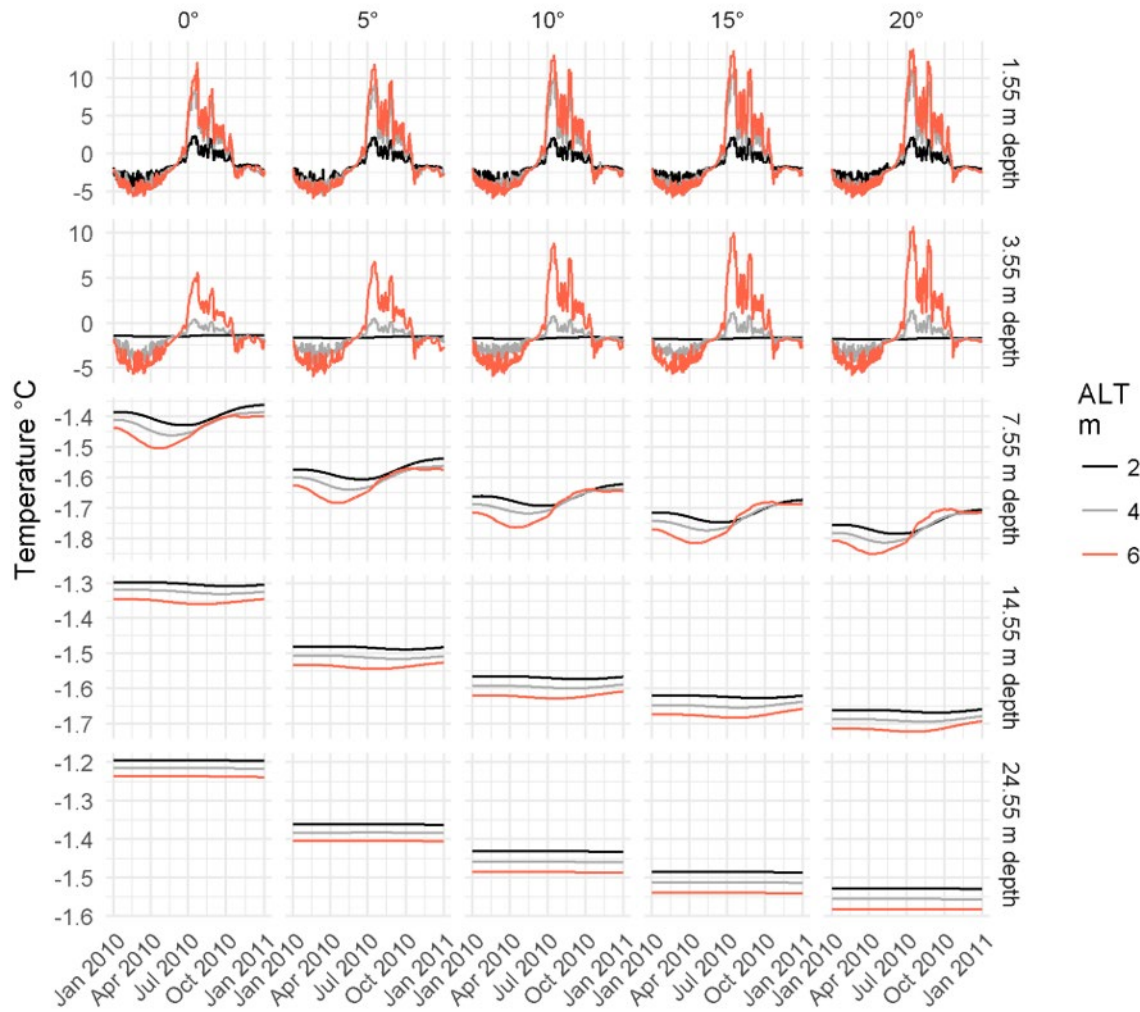*Figure 4 Geometries with a varying slope angle for a rock glacier.*

Figure 5 Ground temperature in °C at several depths corresponding to different slope angles (facets in x-direction) and the different active layer thicknesses (colour scheme).

Both, the increase of the active layer, as well as the increase of slope angle, lead to an increase in convective heat transfer and thus to lower temperatures at depth (Figure 5). The lowering in temperatures with an increase in slope angle can be explained by the larger air velocity in the active layer, as the gravitational force is stronger on a steeper slope. This leads to more convective heat transfer and thus – at least in the middle and lower part of the landform – to colder temperatures. Within a steeper active layer, advective heat transfer (e.g. chimney effect) gains in relevance. The colder conditions linked to the active layer thickness can be directly linked to the Rayleigh number (cf. Eq. 1), which is extensively discussed in paper II and section 7.2. The Rayleigh number has a positive linear relationship to the vertical extension H of the convective porous layer. For larger H, the criterion for natural convection $Ra > Ra_{crit}$ can be met more often during the year leading to longer periods of convection and consequently larger effects on the ground temperatures.

In degrading permafrost environments, the above described cooling effect related to an increase in Ra through active layer thickening might lead to the conclusion that the active layer thickening potentially leads to a positive feedback effect in the form of intensified convective cooling. This presumption needs to be taken with care, as other properties of the active layer, e.g. the permeability, are far more decisive on the convective activity. The sensitivity of the ground temperatures to a change in active layer thickness or slope angle is much smaller compared to the

sensitivity to permeability values (see paper II, Figure 3). *Ra* is in this respect a good indicator to assess the sensitivity of the convective regime in the porous ground to the various influencing variables.

6.3 Influence of atmospheric wind pumping

Wind pumping, i.e. the atmospheric pressure-wind system that directly influences the wind field within the uppermost meters of the ground, is discussed in the literature (Hanson and Hoelzle, 2004; Pruessner et al., 2018). Based on field measurements Hanson and Hoelzle (2004) conclude that the effect is of minor importance, Levintal et al. (2017) conclude that wind pumping is only superficial (down to 0.3 m depth) and less important than free convection. In contrast, Pruessner et al. (2018) links all convective flow in the active layer to wind pumping, including the free convection part through a tuning parameter. Further ongoing studies within the PERMA-XT project may reveal further understanding of the importance of this process through numerical modelling and on-site measurements. Preliminary measurements suggest that the wind pumping is only active close to the surface (0.3 m), the measurements lower down (1.5 m) seem not to be directly influenced by atmospheric flow (Amschwand et al., 2021).
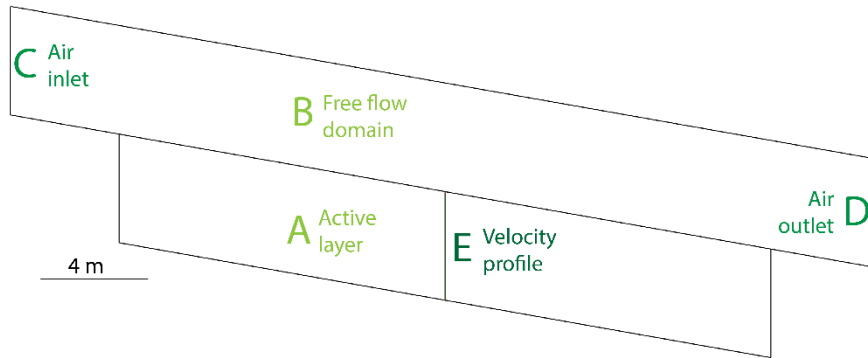

Figure 6 Geometry of active layer (A) with a block of air (B) above which is used to model air entering the porous active layer domain. The flow is governed by an air inlet (C) and outlet (D). The vertical velocity profile (E) is shown in Figure 7.

To assess the potential importance of wind pumping for mountain permafrost, a numerical experiment was conducted within this thesis, revealing that wind pumping is of minor importance, respectively that the here presented porous media approach may not be suited to represent the wind pumping adequately. On a simplified geometry (Figure 6), the following assumptions are made: the coarse-grained active layer (Figure 6 A) is a porous media composed of granite and air with a permeability of $1 * 10^{-6} \, m^2$ and is governed by a extended Darcy-equation (Eq. 4 & 5), more precisely with a Brinkman equation including a Forchheimer drag term (COMSOL, 2018c) to link the free to the porous flow. In the free flow domain (Figure 6 B), the air inlet (Figure 6 C) is driven by a constant flow of $5 \, m \, s^{-1}$ (corresponding to the order of magnitude measured at the Murtèl/Corvatsch meteorological station), the air outlet (Figure 6 D) is a zero-pressure boundary to allow for unrestricted air outflow. The flow is assumed to be purely laminar. With these assumptions, the air flow velocity drops by a factor of 10^4 when entering the porous domain from the free flow domain. The air flow velocity is thus is in the range of the air flow velocity resulting from free convection with a permeability of $1 * 10^{-7} \, m^2$ (Table 2). Since almost no influence of convective heat transfer on ground temperatures can be detected with a of permeability of $1 * 10^{-7} \, m^2$, it can be assumed that the same is true for wind pumping. Due to this strong damping of atmospheric wind effects within

the porous active layer and the so far missing further direct observations (e.g. Hanson and Hoelzle, 2004), wind pumping was not studied any further and the model not developed towards this direction. However, if observational data are available from future projects that indicate the importance of wind pumping, the effect should be treated in a more rigorous modelling setup. Likely, a more explicit approach without a porous media assumption and the integration of turbulent fluxes on a smaller time and spatial scale could lead to more profound insights, but this is beyond the scope of the approach presented in this thesis.

Figure 7 Air velocity profile in the porous media domain (see Figure 6 E).

7 Discussion

7.1 Permeability

Seen over the entire thesis, the most important material property is arguably the intrinsic permeability of the porous media, denoted with κ. Described and discussed extensively in paper II, some of the issues are readdressed here. Permeability is the parameter defining how well the pores of the porous medium are connected and thus how efficient a liquid can move through the porous medium. In distinction, porosity describes only the volumetric ratio of the solid and fluid phase of the porous medium.

The main messages that have to be retained from paper II are the following:

i. The Rayleigh number (section 2.3.2) is especially sensitive to the chosen permeability as it is linearly depending on it and the values may change in orders of magnitude, whereas changes in the order of magnitude in other parameters governing *Ra* would not be physically justifiable.

ii. The Kozeny-Carman relation (Johansen, 1975; Nield and Bejan, 2017) to describe permeability is likely to overestimate the permeability for big (> sand), non-spherical particles (Côté et al., 2011) and has to be used with care in the field of coarse blocky permafrost.

iii. Analogies from engineering sciences for crushed rock layers give a good range of possible permeability values (order of 1 to 3 * 10^{-6} m^2) for a coherent model representation (Côté et al., 2011; Rieksts et al., 2020).

iv. The porous media approach inherently homogenizes the porous layer and site-specific features, like a permeability increase with depth or preferential flow channels, are dismissed. An approach of heterogeneous soil permeability is presented in paper III.

Using a Kozeny-Carman (K-C) relation (paper II, eq. 8) is still the so far most used and best-known way to estimate permeability values of the ground (Nield and Bejan, 2017), certainly also because of its simple applicability. Permeability values range from 10^{-12} to 10^{-9} m^2 for clean sand, from 10^{-9}-10^{-7} m^2 for clean gravel (Nield and Bejan, 2017) to roughly 10^{-7} to 10^{-6} m^2 for crushed rock in an engineering context (Côté et al., 2011; paper II, table 4). It is important to note that the K-C relation has been established experimentally in a bed of perfectly packed spheres of equal size. To correct for different particle sizes, Johansen (1975) proposes to use the harmonic mean of the diameter or specifically for sand the d_{10}, the diameter which 90 % of the particles exceed. A reliable correction factor for larger particles to correct for different sizes or even for the non-spherical aspect of particles does so far not exist. Hence, laboratory experiments try to reduce the uncertainty linked to this parameter. Figure 8 presents the range of values of porosity and particle diameter, which are of interest for coarse blocky permafrost with the resulting permeability values obtained through the K-C relation divided by a correction factor of 4.25. This correction factor is justified by measurements of Côté et al. (2011) that were on average 4.25 times smaller than the value predicted by the K-C relation. The particle diameter has to be interpreted in the sense of Johansen (1975) as a harmonic mean corresponding (more or less) to d_{10}.
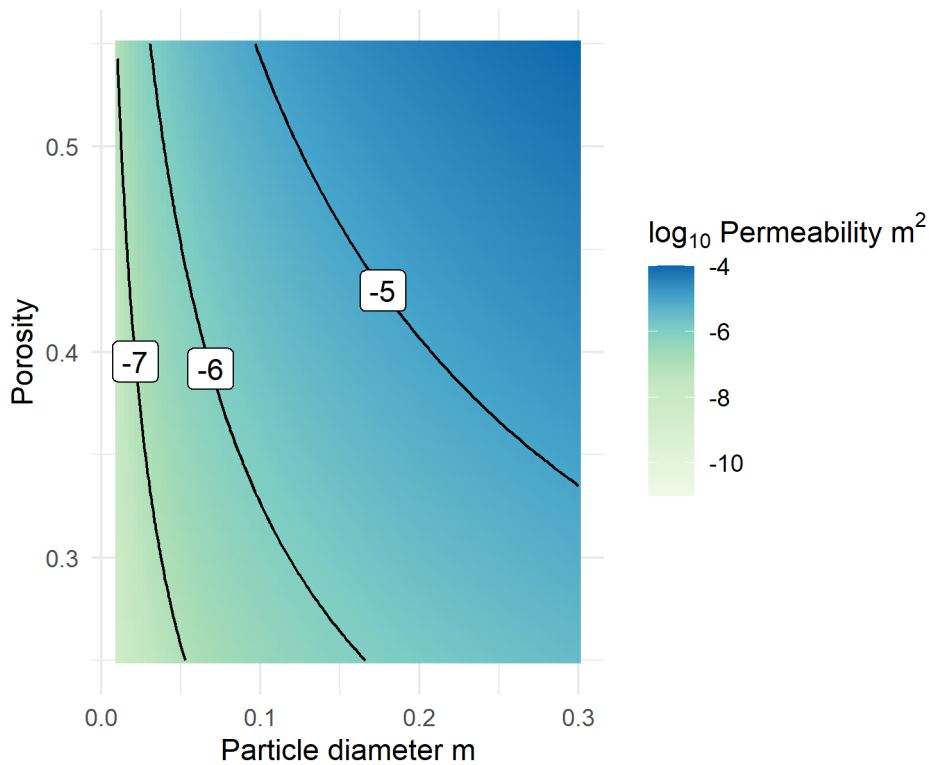
Figure 8 Estimates of permeability values relative to the particle diameter (see text) and to the porosity, obtained using the K-C relation (Johansen, 1975)*, divided by a correction factor of 4.25* (Côté et al., 2011)*.*

Even though Figure 8 gives an overview of the permeability values and allows for a quick estimate, the reliability is strongly limited. It is very important to stress that more research has to be conducted in future in this direction to better understand the permeability of coarse blocky soil in a natural environment, as encountered in mountain permafrost regions around the globe. In model studies, like the here presented thesis, the sensitivity of the permeability needs to be well assessed. This leads to a better understanding of the applicable permeability range in coarse blocky permafrost.

Furthermore, in-situ attempts of measuring permeability may be envisaged. Unfortunately, this is not very easy to carry out. Differential pressure sensors or air tracing experiments may advance the state of knowledge. To better constrain the K-C relation, a better knowledge of the particle size distribution is of importance. This has already been done by Ikeda and Matsuoka (2006) but needs to be more rigorous to be of use for this specific issue. Still, whether this will bring decisive progress is difficult to assess. Geophysical surveys also bear the possibility to infer permeability on larger scales. Lesmes and Friedman (2005) give an overview therein. The potential to determine absolute values of permeability is still quite limited. However, the heterogeneity of permeability in the ground can be approximated using e.g. measured electrical resistivity values – as done and explained in detail in paper III.

7.2 Rayleigh number

The Rayleigh (or Rayleigh-Darcy) number *Ra*, as described in section 2.3.2, is an important concept to understand and characterize the onset and characteristics of convection. *Ra* and the onset of convection at *Ra*$_{crit}$ are in general described by for a flat homogeneous porous layer heated from below (Lapwood, 1948; Nield and Bejan, 2017). Bories and Combarnous (1973) then also considered a sloping porous layer – the case of paper I and II. Paper III deals with a strongly heterogenous sloping porous layer. This is also inherent for studies presenting data and resulting *Ra* measured on-

site (Herz, 2006; Panz, 2008; Wagner et al., 2019). It is further important to keep in mind that the general research background, as well as the application in practice, is often linked to the research field of fossil fuel reservoirs (Bories and Combarnous, 1973; Hewitt et al., 2014; Horton and Rogers, 1945; Lapwood, 1948). Therefore, many of the publications that refer to Ra often are in a context of much lower permeabilities (10^{-12} - 10^{-10} m^2) and a larger spatial extent. Their assumptions may not be directly adopted to convection in a coarse blocky permafrost environment and must be interpreted with a certain degree of caution.

Still, analogies between the theoretical considerations concerning the explanation of the convection regime and the here presented results are of importance. The theoretical foundations of convection in porous media, developed by mathematical methods and laboratory experiments, are themselves a large field of research. A detailed overview (which is far beyond the scope of this thesis) is given by Nield and Bejan (2017). Nevertheless, there are some interesting points of contact. The regime of 2-dimensional Rayleigh-Darcy convection can be summarised as follows (Hewitt et al., 2014; Nield and Bejan, 2017):

- For $Ra < 4\pi^2$ (= Ra_{crit}), there is no convective flow (Lapwood 1948).
- For $4\pi^2 < Ra < 300$, the flow takes the form of large-scale convective rolls.
- At around Ra = 300, instabilities start to develop in form of plumes at the boundary layer and then increase subsequently (Graham and Steen, 1994) till $Ra > 1300$, known as the "high-Ra" range, where the quasi-steady background rolls completely break down (Otero et al., 2004).
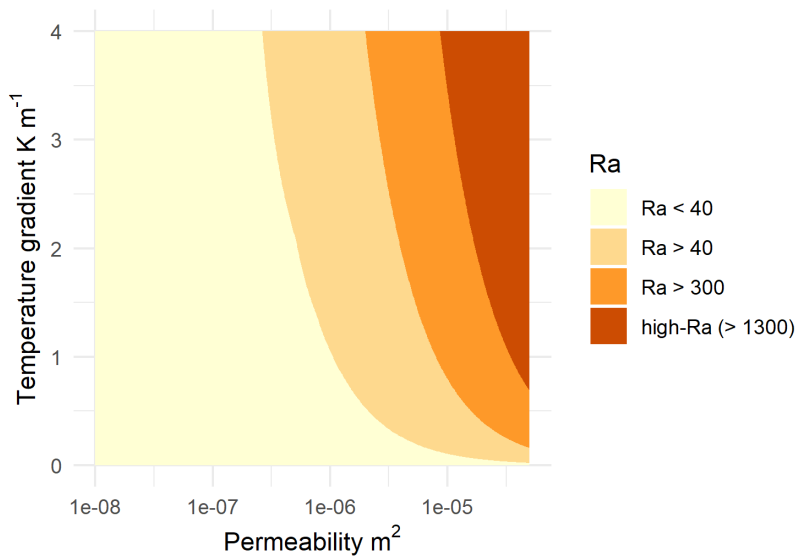

Figure 9 Range of Rayleigh numbers relative to the permeability and the thermal gradient. The parameters governing Ra (section 2.3.2) were chosen according to the Murtèl rock glacier at a reference temperature of 0°C with an ALT of 4m. Note the log scale for the x-axis.

Figure 9 transfers these values to a range that is of relevance for coarse blocky alpine permafrost. The results of paper II fit within this schema. The onset of convection is observed at $Ra \sim 40$ (paper II, figure 7 and 8). Consistent to the theoretical tipping point at $Ra \sim 300$ mentioned in the literature (Nield and Bejan, 2017), the model tends to develop instabilities for $Ra > 300$. If they persist, the model no longer achieves numerical convergence and the calculations can no longer be completed.

Independent of the site, a critical increase in permeability prevents numerical convergence. At Murtèl and Schafberg, this corresponds well to a change in the convection regime observed at $Ra \sim 300$. Numerical experiments at Murtèl and Schafberg showed that a permeability of $5 * 10^{-6}$ m^2 leads to deteriorating results when the maximal thermal gradient (which is within the active layer of Murtèl during winter roughly 3 K m^{-1}) occurs, corresponding to a situation where $Ra > 300$ (Figure 9).

To transfer the concept of Ra to a talus slope, the integration of the slope angle is crucial. A tipping point mentioned in the literature is a slope angle α of about 15°, from where onwards the temperature field differs from a horizontal layer (Bories and Combarnous, 1973). Studies in crushed rock embankments (Zhang et al., 2009) and own results (section 6.1) show that this transition is more gradual. The critical Rayleigh number on a slope describes the destabilization of the initial unicellular flow to a multicellular convection pattern. The transition takes place if $Ra * \cos(\alpha) > Ra_{crit}$ (of 40 resp. 4 π^2) (Bories and Combarnous, 1973; Nield and Bejan, 2017). The changes in the threshold for the occurrence of multicellular convection are relatively small for talus slopes. With a slope of $\alpha = 30°$, the onset of multicellular convection can theoretically be observed at $Ra = 46$, for $\alpha = 40°$ at $Ra = 52$. The larger difference in the results compared to a flat setup lies in the constant presence of a unicellular flow, which is driven by a gravitational downslope movement. As soon as a thermal gradient exists, convective flow takes place. At low flow rates, however, the influence on the ground thermal regime is negligible.

Figure 8 and Figure 9 allow thus for a rough estimation if convective heat transfer is of importance for a specific landform. An estimate of the block size, assumed porosity and temperature data of the active layer, respective an estimate of the temperature gradient within the active layer, allow for a simple, quick guess of the potential Ra. If Ra_{crit} is reached, free convection takes place and gets stronger with an increase in Ra. For talus slopes, unicellular convection happens also for $Ra < Ra_{crit}$. Nevertheless, the modelling results of this thesis suggest that a minimum permeability $> 10^{-7}$ m^2 is required to observe an influence of air convection on the ground thermal regime.

7.3 Validation

7.3.1   Temperature

The validation procedure of the model approach presented in this study has several aspects. The most obvious approach consists of the comparison of the simulation results with measured temperature data in boreholes, presented and discussed extensively in each of the papers. Here, the validations through temperature data of the respective simulation are briefly compared. The validation in paper I is hampered by the relatively simple structure of the model compared to the high complexity of the circulation at the Lapires site and the gaps in the borehole data. In paper III, the model complexity increased by a lot and more processes are included. However, the high complexity of low altitude talus slopes cannot be fully represented by the model. The fit of modelled to measured temperatures is still better compared to paper I. The best fit from modelled to measured data is obtained in paper II. The convection regime at a rock glacier is less complex than at a talus slope. The vertical component of convection is most important which leads to a relatively local convection. In addition, the spatial dimensions of the active layer are relatively small compared to an entire talus slope, resulting in a smaller porous model domain and thus fewer uncertainties. Another important difference is that in paper II the upper boundary is prescribed by the temperature measured in the uppermost thermistor of the boreholes on-site, whereas in the talus slopes (paper I and III) GST loggers located in the vicinity of the borehole are used to define the upper boundary. The use of independent validation data (GST vs borehole) is conceptually better, but a worse fit of modelled data to measured data has to be expected. In general, it is important to keep in mind that, apart from permeability, the model has not been calibrated to any parameters. This would certainly

improve the fit of the modelled to the measured temperatures, but also has the disadvantage that the dominant processes cannot be assessed properly, as they can be masked by calibration.

7.3.2 Air velocity

A further variable that allows for direct comparison with the simulation results is the velocity of the airflow observed in the few available measurements. Measured values from anemometers (Morard, 2011; Morard and Delaloye, 2008) or convective heat coefficient sensors (Panz, 2008) give values on the order of 10^{-1} m s^{-1}, Tanaka et al. (2000) reports of measured wind speed of roughly 0.5 – 1 m s^{-1}. Table 2 gives an overview of the modelled velocities relative to the permeability at the Murtèl rock glacier from the model data set presented in paper II. They are about one to two orders of magnitude smaller than the measured values.

Table 2 Modelled Mean and maximum Darcy velocity magnitude for different permeabilities in the active layer of Murtèl rock glacier. Data is from the model described in paper II. Note that a permeability value of $1 * 10^{-7}$ m^2 has no significant influence on ground temperatures and that best modelling results were obtained with $3 * 10^{-6}$ m^2.

Permeability (m^2)	$1 * 10^{-7}$	$1 * 10^{-6}$	$3 * 10^{-6}$
Mean velocity (m s^{-1})	$1.11 * 10^{-4}$	$1.18 * 10^{-3}$	$3.60 * 10^{-3}$
Max velocity (m s^{-1})	$6.38 * 10^{-4}$	$6.53 * 10^{-3}$	$2.31 * 10^{-2}$

It is relatively difficult to compare the velocities occurring in the model with real measurements. The modelled velocity is averaged over the entire porous medium and the measurements always take place in cavities - usually in particularly well-developed ones. One possibility is to simply correct the airflow for the porosity by dividing the velocity by 0.5, the porosity of the active layer of Murtèl in the model (paper II). Tanaka et al. (2000) even suggest that the outlet area shrinks to 10^{-3} of the surface area for a wind hole in a talus slope, but a correction factor of 10^3 would potentially lead to a slight overestimation of the convective air flow velocity at higher permeability values (Table 2). A correction based on porosity (division by 0.5) to account for the porous media approach in turn leads still to an underestimation by the modelled velocities. As the measurements are subject to quite high uncertainty and the modelled values are below the typical accuracy of the measurement devices (which is ≥ 10^{-1} m s^{-1}: Anemoment, 2021; Panz, 2008), a sound conclusion is not possible. Of relevance, especially for future model attempts, is the range of velocity, where convection becomes important. At the order of 10^{-4} m s^{-1} (corresponding to the permeability of $1 * 10^{-7}$ m^2) the convective heat transfer is negligible and gains in influence from 10^{-3} m s^{-1} onwards. This corresponds also to published values for pore air flux velocities in cold region engineering modelling by Goering (2003; mean winter velocity of $3.5 * 10^{-3}$ m s^{-1}, mean summer velocity of $1.6 * 10^{-3}$ m s^{-1}), Lebeau and Konrad (2016; annual fluctuations between 0.5 and $5.5 * 10^{-3}$ m s^{-1}) or Pham et al. (2008; Range of air velocity of $9.4 * 10^{-4}$ - $2.6 * 10^{-3}$ m s^{-1}).

7.3.3 Process

Validation can also be understood as a validation of the observed processes and the confirmation of the conceptual models, which are derived from field observations. In this respect, this thesis can be seen as an important contribution. Convective airflow has been observed in the field and serves as an explanation for cold microclimates in many sites and landforms, whether it be on low elevation talus slopes (Delaloye et al., 2003; Gude et al., 2003; Kneisel et al., 2000; Popescu et al., 2017; Wakonigg, 1996; Zacharda et al., 2005 and many more), in alpine talus slopes (Delaloye and Lambiel, 2005; Lambiel and Pieracci, 2008; Scapozza et al., 2015), in rock glaciers (Hanson and Hoelzle, 2004) or

coarse blocky surfaces in more general terms (Gubler et al., 2011; Hoelzle et al., 1999; Schneider et al., 2012). The here presented papers show now explicit model simulations of the observed air convection in the ground and can confirm that this is a relevant - if not even the dominant - process governing the ground thermal regime at many sites with a coarse blocky surface cover.

To weigh the importance of convection to other heat transfer processes, it is further important to make a quantitative statement about the magnitude of the convective heat flux. Figure 10 gives an overview of the monthly mean vertical heat fluxes at the upper boundary of the active layer at the Murtèl rock glacier (paper II) in the middle of the domain. The standard deviation indicates the spread of the values. When the convective heat flux becomes efficient, especially at a permeability value of $3 * 10^{-6} \, m^2$, the mean values are not reflecting the true dynamics of the system, because positive and negative anomalies will be averaged. The standard deviation (Figure 10), however, can be interpreted as a measure of these dynamics, resulting from either stationary or unsteadily moving convection cells.
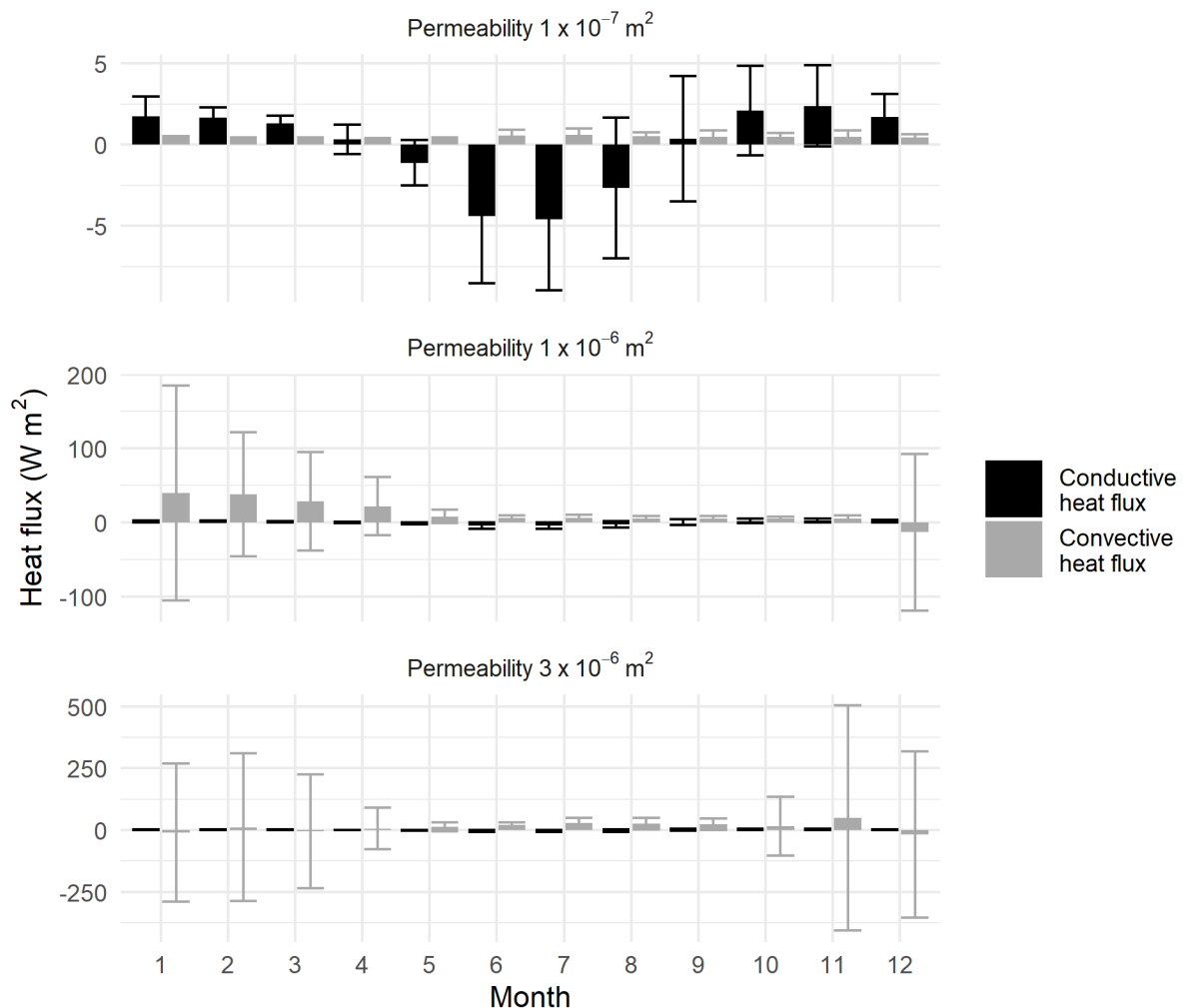

Figure 10 Vertical conductive (black) and convective (grey) monthly mean heat flux at the upper boundary of the active layer at the Murtèl rock glacier. The bars indicate the monthly mean with the corresponding standard deviation, the different panels indicate a different permeability in the active layer. Data presented stem from the model runs in paper II. Note that the y-scale is different for the heat fluxes of the various corresponding permeability values.

The interpretation of this data illustrates the difficulties of compressing a two-dimensional model result to a one-dimensional quantification which is needed to compare the model data to existing measurements (Mittaz et al., 2000; Scherler et al., 2014) or previous model results (Scherler et al., 2014). Reported deviations of the measured energy balance at Murtèl, which can potentially be attributed to convective processes, are of 78 Wm^2 (-130 Wm^2) in winter (summer) (Mittaz et al., 2000), or in a modelled heat source/sink approach of 28.9 Wm^2 (-26 Wm^2) (Scherler et al., 2014). Although a reliable quantitative comparison has proven to be difficult, the following qualitative statements can be made as a direct interpretation of the observed heat fluxes:

i. With a low permeability (1 * 10^{-7} m^2), conductive heat flux prevails. The vertical convective flux is due to the sloping domain, showing a steady gravitational downflow.

ii. With a permeability of 1 * 10^{-6} m^2, the convection is relatively steady and the mean convective heat flux is meaningful and shows a seasonal cycle. During winter, the mean convective heat flux is considerably larger than the conductive heat flux.

iii. The high permeability of 3 * 10^{-6} m^2, which yields the best reproduction of the thermal behaviour of the Murtèl rock glacier (paper II), leads to higher Ra and the mean values of the convective heat flux on a point-scale depend strongly on the occurrence and the stability of convection cells. However, the temperature trend at the depth of zero annual amplitude, which is somewhat of a natural mean value, is modelled consistently (paper II, Figure 3).

iv. An effective autumn cooling takes only place with a permeability of 3 * 10^{-6} m^2 (see the standard deviation of November on Figure 10), which is also observed in the modelled flow patterns (paper II, Figure 8): A lower permeability implies higher inertia preventing the onset of convection in November.

v. Ground air convection seems to explain the observed offset in the energy balance calculations and simulations (Mittaz et al., 2000; Scherler et al., 2014) during winter. During summer, the convective heat flux is relatively small and stable and seems not to explain the measured and modelled differences in the energy balance.

7.4 Relevance to other fields

7.4.1 Permafrost evolution

Permafrost temperatures were warming in the last decades in the alps (Etzelmüller et al., 2020; Harris et al., 2003) and with the projected climate warming, the increase in permafrost temperatures – as projected by model simulations – is likely to continue in the future (Marmy et al., 2016; Scherler et al., 2013). This thesis is not a direct contribution to the understanding of the future evolution of permafrost, the objectives were set towards a better process understanding, motivated by the shortcomings that the aforementioned studies highlighted. First, the here presented results support strongly the importance of ground convection – a process which cannot be neglected for present climatic conditions. Indications on how this process develops under changing climatic conditions can also be derived from the Rayleigh number Ra. An important parameter of Ra is the temperature gradient in the active layer, which is also subject to changes under a warming climate. The temperature gradient is of importance during the winter, when the outer temperatures are colder than the active layer temperatures. Table 3 in paper II presents critical temperature gradients which are required to reach Ra_{crit} for the rock glaciers Murtèl and Schafberg. Under a warming climate, the critical gradients are less likely to be reached. The same applies for talus slopes, with the exception that a positive gradient, i.e. warmer outside temperatures, additionally has a warming effect on talus temperatures as the summer advection is then more effective. Further, a potential feedback effect is described by Ra – the thicker the active layer, the higher Ra and thus the more often the Ra_{crit} is reached, which is favourable for the occurrence of free convection and the related ground cooling.

This is contradicted by the fact that at sites where convection is of high importance, a real active layer thickening keeping a high (air) permeability is not likely. For example at sites like Murtèl, ground subsidence probably dominates (Scherler et al., 2013) or at Schafberg the water content in the AL is increasing (Kenner et al., 2019b), which prevents air circulation. In addition, the active layer thickening in ice-rich landforms is a relatively slow process (PERMOS, 2019), while the temperature gradient is subject to larger variations on a much smaller time scale.

This brief assessment of the evolution of convection in a warming climate based on *Ra* can be summarised as follows: provided that free convection of air is considered in the modelling approach, no surprising feedback effects are to be expected. Ground convection has the potential to amplify cold periods because it is more effective with higher negative temperature gradients. Still, on the long-term, the warming trend will weaken the convective cooling effect because the occurrence of high temperature gradients is less frequent.

7.4.2   Permafrost mapping

Permafrost mapping is either done by pure statistical approaches (e.g. Boeckli et al., 2012; Deluigi et al., 2017), with physically-based distributed models (e.g. Westermann et al., 2013) or on combined approaches (e.g. Kenner et al., 2019a). To date, however, all approaches lack the integration of an explicit formulation of air convection in the ground, and most of them report shortcomings related to the representation of permafrost in coarse blocky ground.

In this field, the present thesis rather emphasizes the importance of convection than proposes a solution. In a statistical approach of permafrost modelling, models should account for the cold temperature offset occurring through air convection in the ground when the ground is covered – or consists of – coarse blocks. This is generally independent of the existence of permafrost or permafrost related landforms. Furthermore, in physically-based distribution models, convection needs to be accounted for, even if it is only in a parametrised form. The challenge herein again lies in the accuracy of the model properties, which are often obtained through remote sensing (e.g. Westermann et al., 2013). This stresses the importance of developing reliable ground cover data from remote sensing imagery to represent this process on a large spatial scale. Another remark may be made on the occurrence and perseverance of ground ice: Kenner et al. (2019a) present a mapping approach that differentiates between ice-poor and ice-rich permafrost, integrating mass wasting processes to represent the latter. This mass wasting process not only favours the burial of snow, as described in the aforementioned publication. Sediments deposed by mass wasting in the alpine environment create favourable conditions for air convection in the ground, which in turn also has the potential to govern the aggregation of ground ice (paper III).

7.4.3   Debris covered glaciers

A short note can be made on debris-covered glaciers. The debris cover of a glacier influences the energy balance of the subsurface of a glacier and leads thus to a difference in mass balance compared to a debris-free glacier (Nicholson and Benn, 2006). Ample work has been done on this research subject – an introduction and a review are beyond the scope of this thesis. Nevertheless, a very simple analogy is possible. From the point of view of heat transfer processes, neglecting temporal dimensions, hydrological, kinematic and spatial processes, a debris-covered glacier is somewhat similar to an ice-rich rock glacier, having a layer of blocks on top of the ice. The main differences are in the composition and thickness of the debris layer and the lower thermal boundary of the debris layer, at least for temperate glaciers. Explicit modelling of the heat transfer in the debris layer of a debris-covered glacier has been performed on different complexity scales, at times also accounting for non-conductive heat transfer modes, but neglecting convective airflow within the porous debris layer (Evatt et al., 2015; Nicholson and Benn, 2006; Reid and Brock, 2010). The

aforementioned modelling approaches deal with relatively thin debris layers (centimetres up to several decimetres) with relatively low porosity, where the neglect of air convection in the ground is valid because Ra is never close to Ra_{crit}. To my knowledge, thicker debris layers with coarse blocks on glaciers have not been subject to modelling attempts yet. Their extent (and thus relevance) may be quite small, but they can be observed. There, convective airflow would account for a significant share of heat transfer in the debris layer and must be considered.

7.5 Future challenges

The future challenges resulting from this thesis are manifold. The first field is the improvement of the model approach itself. Technically, a major step would be a model development for a three-phase flow with phase change, allowing for water and air to circulate and interact in the porous media domain, and thus also for ice to build up and melt in direct interaction with the convective air circulation. This would also include the flow of water vapour in the air, which allows for the integration of evaporation and sublimation (eg. hoar formation) in the model, processes that are of minor importance compared to the air convection, but are still observed and of relevance for the heat transfer. Furthermore, an approach going beyond the porous media assumption with an explicit integration of flow channels and real-scale pore flow (ongoing attempts by the PERMA-XT project of M. Scherler) may reveal further insights on the convection regime, especially on smaller timescales and on the interaction with the atmospheric flow at the boundary to the atmosphere.

However, model advances are often also hampered by the lack of conceptual understanding or the lack of data, whether it be for constraining the model or for validation. There, the main challenge is to determine the permeability of the coarse blocky layer. To integrate water, the definition of the boundaries and initial conditions remains very challenging – where is water, where does it originate from and where does it enter and leave the coarse blocky layer? Furthermore, a sound validation of the convection process is still not possible, as no reliable long-term data of direct convection related measurements, as air or heat flow measurements, is available.

Beyond possible model improvements, the challenge lies also in the integration of air convection in long-term modelling to improve projections of permafrost evolution. There, this thesis provides a concept that can be pursued: To improve parametrization, comparable to a heat sink/source term, a parametrization using Ra could improve the timing and the intensity level of convection and would not lead to the considerable additional computational effort. Integrating an explicit formulation of the two-dimensional convection is, at least for spatially distributed models, computationally quite expensive and not very simple to define. This is less of an issue on site-specific two- or even three-dimensional models and should be considered in future model attempts.

8 Conclusion

The here presented thesis contributes towards a better understanding of the influence of free convection of air on the ground thermal regime in coarse blocky mountain permafrost by means of numerical modelling. The main advances from a modelling perspective are that the process of air convection within the ground is modelled explicitly using a physics-based approach. Solving for conduction coupled with Darcy's law adopting the Boussinesq approximation to describe convective airflow in the porous medium on a two-dimensional domain allows for a robust representation of ground air convection. The modelling approach was applied to three different types of landforms – alpine talus slopes, rock glaciers and low-altitude talus slopes. At all sites, convection has been shown to play an important role. This in accordance with the expectations; the novelty therein is the integration and representation in a numerical modelling framework. The modelling approach has evolved and grown in complexity over the course of the thesis, allowing for the integration and representation of more and more processes. A physically based, explicit representation on two spatial dimensions of air convection in the ground in the context of alpine permafrost has only been covered by this thesis so far.

The main findings can be briefly summarised as follows:

- Over all the modelled landforms, ground convection has been shown to have a cooling effect on the ground. Colder temperatures are modelled when accounting not only for conduction but also for convection. Air convection in the coarse blocky ground is a crucial process to remodel the measured temperatures in boreholes. A conduction-dominated model approach yields warmer than measured temperatures.

- In *talus slopes*, the simulations show that a seasonally reversing circulation develops due to free convection without external forcing. The altering convective air flow leads to a cooling of the lower part of the slope. It therefore has a significant influence on the thermal regime of a talus slope. The findings thus confirm that the chimney effect, respectively the advection along a slope, is a central thermal process in a talus slope.

- The model results in a *low-altitude cold talus slope* showed that enhanced ground cooling by air convection can be strong enough to aggregate ice in a water-bearing substrate and therefore regulate the existence or persistence of permafrost, especially at its lower altitudinal margin or even below. The complex heterogeneity of low altitude cold talus slopes is not yet fully understood and the model therefore represents it by integrating geophysical data to approximate the subsurface heterogeneity and by damping summer convection, as a parameterization of different flow paths.

- In *rock glaciers*, free convection in the active layer is shown to have a major influence on the ground thermal regime of the whole landform. Even at depth of the zero-annual amplitude, the temperatures are significantly lower when accounting for convection. In the active layer of rock glaciers, the convection is characterised mainly by vertical convection cells. The higher the permeability of the active layer, the higher the convective activity and thus also the cooling effect on the ground temperatures. Convection cells occur only when the outside air temperature is colder than the inside talus temperature and the density stratification of the air is thus unstable. The model results show that the Rayleigh number is a good indicator of the potential and the onset of air convection in the ground.

− The Rayleigh number is shown to be a good dimensionless number to characterize the convection regime of the coarse blocky permafrost substratum. The most important parameters in the context of coarse blocky permafrost governing the Rayleigh number are the temperature gradient within the ground and the permeability of the ground. The temperature gradient can be measured (or modelled), the permeability is subject to greater uncertainty.

− This thesis showed that permeability estimations using the Kozeny-Carman relation have to be used with care, that analogies to cold engineering sciences give a good starting point and that permeability values in the range of 1 - 3 * 10^{-6} m^2 enable a consistent representation of ground convection in coarse blocky permafrost, as they led to the best model results.

− Future improvements of the model approach can may be achieved by a validation that goes beyond temperature data and the confirmation of conceptual models, for example with air or heat flow measurements. In addition, efforts should be made to better delimit the range of permeability values by specific measurements. From the model development point of view, an integration of two-phase flow would be a significant step forward: It would allow to model water and air fluxes simultaneously, optimally also considering latent heat exchange.

Data availability

The model files reproducing the results from papers I, II and III can be accessed through the online repository *figshare* with the DOI 10.6084/m9.figshare.16793218. They may be accessed and reused, but the authorship needs to be credited.

The model file from paper I runs best in GeoStudio2012 with active licenses for TEMP/W, SEEP/W and AIR/W. The model files of papers II and III were developed in COMSOL Multiphysics 5.3 and 5.6 respectively. An update to a newer version has to be performed with care as some features may be deprecated in newer versions.

The model boundary and validation data are in general available throughout the PERMOS network (PERMOS, 2019) either in their online data server or on request and it is described in the respective publication which datasets were used. Boundary data with gap-filling of papers II and III can be found in the respective supplementary material section.

References

Publications related to this thesis

PAPER I

Wicky, J. and Hauck, C. (2017). Numerical modelling of convective heat transport by air flow in permafrost talus slopes. *The Cryosphere* 11(3): 1311-1325.

PAPER II

Wicky, J. and Hauck, C. (2020). Air Convection in the Active Layer of Rock Glaciers. *Frontiers in Earth Science* 8: 335.

PAPER III

Wicky, J., Hilbich, C., Delaloye, R. and Hauck, C. (in prep.). Modelling the link between air convection and the formation of short-term permafrost in low altitude cold talus slopes. Submission to *Permafrost and periglacial Processes* foreseen.

Conference contributions

Wicky, J. and Hauck, C. (2020a). The thermal behavior of a low elevation cold talus slope: Insights through numerical modelling. SGM 2020, Zurich, Switzerland (Poster).

Wicky, J. and Hauck, C. (2019c). Thermal effects of natural air convection in the active layer of rock glaciers. SGM 2019, Freiburg, Switzerland (Poster).

Wicky, J. and Hauck, C. (2019b). Numerical Modelling of Convective Heat Transfer in Porous Permafrost in the Swiss Alps. COMSOL Geoscience Day 2019, Fribourg, Switzerland (Keynote Talk).

Wicky, J. and Hauck, C. (2019a). Air Convection Within the Active Layer of an Alpine Rock Glacier: A Numerical Modelling Approach. EGU 2019, Vienna, Austria (Talk).

Wicky, J. and Hauck, C. (2018d). Assessing the influence of convection in the active layer of a rock glacier on ground temperatures. SGM 2018, Bern, Switzerland (Talk).

Wicky, J. and Hauck, C. (2018c). Modelling Convective Heat Transfer in the Porous Active Layer of an Alpine Rock Glacier. COMSOL Conference 2018, Lausanne, Switzerland (Paper, Poster).

Wicky, J. and Hauck, C. (2018b). Convective Heat Transfer in Coarse Permafrost Substrate - A Numerical Model Study in the Swiss Alps. EUCOP 2018, Chamonix, France (Poster).

Wicky, J. and Hauck, C. (2018a). Modelling Convective Heat Transfer in Alpine Permafrost. POLAR 2018, Davos, Switzerland (Talk).

Wicky, J. and Hauck, C. (2017a). Influence of slope angle on the convective heat transfer in porous permafrost substrate. SGM 2017, Davos, Switzerland (Poster).

Cited literature

Amschwand, D., Scherler, M., Hoelzle, M., Krummenacher, B., Haberkorn, A., and Gubler, H.-U. (2021). Novel subsurface measurement setup to investigate heat transfer processes within the debris mantle of rock glacier Murtèl (Engadine, eastern Swiss Alps). in *Regional Conference on Permafrost & 19th International Conference on Permafrost Engineering, Boulder (CO),*

USA/virtual conference, Oct 24–29.

Anemoment (2021). *TriSonica Mini Wind & Weather Sensor Datasheet*. Longmont, US: Anemoment LLC.

Arenson, L. U., Hauck, C., Hilbich, C., Seward, L., Yamamoto, Y., and Springman, S. M. (2010). Sub-surface Heterogeneities in the Murtèl-Corvatsch Rock Glacier, Switzerland. *Geo 2010. 62nd Can. Geotech. Conf.*, 1494–1500.

Arenson, L. U., Hoelzle, M., and Springman, S. (2002). Borehole deformation measurements and internal structure of some rock glaciers in Switzerland. *Permafr. Periglac. Process.* 13, 117–135. doi:10.1002/ppp.414.

Arenson, L. U., Pham, H., Klassen, R., and Sego, D. C. (2007). Heat convection in coarse waste rock piles. *OttawaGeo2007 60th Can. Geotech. Conf.*, 1500–1507.

Arenson, L. U., and Sego, D. C. (2006). Considering convective air fluxes in the design of engineered structures in cold regions. *Sea to Sky Geotech. 59th Can. Geotech. Conf.*, 1033–1040.

Balch, E. S. (1900). *Glacieres, or Freezing Caverns*. Philadelphia: Allen Lane & Scott.

Barsch, D. (1996). *Rockglaciers : Indicators for the Present and Former Geoecology in High Mountain Environments*. Berlin, Heidelberg: Springer.

Biskaborn, B. K., Smith, S. L., Noetzli, J., Matthes, H., Vieira, G., Streletskiy, D. A., et al. (2019). Permafrost is warming at a global scale. *Nat. Commun.* 10, 1–11. doi:10.1038/s41467-018-08240-4.

Boeckli, L., Brenning, A., Gruber, S., and Noetzli, J. (2012). A statistical approach to modelling permafrost distribution in the European Alps or similar mountain ranges. *Cryosph.* 6, 125–140. doi:10.5194/tc-6-125-2012.

Bories, S. A., and Combarnous, M. A. (1973). Natural convection in a sloping porous layer. *J. Fluid Mech.* 57, 63–79. doi:10.1017/S0022112073001023.

Cicoira, A., Beutel, J., Faillettaz, J., Gärtner-Roer, I., and Vieli, A. (2019). Resolving the influence of temperature forcing through heat conduction on rock glacier dynamics: a numerical modelling approach. *Cryosph.* 13, 927–942. doi:10.5194/tc-13-927-2019.

COMSOL (2018a). *COMSOL Multiphysics Reference Manual*. Stockholm, Sweden: COMSOL AB.

COMSOL (2018b). *Heat Transfer Module. Users Guide.* Stockholm, Sweden: COMSOL AB.

COMSOL (2018c). *Subsurface Flow Module. Users Guide.* Stockholm, Sweden: COMSOL AB.

Côté, J., Fillion, M.-H., and Konrad, J.-M. (2011). Intrinsic permeability of materials ranging from sand to rock-fill using natural air convection tests. *Can. Geotech. J.* 48, 679–690. doi:10.1139/t10-097.

Darrow, M. M., and Jensen, D. D. (2016). Modeling the performance of an air convection embankment (ACE) with thermal berm over ice-rich permafrost, Lost Chicken Creek, Alaska. *Cold Reg. Sci. Technol.* 130, 43–58. doi:10.1016/j.coldregions.2016.07.012.

Delaloye, R. (2004). Contribution à l'étude du pergélisol de montagne en zone marginale. *GeoFocus No. 10*, 244.

Delaloye, R., and Lambiel, C. (2005). Evidence of winter ascending air circulation throughout talus slopes and rock glaciers situated in the lower belt of alpine discontinuous permafrost (Swiss Alps). *Nor. Geogr. Tidsskr.* 59, 194–203. doi:10.1080/00291950510020673.

Delaloye, R., Reynard, E., Lambiel, C., Marescot, L., and Monnet, R. (2003). Thermal anomaly in a cold scree slope (Creux du Van, Switzerland). *Proc. Eighth Int. Conf. Permafr.*, 175–180.

Deluigi, N., Lambiel, C., and Kanevski, M. (2017). Data-driven mapping of the potential mountain permafrost distribution. *Sci. Total Environ.* 590–591, 370–380. doi:10.1016/j.scitotenv.2017.02.041.

Edenborn, H. M., Sams, J. I., and Kite, J. S. (2012). Thermal Regime of a Cold Air Trap in Central Pennsylvania, USA: The Trough Creek Ice Mine. *Permafr. Periglac. Process.* 23, 187–195. doi:10.1002/ppp.1742.

Etzelmüller, B. (2013). Recent advances in mountain permafrost research. *Permafr. Periglac. Process.* 24, 99–107. doi:10.1002/ppp.1772.

Etzelmüller, B., Guglielmin, M., Hauck, C., Hilbich, C., Hoelzle, M., Isaksen, K., et al. (2020). Twenty years of European mountain permafrost dynamics-the PACE legacy. *Environ. Res. Lett.* 15. doi:10.1088/1748-9326/abae9d.

Evatt, G. W., Abrahams, I. D., Heil, M., Mayer, C., Kingslake, J., Mitchell, S. L., et al. (2015). Glacial melt under a porous debris layer. *J. Glaciol.* 61, 825–836. doi:10.3189/2015JoG14J235.

Faimon, J., and Lang, M. (2013). Variances in airflows during different ventilation modes in a dynamic U-shaped cave. *Int. J. Speleol.* 42, 115–122. doi:10.5038/1827-806X.42.2.3.

FOEN (2005). *Map of potential permafrost distribution in Switzerland*. Federal Office for the Environment FOEN.

Fourier, J. B. J. (1822). *Théorie analytique de la chaleur*. Paris: Chez Firmin Didot, père et fils.

GeoStudio (2013a). *Air Flow Modeling with AIR/W2012. An Engineering Methodology. September 2013 Edition*. GEO-SLOPE International, Ltd., Calgary, Alberta, Canada.

GeoStudio (2013b). *Seepage Modeling with SEEP/W2012. An Engineering Methodology. September 2013 Edition*. GEO-SLOPE International, Ltd., Calgary, Alberta, Canada.

GeoStudio (2013c). *Thermal Modeling with TEMP/W2012. An Engineering Methodology. September 2013 Edition*. GEO-SLOPE International, Ltd., Calgary, Alberta, Canada.

Geotest (1990). Schafberg (Pontresina). Geophysikalische Untersuchungen im Rahmen des Permafrostprojektes. *Geotest Bericht Nr. 89035*.

Goering, D. J. (2003). Passively Cooled Railway Embankments for Use in Permafrost Areas. *J. Cold Reg. Eng.* 17, 119–133. doi:10.1061/(asce)0887-381x(2003)17:3(119).

Goering, D. J., and Kumar, P. (1996). Winter-time convection in open-graded embankments. *Cold Reg. Sci. Technol.* 24, 57–74. doi:10.1016/0165-232X(95)00011-Y.

Graham, M. D., and Steen, P. H. (1994). Plume formation and resonant bifurcations in porous-media convection. *J. Fluid Mech.* 272, 67–90. doi:10.1017/S0022112094004386.

Gruber, S., and Hoelzle, M. (2008). The cooling effect of coarse blocks revisited: A modeling study of a purely conductive mechanism. *Proc. Ninth Int. Conf. Permafr.*, 557–561.

Gubler, S., Fiddes, J., Keller, M., and Gruber, S. (2011). Scale-dependent measurement and analysis of ground surface temperature variability in alpine terrain. *Cryosph.* 5, 431–443. doi:10.5194/tc-5-431-2011.

Gude, M., Dietrich, S., Mausbacher, R., Hauck, C., Molenda, R., Ruzicka, V., et al. (2003). Probable occurrence of sporadic permafrost in non-alpine scree slopes in central Europe. *Proc. 8th Int.*

Conf. Permafr., 331–336.

Guodong, C., Yuanming, L., Zhizhong, S., and Fan, J. (2007). The 'thermal semi-conductor' effect of crushed rocks. *Permafr. Periglac. Process.* 18, 151–160. doi:10.1002/ppp.575.

Haberkorn, A., Wever, N., Hoelzle, M., Phillips, M., Kenner, R., Bavay, M., et al. (2017). Distributed snow and rock temperature modelling in steep rock walls using Alpine3D. *Cryosph.* 11, 585–607. doi:10.5194/tc-11-585-2017.

Haeberli, W., Hunder, J., Keusen, H.-R., Pika, J., and Röthlisberger, H. (1988). Core drilling through rock-glacier permafrost. *Proc. Fifth Int. Conf. Permafr.*, 937–942.

Haeberli, W., Noetzli, J., Arenson, L., Delaloye, R., Gärtner-Roer, I., Gruber, S., et al. (2011). Mountain permafrost: Development and challenges of a young research field. *J. Glaciol.* 56, 1043–1058. doi:10.3189/002214311796406121.

Hanson, S., and Hoelzle, M. (2004). The thermal regime of the active layer at the Murtèl rock glacier based on data from 2002. *Permafr. Periglac. Process.* 15, 273–282. doi:10.1002/ppp.499.

Harris, C., Arenson, L. U., Christiansen, H. H., Etzelmüller, B., Frauenfelder, R., Gruber, S., et al. (2009). Permafrost and climate in Europe: Monitoring and modelling thermal, geomorphological and geotechnical responses. *Earth-Science Rev.* 92, 117–171. doi:10.1016/j.earscirev.2008.12.002.

Harris, C., Mühll, D. V., Isaksen, K., Haeberli, W., Sollid, J. L., King, L., et al. (2003). Warming permafrost in European mountains. *Glob. Planet. Change* 39, 215–225. doi:10.1016/j.gloplacha.2003.04.001.

Harris, S. A., and Pedersen, D. E. (1998). Thermal regimes beneath coarse blocky materials. *Permafr. Periglac. Process.* 9, 107–120. doi:10.1002/(SICI)1099-1530(199804/06)9:2<107::AID-PPP277>3.0.CO;2-G.

Hasler, A., Gruber, S., Font, M., and Dubois, A. (2011). Advective heat transport in frozen rock clefts: Conceptual model, laboratory experiments and numerical simulation. *Permafr. Periglac. Process.* 22, 378–389. doi:10.1002/ppp.737.

Heinze, T. (2020). Possible effect of flow velocity on thawing rock-water-ice systems under local thermal non-equilibrium conditions. *Cold Reg. Sci. Technol.* 170, 102940. doi:10.1016/j.coldregions.2019.102940.

Herz, T. (2006). *Das Mikroklima grobblockiger Schutthalden der alpinen Periglazialstufe und seine Auswirkungen auf Energieaustauschprozesse zwischen Atmosphäre und Lithosphäre*. PhD Thesis: Justus-Liebig-Universität Gießen.

Hewitt, D. R., Neufeld, J. A., and Lister, J. R. (2014). High Rayleigh number convection in a three-dimensional porous medium. *J. Fluid Mech.* 748, 879–895. doi:10.1017/jfm.2014.216.

Hilbich, C. (2010). Time-lapse refraction seismic tomography for the detection of ground ice degradation. *Cryosphere* 4, 243–259. doi:10.5194/tc-4-243-2010.

Hilbich, C., Marescot, L., Hauck, C., Loke, M. H., and Mäusbacher, R. (2009). Applicability of electrical resistivity tomography monitoring to coarse blocky and ice-rich permafrost landforms. *Permafr. Periglac. Process.* 20, 269–284. doi:10.1002/ppp.652.

Hoelzle, M. (1996). Mapping and modelling of mountain permafrost distribution in the Alps. *Nor. Geogr. Tidsskr.* 50, 11–50.

Hoelzle, M., Mittaz, C., Etzelmüller, B., and Haeberli, W. (2001). Surface energy fluxes and distribution models of permafrost in European mountain areas: an overview of current

developments. *Permafr. Periglac. Process.* 12, 53–68. doi:10.1002/ppp.385.

Hoelzle, M., Wagner, S., Kääb, A., and Vonder Mühll, D. (1998). Surface movement and internal deformation of ice-rock mixtures within rock glaciers at Pontresina-Schafberg, Upper Engadin, Switzerland. *Proc. Seventh Int. Conf. Permafrost, Yellowknife*, 465–471.

Hoelzle, M., Wegmann, M., and Krummenacher, B. (1999). Miniature temperature dataloggers for mapping and monitoring of permafrost in high mountain areas: First experience from the Swiss Alps. *Permafr. Periglac. Process.* 10, 113–124. doi:10.1002/(SICI)1099-1530(199904/06)10:2<113::AID-PPP317>3.0.CO;2-A.

Horton, C. W., and Rogers, F. T. (1945). Convection Currents in a Porous Medium. *J. Appl. Phys.* 16, 367–370. doi:10.1063/1.1707601.

Ikeda, A., and Matsuoka, N. (2006). Pebbly versus bouldery rock glaciers: Morphology, structure and processes. *Geomorphology* 73, 279–296. doi:10.1016/j.geomorph.2005.07.015.

Johansen, O. (1975). *Thermal Conductivity of Soils*. PhD Thesis: University of Trondheim, Trondheim, Norway. CRREL Draft English Translation 637, US Army Corps of Engineers, Cold Regions Research and Engineering Laboratory, Hanover, N.H.

Jones, D. B., Harrison, S., Anderson, K., and Betts, R. A. (2018). Mountain rock glaciers contain globally significant water stores. *Sci. Rep.* 8, 1–10. doi:10.1038/s41598-018-21244-w.

Juliussen, H., and Humlum, O. (2008). Thermal regime of openwork block fields on the mountains Elgåhogna and Sølen, central-eastern Norway. *Permafr. Periglac. Process.* 19, 1–18. doi:10.1002/ppp.607.

Kane, D. L., Hinkel, K. M., Goering, D. J., Hinzman, L. D., and Outcalt, S. I. (2001). Non-conductive heat transfer associated with frozen soils. *Glob. Planet. Change* 29, 275–292. doi:10.1016/S0921-8181(01)00095-9.

Keller, F. (1992). Automated mapping of mountain permafrost using the program PERMAKART within the geographical information system ARC/INFO. *Permafr. Periglac. Process.* 3, 133–138. doi:10.1002/ppp.3430030210.

Kenner, R., Noetzli, J., Hoelzle, M., Raetzo, H., and Phillips, M. (2019a). Distinguishing ice-rich and ice-poor permafrost to map ground temperatures and ground ice occurrence in the Swiss Alps. *Cryosphere* 13, 1925–1941. doi:10.5194/tc-13-1925-2019.

Kenner, R., Pruessner, L., Beutel, J., Limpach, P., and Phillips, M. (2019b). How rock glacier hydrology, deformation velocities and ground temperatures interact: Examples from the Swiss Alps. *Permafr. Periglac. Process.*, 12–14. doi:10.1002/ppp.2023.

Kneisel, C., Hauck, C., and Mühll, D. V. (2000). Permafrost below the Timberline confirmed and characterized by geoelectrical resistivity measurements, Bever Valley, eastern Swiss Alps. *Permafr. Periglac. Process.* 11, 295–304. doi:10.1002/1099-1530(200012)11:4<295::AID-PPP353>3.0.CO;2-L.

Koenig, C. E. M., Arenson, L. U., Hilbich, C., and Hauck, C. (2021). Modelling Water Release from Degrading Permafrost in Arid Mountain Environments. in *Regional Conference on Permafrost & 19th International Conference on Permafrost Engineering, Boulder (CO), USA/virtual conference, Oct 24–29*.

Lambiel, C. (2006). *Le pergélisol dans les terrains sédimentaires à forte déclivité: distribution, régime thermique et instabilités*. PhD Thesis, Université de Lausanne.

Lambiel, C., and Pieracci, K. (2008). Permafrost distribution in talus slopes located within the alpine

periglacial belt, Swiss Alps. *Permafr. Periglac. Process.* 19, 293–304. doi:10.1002/ppp.624.

Lapwood, E. R. (1948). Convection of a fluid in a porous medium. in *Mathematical Proceedings of the Cambridge Philosophical Society* (Cambridge University Press), 508–521.

Lebeau, M., and Konrad, J. M. (2009). Natural convection of compressible and incompressible gases in undeformable porous media under cold climate conditions. *Comput. Geotech.* 36, 435–445. doi:10.1016/j.compgeo.2008.04.005.

Lebeau, M., and Konrad, J. M. (2016). Non-Darcy flow and thermal radiation in convective embankment modeling. *Comput. Geotech.* 73, 91–99. doi:10.1016/j.compgeo.2015.11.016.

Lendemer, J. C., Edenborn, H. M., and Harris, R. C. (2009). Contributions to the lichen flora of Pennsylvania: Notes on the lichens of a remarkable talus slope in Huntingdon County. *Opusc. Philolichenum* 6, 125–136.

Lesmes, D. P., and Friedman, S. P. (2005). "Relationships between the Electrical and Hydrogeological Properties of Rocks and Soils," in, eds. Y. Rubin and S. S. Hubbard (Springer. Printed in the Netherlands.), 87–128. doi:10.1007/1-4020-3102-5_4.

Levintal, E., Dragila, M. I., Kamai, T., and Weisbrod, N. (2017). Free and forced gas convection in highly permeable, dry porous media. *Agric. For. Meteorol.* 232, 469–478. doi:10.1016/j.agrformet.2016.10.001.

Luethi, R., Phillips, M., and Lehning, M. (2017). Estimating Non-Conductive Heat Flow Leading to Intra-Permafrost Talik Formation at the Ritigraben Rock Glacier (Western Swiss Alps). *Permafr. Periglac. Process.* 28, 183–194. doi:10.1002/ppp.1911.

Luetscher, M., and Jeannin, P.-Y. (2004). A process-based classification of alpine ice caves. *Theor. Appl. Karstology* 17, 5–10.

Maierhofer, T., Hauck, C., Hilbich, C., Kemna, A., and Flores-Orozco, A. (2021). Spectral Induced Polarization imaging to investigate an ice-rich mountain permafrost site in Switzerland. *Cryosph. Discuss.* 2021, 1–36. doi:10.5194/tc-2021-234.

Marmy, A., Rajczak, J., Delaloye, R., Hilbich, C., Hoelzle, M., Kotlarski, S., et al. (2016). Semi-automated calibration method for modelling of mountain permafrost evolution in Switzerland. *Cryosph.* 10, 2693–2719. doi:10.5194/tc-10-2693-2016.

Maurer, H., and Hauck, C. (2007). Geophysical imaging of alpine rock glaciers. *J. Glaciol.* 53, 110–120. doi:10.3189/172756507781833893.

Meyer, C., Meyer, U., Pflitsch, A., and Maggi, V. (2016). Analyzing airflow in static ice caves by using the calcFLOW method. *Cryosphere* 10, 879–894. doi:10.5194/tc-10-879-2016.

Millar, C. I., Westfall, R. D., and Delany, D. L. (2016). Thermal Components of American Pika Habitat—How does a Small Lagomorph Encounter Climate? *Arctic, Antarct. Alp. Res.* 48, 327–343. doi:10.1657/AAAR0015-046.

Mittaz, C., Hoelzle, M., and Haeberli, W. (2000). First results and interpretation of energy-flux measurements over Alpine permafrost. *Ann. Glaciol.* 31, 275–280. doi:10.3189/172756400781820363.

Mollaret, C., Hilbich, C., Pellet, C., Flores-Orozco, A., Delaloye, R., and Hauck, C. (2019). Mountain permafrost degradation documented through a network of permanent electrical resistivity tomography sites. *Cryosph.* 13, 2557–2578. doi:10.5194/tc-13-2557-2019.

Mollaret, C., Wagner, F. M., Hilbich, C., Scapozza, C., and Hauck, C. (2020). Petrophysical Joint

Inversion Applied to Alpine Permafrost Field Sites to Image Subsurface Ice, Water, Air, and Rock Contents. *Front. Earth Sci.* 8. doi:10.3389/feart.2020.00085.

Moore, J. R., Gischig, V., Katterbach, M., and Loew, S. (2011). Air circulation in deep fractures and the temperature field of an alpine rock slope. *Earth Surf. Process. Landforms* 36, 1985–1996. doi:10.1002/esp.2217.

Morard, S. (2011). Effets de la circulation d'air par effet de cheminée dans l'évolution du régime thermique des éboulis froids de basse et moyenne altitude. *GeoFocus*, 224.

Morard, S., and Delaloye, R. (2008). Airflow velocity measurements in ventilated porous debris accumulations. *Abstr. Vol. 6th Swiss Geosci. Meet.*, 192–193.

Morard, S., Delaloye, R., and Lambiel, C. (2010). Pluriannual thermal behavior of low elevation cold talus slopes in western Switzerland. *Geogr. Helv.* 65, 124–134. doi:10.5194/gh-65-124-2010.

Mottaghy, D., and Rath, V. (2006). Latent heat effects in subsurface heat transport modelling and their impact on palaeotemperature reconstructions. *Geophys. J. Int.* 164, 236–245. doi:10.1111/j.1365-246X.2005.02843.x.

Nicholson, L., and Benn, D. I. (2006). Calculating ice melt beneath a debris layer using meteorological data. *J. Glaciol.* 52, 463–470. doi:10.3189/172756506781828584.

Nield, D. A., and Bejan, A. (2017). *Convection in porous media*. Cham: Springer doi:10.1007/978-3-319-49562-0.

Noetzli, J., and Gruber, S. (2009). Transient thermal effects in Alpine permafrost. *Cryosph.* 3, 85–99. doi:10.5194/tc-3-85-2009.

Otero, J., Dontcheva, L. A., Johnston, H., Worthing, R. A., Kurganov, A., Petrova, G., et al. (2004). High-Rayleigh-number convection in a fluid-saturated porous layer. *J. Fluid Mech.* 500, 263–281. doi:10.1017/S0022112003007298.

Panz, M. (2008). *Analyse von Austauschprozessen in der Auftauschicht des Blockgletschers Murtèl-Corvatsch, Oberengadin*. Master Thesis (unpublished): Ruhr Universität.

Pellet, C., and Hauck, C. (2017). Monitoring soil moisture from middle to high elevation in Switzerland: Set-up and first results from the SOMOMOUNT network. *Hydrol. Earth Syst. Sci.* 21, 3199–3220. doi:10.5194/hess-21-3199-2017.

PERMOS (2016). *PERMOS Database*. Fribourg, Switzerland: Swiss Permafrost Monitoring Network doi:http://dx.doi.org/10.13093/permos-2016-01.

PERMOS (2019). *PERMOS Database*. Fribourg and Davos, Switzerland: Swiss Permafrost Monitoring Network. doi:10.13093/permos-2019-01.

Pewe, T. L. (1983). Alpine permafrost in the contiguous United States: a review. *Arct. Alp. Res.* 15, 145–156. doi:10.2307/1550917.

Pham, H., Arenson, L. U., and Sego, D. C. (2008). Numerical analysis of forced and natural convection in waste-rock piles in permafrost environments. *Proc. Ninth Int. Conf. Permafr.*, 1411–1416.

Pham, N., Amos, R., Blowes, D., Smith, L., and Sego, D. (2015). The Diavik Waste Rock Project : Heat Transfer in a Large Scale Waste Rock Pile Constructed in a Permafrost Region. *10th Int. Conf. Acid Rock Drain. IMWA Annu. Conf.*, 1–11.

Phillips, M., Mutter, E. Z., Kern-Luetschg, M., and Lehning, M. (2009). Rapid degradation of ground ice in a ventilated talus slope: Flüela Pass, Swiss Alps. *Permafr. Periglac. Process.* 20, 1–14. doi:10.1002/ppp.638.

Popescu, R., Vespremeanu-Stroe, A., Onaca, A., Vasile, M., Cruceru, N., and Pop, O. (2017). Low-altitude permafrost research in an overcooled talus slope–rock glacier system in the Romanian Carpathians (Detunata Goală Apuseni Mountains). *Geomorphology* 295, 840–854. doi:10.1016/j.geomorph.2017.07.029.

Pruessner, L., Huss, M., Phillips, M., and Farinotti, D. (2021). A Framework for Modeling Rock Glaciers and Permafrost at the Basin-Scale in High Alpine Catchments. *J. Adv. Model. Earth Syst.* 13. doi:10.1029/2020MS002361.

Pruessner, L., Phillips, M., Farinotti, D., Hoelzle, M., and Lehning, M. (2018). Near-surface ventilation as a key for modeling the thermal regime of coarse blocky rock glaciers. *Permafr. Periglac. Process.* 29, 152–163. doi:10.1002/ppp.1978.

Reid, T. D., and Brock, B. W. (2010). An energy-balance model for debris-covered glaciers including heat conduction through the debris layer. *J. Glaciol.* 56, 903–916. doi:10.3189/002214310794457218.

Rieksts, K., Hoff, I., Scibilia, E., and Côté, J. (2020). Establishment of intrinsic permeability of coarse open-graded materials: Review and analysis of existing data from natural air convection tests. *Minerals* 10, 1–22. doi:10.3390/min10090767.

Sawada, Y., Ishikawa, M., and Ono, Y. (2003). Thermal regime of sporadic permafrost in a block slope on Mt. Nishi-Nupukaushinupuri, Hokkaido Island, Northern Japan. *Geomorphology* 52, 121–130. doi:10.1016/S0169-555X(02)00252-0.

Scapozza, C. (2013). *Stratigraphie, morphodynamiqe, paléoenvironnements des terrains sédimentaires meubles à forte déclivité du domaine périglaciaire alpin*. PhD Thesis, Université de Lausanne.

Scapozza, C., Baron, L., and Lambiel, C. (2015). Borehole logging in Alpine periglacial talus slopes (Valais, Swiss Alps). *Permafr. Periglac. Process.* 26, 67–83. doi:10.1002/ppp.1832.

Scherler, M., Hauck, C., Hoelzle, M., and Salzmann, N. (2013). Modeled sensitivity of two alpine permafrost sites to RCM-based climate scenarios. *J. Geophys. Res. Earth Surf.* 118, 780–794. doi:10.1002/jgrf.20069.

Scherler, M., Hoelzle, M., Huss, M., and Hauck, C. (2018). Present and future runoff regimes at Murtel-Corvatsch rock glacier. in *5th European Conference on Permafrost, June 23-July 1, Chamonix, France*, 990–991.

Scherler, M., Schneider, S., Hoelzle, M., and Hauck, C. (2014). A two-sided approach to estimate heat transfer processes within the active layer of the Murtèl-Corvatsch rock glacier. *Earth Surf. Dyn.* 2, 141–154. doi:10.5194/esurf-2-141-2014.

Schneider, S., Hoelzle, M., and Hauck, C. (2012). Influence of surface and subsurface heterogeneity on observed borehole temperatures at a mountain permafrost site in the Upper Engadine, Swiss Alps. *Cryosph.* 6, 517–531. doi:10.5194/tc-6-517-2012.

Schorghofer, N., Leopold, M., and Yoshikawa, K. (2017). State of High-Altitude Permafrost on Tropical Maunakea Volcano, Hawaii. *Permafr. Periglac. Process.* 28, 685–697. doi:10.1002/ppp.1954.

Schwindt, D. (2013). *Permafrost in ventilated talus slopes below the timberline*. PhD Thesis, Bayerische Julius-Maximilians-Universität Würzburg.

Stocker-Mittaz, C., Hoelzle, M., and Haeberli, W. (2002). Modelling alpine permafrost distribution based on energy-balance data: a first step. *Permafr. Periglac. Process.* 13, 271–282. doi:10.1002/ppp.426.

Sun, B., Yang, L., Liu, Q., and Xu, X. (2010). Numerical modelling for crushed rock layer thickness of highway embankments in permafrost regions of the Qinghai-Tibet Plateau. *Eng. Geol.* 114, 181–190. doi:10.1016/j.enggeo.2010.04.014.

Tanaka, H. L., Nohara, D., and Yokoi, M. (2000). Numerical Simulation of Wind Hole Circulation and Summertime Ice Formation at Ice Valley in Kora and Nakayama in Fukushima, Japan. *J. Meteorol. Soc. Japan* 79, 611–630.

van Everdingen, R. O. (1998). Glossary of Permafrost and Related Ground-Ice Terms. *Int. Permafr. Assoc. IPA*.

VAW (1991). Pontresina Schafberg. Bericht über die geophysikalischen Sondierungen im Permafrostbereich der Lawinenverbauungszone. *Bericht VAW/ETHZ Nr. 80.1*.

VAW (1992). Pontresina Schafberg. Bericht über die geophysikalischen Sondierungen im Grenzbereich des alpinen Permafrostes im Val Clüx. *Bericht VAW/ETHZ Nr. 80.4*.

Vonder Mühll, D. S., Arenson, L. U., and Springman, S. M. (2003). Temperature conditions in two Alpine rock glaciers. *Proc. Eighth Int. Conf. Permafr.*, 1195–1200.

Vonder Mühll, D. S., and Haeberli, W. (1990). Thermal Characteristics of the Permafrost within an Active Rock Glacier (Murtèl/Corvatsch, Grisons, Swiss Alps). *J. Glaciol.* 36, 151–158. doi:10.3189/S0022143000009382.

Vonder Mühll, D. S., Hauck, C., and Lehmann, F. (2000). Verification of geophysical models in Alpine permafrost using borehole information. *Ann. Glaciol.* 31, 300–306. doi:10.3189/172756400781820057.

Vonder Mühll, D. S., and Holub, P. (1992). Borehole logging in alpine permafrost, upper Engadin, Swiss Alps. *Permafr. Periglac. Process.* 3, 125–132. doi:10.1002/ppp.3430030209.

Wagner, T., Pauritsch, M., Mayaud, C., Kellerer-Pirklbauer, A., Thalheim, F., and Winkler, G. (2019). Controlling factors of microclimate in blocky surface layers of two nearby relict rock glaciers (Niedere Tauern Range, Austria). *Geogr. Ann. Ser. A, Phys. Geogr.* 101, 310–333. doi:10.1080/04353676.2019.1670950.

Wakonigg, H. (1996). Unterkühlte Schutthalden. *Arb. aus dem Inst. für Geogr. der Karl-Franzens-Universität Graz* 33, 209–223.

Wang, H., Sun, H., Ge, X., Chen, J., and Zhu, D. (2021). Cooling effect of a composite embankment for wide expressways in permafrost regions: a three-dimensional numerical analysis. *Eur. J. Environ. Civ. Eng.* 25, 857–875. doi:10.1080/19648189.2018.1552204.

Weisbrod, N., Dragila, M. I., Nachshon, U., and Pillersdorf, M. (2009). Falling through the cracks: The role of fractures in Earth-atmosphere gas exchange. *Geophys. Res. Lett.* 36, 1–5. doi:10.1029/2008GL036096.

Westermann, S., Schuler, T. V., Gisnås, K., and Etzelmüller, B. (2013). Transient thermal modeling of permafrost conditions in Southern Norway. *Cryosph.* 7, 719–739. doi:10.5194/tc-7-719-2013.

Zacharda, M., Gude, M., Kraus, S., Hauck, C., Molenda, R., and Růžička, V. (2005). The relict mite Rhagidia gelida (Acari, Rhagidiidae) as a biological cryoindicator of periglacial microclimate in European highland screes. *Arctic, Antarct. Alp. Res.* 37, 402–408. doi:10.1657/1523-0430(2005)037[0402:TRMRGA]2.0.CO;2.

Zacharda, M., Gude, M., and Růžička, V. (2007). Thermal regime of three low elevation scree slopes in central Europe. *Permafr. Periglac. Process.* 18, 301–308. doi:10.1002/ppp.598.

Zhang, M., Cheng, G., and Li, S. (2009). Numerical study on the influence of geometrical parameters on natural convection cooling effect of the crushed-rock revetment. *Sci. China, Ser. E Technol. Sci.* 52, 539–545. doi:10.1007/s11431-008-0329-9.

Zhang, M., Lai, Y., Li, D., Chen, W., and Tong, G. (2013). Experimental study on ventilation characteristics of a concrete-sphere layer and a crushed-rock layer. *Int. J. Heat Mass Transf.* 59, 407–413. doi:10.1016/j.ijheatmasstransfer.2012.12.013.

Acknowledgments

Curriculum vitae

Personal Details

Name	Jonas Wicky
Adress	Dahliaweg 14 3004 Bern
E-mail	jonas.wicky@unifr.ch mail@jonaswicky.ch
Mobile	+41 79 721 25 75
Languages	German (mother tongue), French (bilingual), English (good knowledge)

Education

2017 - 2022	**PhD at the Cryosphere Research Group, Dep. of Geosciences, University of Fribourg with the title :** Air Convection in Coarse Blocky Permafrost: A Numerical Modelling Approach to Improve the Understanding of the Ground Thermal Regime
2012 – 2015	**Master of Science in Geography at the University of Fribourg** Option Dynamics in Glaciology and Geomorphology
2008 – 2012	**Bachelor of Science in Geography at the University of Fribourg** Minor in Informatics & Earth science
2004 – 2008	**Matura at Kollegium Sankt Michael in Fribourg** Main subject Mathematics & Physics

Professional activities

Since 2020	**Mountain Guide UIAGM/IFMGA**
2016- 2017	**Research Assistant PERMOS Office, University of Fribourg & SLF**
2016	**Graduate assistant at the Dep. of Geosciences, University of Fribourg** Geophysics in Chile
2015 - 2016	**Temporary technical employee at Swiss Federal Institute for Forest, Snow and Landscape Research WSL** Field team Swiss natural forest reserves / Field work in Ukraine
2013 - 2014	**sCOOL-Animateur at the Swiss Orienteering Federation** Orienteering course education at primary school level
2012	**Civil Service at Swiss Federal Institute for Forest, Snow and Landscape Research WSL** Unit stand dynamics and silviculture